学 位 論 文

Metal-responsive Bifacial DNA Base Pairing based on 5-Hydroxyuracil Nucleobase

（5-ヒドロキシウラシル核酸塩基を用いた
金属応答性二面型 DNA 塩基対の開発）

平成２８年１２月博士（理学）申請

東京大学大学院理学系研究科
化学専攻

西 山　康 太 郎

Abstract

1. Introduction

DNA molecules form duplexes, triplexes, and other higher-order structures in a sequence-specific manner. Thus, DNAs have great potential to serve as building blocks of nanoarchitectures and nanomachines. We and other groups have developed artificial metallo-DNAs, which contain an unnatural nucleobase pair formed through metal coordination bonding instead of natural hydrogen-bonding.[1] The metal-mediated base pairing allows thermal stabilization of self-assembled and folded DNA structures and thereby metal-induced DNA structural conversion. Moreover, introduction of multiple metal-mediated base pairs provides the fundamentals for precise metal arrangement in the DNA helical structures.

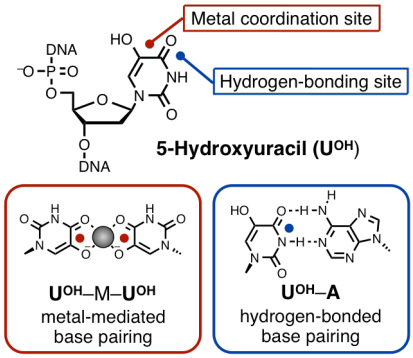

Figure 1. Metal-responsive bifacial DNA base pairing of 5-hydroxyuracil ($\mathbf{U}^{\mathbf{OH}}$) nucleobase. $\mathbf{U}^{\mathbf{OH}}$ base forms both a metal-mediated base pair ($\mathbf{U}^{\mathbf{OH}}$–M–$\mathbf{U}^{\mathbf{OH}}$) and a hydrogen-bonded base pair ($\mathbf{U}^{\mathbf{OH}}$–**A**).

In this study, I have utilized a 5-hydroxyuracil ($\mathbf{U}^{\mathbf{OH}}$) nucleobase for metal-responsive "*bifacial*" nucleobase pairing (Figure 1). The 4-carbonyl and 5-hydroxy groups of $\mathbf{U}^{\mathbf{OH}}$ nucleobase can serve as a bidentate metal ligand, in which its uracil scaffold is maintained as a hydrogen bond donor/acceptor site. Therefore, it was expected that the $\mathbf{U}^{\mathbf{OH}}$ nucleobase may form a metal-mediated base pair ($\mathbf{U}^{\mathbf{OH}}$–M–$\mathbf{U}^{\mathbf{OH}}$, M = metal ion) as well as a hydrogen-bonded base pair with adenine (**A**) nucleobase ($\mathbf{U}^{\mathbf{OH}}$–**A**), leading to stabilization effects and dynamic switching functions based on the metal-responsive *bifacial* base pairing.

2. Metal-mediated DNA base pairing of 5-hydroxyuracil nucleobases

This study aimed to construct novel metallo-DNA duplexes through the formation of metal-mediated $\mathbf{U}^{\mathbf{OH}}$–M–$\mathbf{U}^{\mathbf{OH}}$ base pairs. A DNA duplex **1**·**2**, containing three $\mathbf{U}^{\mathbf{OH}}$–$\mathbf{U}^{\mathbf{OH}}$ base pairs, was synthesized by a DNA synthesizer (Figure 2a).[2,3] The effects of metal ions on the thermal stability of DNA duplex **1**·**2** were estimated by melting experiments. The melting temperature (T_m) of the DNA duplex **1**·**2** (Figure 2b) was increased upon addition of Zn^{II} (ΔT_m = + 13 °C) or a series of lanthanide ions [e.g. Gd^{III} (ΔT_m = + 18 °C)]. The results suggest that the formation of $\mathbf{U}^{\mathbf{OH}}$–M–$\mathbf{U}^{\mathbf{OH}}$ base pairs conferred interstrand crosslinking through the metal coordination bonds. In particular, some lanthanide ions including Gd^{III} exhibited significant duplex stabilization. UV absorption-based titration experiment was then conducted for the DNA duplex **1**·**2** with Gd^{III} ions. A new UV absorption band around 310 nm gradually increased until the ratio of [Gd^{III}] to [duplex **1**·**2**] reached 3.0. In addition, ESI-TOF mass analysis proved the formation of a trinuclear Gd^{III} complex (**1**·**2**·$\mathbf{Gd}^{\mathbf{III}}_3$) (found: 1368.77 ($z$ = 7); calcd for [**1** + **2** + 3Gd –16H]$^{7-}$: 1368.73) with three $\mathbf{U}^{\mathbf{OH}}$–Gd^{III}–$\mathbf{U}^{\mathbf{OH}}$ base pairs inside the DNA duplex **1**·**2** (Figure 2c).

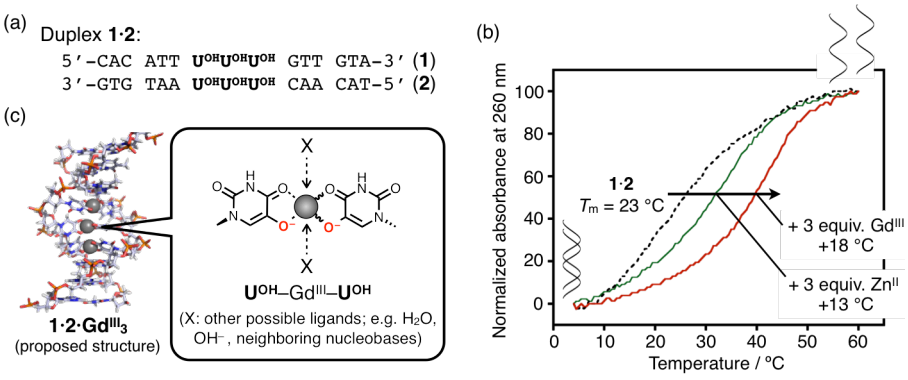

Figure 2. Construction of novel metallo-DNA duplexes based on $\mathbf{U}^{\mathbf{OH}}$ nucleobases. (a) DNA sequences. (b) Effects of metal ions on the melting behaviors of the DNA duplex **1**·**2**. [duplex] = 2 μM, [$GdCl_3$]/[duplex] or [$ZnSO_4$]/[duplex] = 0, 3 in 10 mM HEPES buffer (pH 8.0), 100 mM NaCl. (c) A proposed structure of the metallo-DNA **1**·**2**·$\mathbf{Gd}^{\mathbf{III}}_3$.

Circular dichroic analysis was further conducted to

clarify the DNA structure. As a result, Cotton effects of typical B-form DNA duplex were observed even in the presence of 3 equiv. of Gd^{III} ions although the intensity was decreased. This observation suggests that the Gd^{III} complex of duplex **1·2** has a structure similar to B-form, which was further confirmed by NMR spectroscopy.

Taken all together, the formation of metallo-DNA duplexes containing $\mathbf{U^{OH}}$–M–$\mathbf{U^{OH}}$ (M = Zn^{II}, Gd^{III} etc.) was successfully demonstrated. This metal-mediated base pairing thermally stabilizes the resulting DNA duplexes, allowing quantitative assembly of Gd^{III} ions inside double-stranded DNA structures.

3. Metal-mediated regulation of DNA hybridization preference using 5-hydroxyuracils

A $\mathbf{U^{OH}}$ nucleobase also forms a hydrogen-bonded $\mathbf{U^{OH}}$–**A** base pair (**A** = adenine). I expected that the stability of the $\mathbf{U^{OH}}$–**A** base pair can be controlled by metal complexation. Firstly, the effect of metal ions was examined on the stability of DNA duplex **1·2A**, containing three $\mathbf{U^{OH}}$–**A** base pairs in the central region (Figure 3a). The melting temperature (T_m) of duplex **1·2A** was decreased by 14 °C upon addition of 3 equiv. of Gd^{III} (Figure 3b; **X** = **A**). In addition, its UV absorption spectral changes suggested the binding of Gd^{III} to the metal coordination site of $\mathbf{U^{OH}}$ nucleobase concurrently with deprotonation of the 5-hydroxy group of $\mathbf{U^{OH}}$. This destabilization effect was not observed with the other DNA duplexes containing three mismatched base pairs [$\mathbf{U^{OH}}$–**X**; **X** = **T** (thymine), **G** (guanine), or **C** (cytosine)] (Figure 3). These results indicate that the hydrogen bonding between $\mathbf{U^{OH}}$ and **A** nucleobases was weakened by the binding of metal ions to $\mathbf{U^{OH}}$–**A** base pairs presumably due to the electronic and steric effects. Thus, the $\mathbf{U^{OH}}$–**A**-containing DNA duplex was selectively destabilized through the Gd^{III} complexation of $\mathbf{U^{OH}}$ bases.

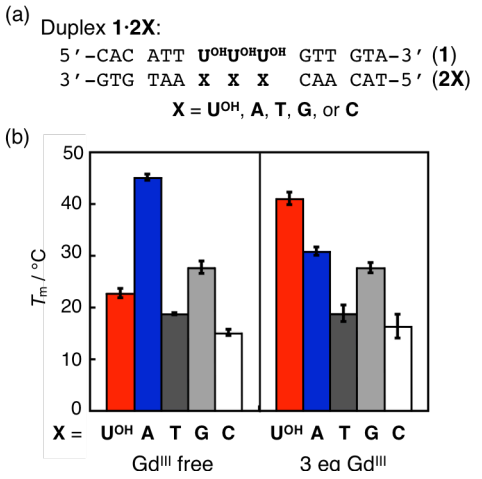

Figure 3. Hybridization preference of $\mathbf{U^{OH}}$-containing DNA strands. (a) DNA sequences. (b) Melting temperatures (T_m) of the DNA duplexes **1·2X**. [duplex] = 2 μM, [$GdCl_3$]/[duplex] = 0, 3 in 10 mM HEPES buffer (pH 8.0), 100 mM NaCl. Error bars indicate the standard deviations.

Next, I examined the hybridization preference of the $\mathbf{U^{OH}}$-containing DNA strands. In the absence of Gd^{III} ion (Figure 3b, left), the DNA duplex **1·2A** was more stable than the duplex **1·2** due to the hydrogen-bonded $\mathbf{U^{OH}}$–**A** base pairing. In the presence of 3 equiv. of Gd^{III} ions (Figure 3b, right), the DNA duplex **1·2** was more stable because of the stabilization through the $\mathbf{U^{OH}}$–Gd^{III}–$\mathbf{U^{OH}}$ base pairing as well as the destabilization of duplex **1·2A** based on the Gd^{III} complexation of $\mathbf{U^{OH}}$–A base pairs. Thus, the hybridization preference of DNA strand containing $\mathbf{U^{OH}}$ nucleobases was significantly influenced by the Gd^{III} complexation.

In addition, I investigated pH dependence of the metal-induced stabilization and destabilization of the $\mathbf{U^{OH}}$-containing DNA duplexes. Melting experiments revealed that Zn^{II} ion affected the duplex stability in a pH-dependent manner. Upon addition of 3 equiv. of Zn^{II}, the T_m value of the DNA duplex **1·2** was increased by 13 °C and 22 °C at pH 8.0 and 9.0, respectively, while it was hardly changed at pH 7.0. Furthermore, UV absorption spectral changes indicated that the metal complexation occurred only under basic conditions. These results are well consistent with the fact that the metal complexation of $\mathbf{U^{OH}}$ nucleobases is accompanied with deprotonation of the 5-hydroxy group, whose pK_a value is 7.7.[4] In addition, the Zn^{II} addition was found to induce thermal destabilization of duplex **1·2A** in a pH-dependent manner. Therefore, the thermal stability of $\mathbf{U^{OH}}$-containing duplex can be controlled not only by metal ions but also by pH when Zn^{II} was employed.

4. Metal-driven DNA strand exchange reactions through base pair switching of 5-hydroxyuracils

Next, I examined DNA strand exchange reactions through the metal-driven base pair switching between $\mathbf{U^{OH}}$–

A and $\mathbf{U}^{\mathbf{OH}}$–Gd^{III}–$\mathbf{U}^{\mathbf{OH}}$ base pairs (Figure 4a). It was expected that the exchange reactions could take place reversibly and isothermally based on the metal-mediated stabilization and destabilization. Then, native polyacrylamide gel electrophoresis (PAGE) analysis was conducted to investigate the effects of Gd^{III} on the hybridization preference of the template DNA strand **1**. A mixture of DNAs **1**, the complementary strands **2**, and **2A** was annealed to obtain thermodynamically stable products, in which the strand **2A** was labeled with a fluorescence tag (FAM) for gel analysis. Whereas the duplex **1·2A** containing three $\mathbf{U}^{\mathbf{OH}}$–**A** base pairs was quantitatively formed in the absence of Gd^{III}, the metallo-DNA duplex **1·2** with Gd^{III} was formed in ~40% yield in the presence of 3 equiv. of Gd^{III}. After optimization of experimental conditions, I found that another template DNA **3** containing four $\mathbf{U}^{\mathbf{OH}}$ nucleobases and complementary DNA strands **4** and **4A** (Figure 4b, left) in the presence of 6 equiv. of Gd^{III} preferentially generated metallo-DNA **3·4** with Gd^{III} in ~80% yield. These results show that the hybridization preference can be controlled by Gd^{III} complexation based on the *bifacial* behaviors of $\mathbf{U}^{\mathbf{OH}}$ nucleobases.

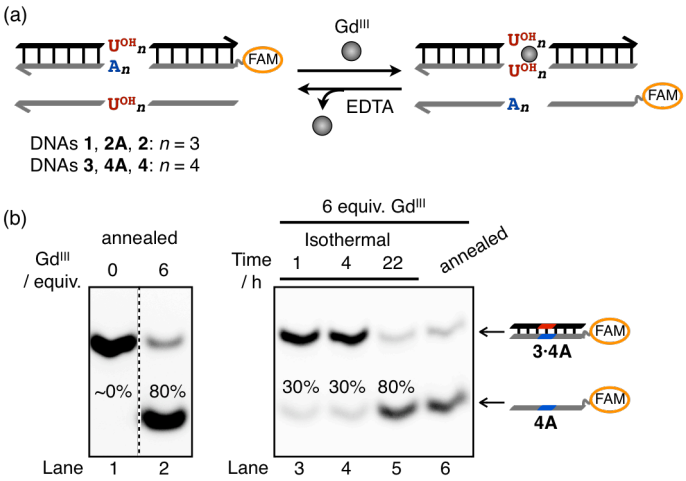

Figure 4. Metal-responsive DNA strand exchange reactions through the base pair switching of $\mathbf{U}^{\mathbf{OH}}$ nucleobases. (a) Schematic representation of the metal-responsive strand exchange and DNA sequences. (b) Native PAGE for DNAs **3**, **4A** and **4**. [DNA] = 2 μM for each, $[GdCl_3]/[DNA]$ = 0 or 6 in 10 mM HEPES buffer (pH 8.0), 100 mM NaCl. The reaction mixture was annealed after (lanes 2, 6) or before adding Gd^{III} ions (lanes 3–5). 20% acrylamide gel in TAMg buffer (pH 8.0; 40 mM Tris, 7.6 mM $MgCl_2$, 1.4 mM acetic acid), 4 °C.

I subsequently investigated whether the DNA strand exchange reactions take place under isothermal conditions, that is, without the annealing process. A mixture of DNA duplex **3·4A**, which contains four $\mathbf{U}^{\mathbf{OH}}$–**A** base pairs, and single strand **4** was prepared in the absence of Gd^{III} ion. After addition of 6 equiv. of Gd^{III}, the reaction mixture was incubated at 30 °C for 22 h and the products were analyzed by native PAGE analysis. The result showed that the duplex **3·4A** was converted to the metallo-DNA duplex **3·4** with Gd^{III} in ~80% yield (Figure 4b, right). Furthermore, when 6 equiv. of EDTA was added to remove Gd^{III}, the reverse reaction proceeded quickly and quantitatively. The result shows that this strand exchange reaction is reversible. Consequently, the introduction of *bifacial* $\mathbf{U}^{\mathbf{OH}}$ nucleobases into DNA allows reversible metal-responsive DNA strand exchange reactions, which may possibly serve as a motive power in DNA-based nanomachines.

5. Metal-responsive triplex-forming oligonucleotides with 5-hydroxyuracils

Triple-stranded DNAs are generally formed based on the sequence-specific recognition of a DNA duplex with a triplex-forming oligonucleotide (TFO), that is, the formation of base triplets such as **T**•**A**–**T** and $\mathbf{C}^{+}$•**G**–**C** ($\mathbf{C}^{+}$ is protonated **C**). The binding of TFO inhibits access of proteins as shown in RNA polymerase and histone to the template DNA, which would be utilized to artificially regulate gene expression.[5] It was expected that $\mathbf{U}^{\mathbf{OH}}$ nucleobase would form a $\mathbf{U}^{\mathbf{OH}}$•**A**–**T** base triplet leading to a triplex structure like the canonical **T**•**A**–**T** base triplet, and that metal complexation of the $\mathbf{U}^{\mathbf{OH}}$•**A**–**T** base triplet may cause dissociation of TFO from the main duplex structure (Figure 5a). Thus, the $\mathbf{U}^{\mathbf{OH}}$-containing TFO would be applied for the regulation of transcription in response to metal ions. As the first step, I investigated the thermal stability of a triple-stranded DNA based on metal complexation of $\mathbf{U}^{\mathbf{OH}}$ nucleobases. Thermal melting behaviors of a triple-stranded DNA consisting of a $\mathbf{U}^{\mathbf{OH}}$-containing TFO ($\mathbf{U}^{\mathbf{OH}}$-TFO) and a target natural duplex (dsDNA) were analyzed with or without Gd^{III} ions (Figure 5b, c). The first transition was ascribable to the dissociation of $\mathbf{U}^{\mathbf{OH}}$-TFO from dsDNA, and the second transition was due to the dissociation of dsDNA into the single strands. Upon addition of 3 equiv. of Gd^{III} ions, the

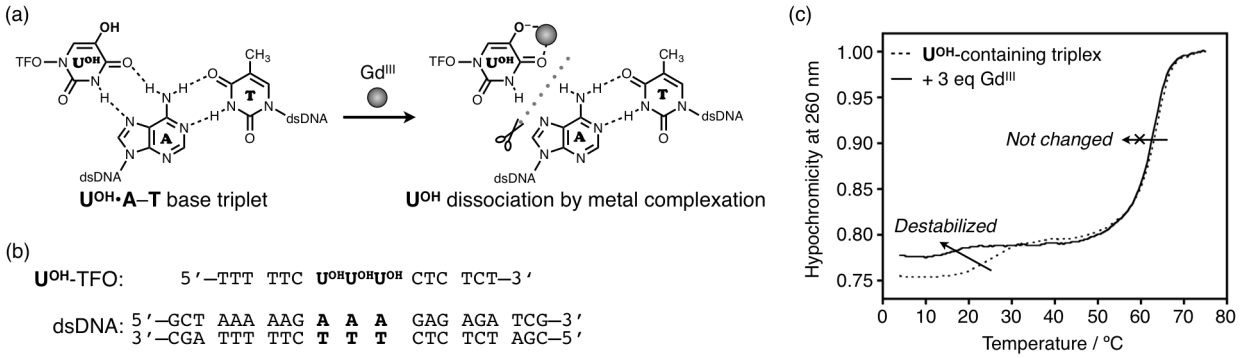

Figure 5. $\mathbf{U^{OH}}$-containing triplex-forming oligonucleotide ($\mathbf{U^{OH}}$-TFO) for metal-responsive structural conversion between triplex and duplex. (a) Metal complexation of $\mathbf{U^{OH}}$•**A**–**T** base triplet. (b) Sequences of DNA strands employed. (c) Melting curves of the $\mathbf{U^{OH}}$-containing triplex ($\mathbf{U^{OH}}$-TFO + dsDNA). [DNA] = 1.5 μM for each, [$GdCl_3$]/[triplex] = 0 or 3 in 10 mM HEPES buffer (pH 7.0), 140 mM NaCl, 10 mM $MgCl_2$, 0.2 °C/min.

triplex was thermally destabilized. In contrast, the thermal stability of dsDNA was hardly perturbed by the Gd^{III} addition. Thus, the binding affinity of the $\mathbf{U^{OH}}$-TFO to the natural DNA duplexes can be regulated in response to Gd^{III} ions. This metal-triggered dissociation of $\mathbf{U^{OH}}$-TFO would be applied for the regulation of biological functions such as transcription.

6. Conclusion

I have successfully developed metal-responsive *bifacial* DNA base pairing based on 5-hydroxyuracil ($\mathbf{U^{OH}}$) nucleobase. (i) Metal-mediated $\mathbf{U^{OH}}$–M–$\mathbf{U^{OH}}$ base pairing stabilized the DNA duplex in response to Zn^{II} and lanthanide metal ions such as Gd^{III}, whereas hydrogen-bonded $\mathbf{U^{OH}}$–**A** base pairing was destabilized by these metal ions. (ii) The thermal stability of Zn^{II}-mediated base pairs can be controlled by pH changes. (iii) The *bifacial* base pairing was applied to the metal-responsive DNA strand exchange reactions through the reversible base pair switching of $\mathbf{U^{OH}}$ nucleobases. (iv) The binding affinity of the triplex-forming DNA oligonucleotide ($\mathbf{U^{OH}}$-TFO) to dsDNA was regulated in response to Gd^{III} addition.

The metal-responsive stability controls and DNA strand exchange reactions would be applied for reversible regulation of DNA nanostructures such as DNA origami, DNA polyhedral, and logic gate. The $\mathbf{U^{OH}}$-TFO could serve as an artificial transcription factor to dynamically control gene expression. Thus, I believe that the metal-responsive *bifacial* base pairing developed in this study would greatly contribute to the development of DNA nanotechnology.

References

[1] Y. Takezawa, M. Shionoya, *Acc. Chem. Res.* **2012**, *45*, 2066. [2] J. Fujimoto, L. Tran, L. C. Sowers, *Chem. Res. Toxicol.* **1997**, *10*, 1254. [3] M. L. Morningstar, D. A. Kreutzer, J. M. Essigmann, *Chem. Res. Toxicol.* **1997**, *10*, 1345. [4] C. J. La Francois, Y. H. Jang, T. Cagin, W. A. Goddard, III, L. C. Sowers, *Chem. Res. Toxicol.* **2000**, *13*, 462. [5] B. P. Casey, P. M. Glazer, *Prog. Nucleic Acid Res. Mol. Biol.* **2001**, *67*, 163.

Abbreviations

Abs	absorbance
CD	circular dichroic
CHES	*N*-Cyclohexyl-2-aminoethanesulfonic acid
COSY	correlation spectroscopy
DNA	deoxyribonucleic acid
DQF	double quantum filter
ESI	electron spray ionization
FAM	carboxyfluorescein
HEPES	4-(2-hydroxyethyl)-1-piperazineethanesufonic acid
HSAB	hard-soft acid-base
Hz	hertz
M	molar
MS	mass spectrometry
m/*z*	mass-to-charge ratio
NMR	nuclear magnetic resonance
NOESY	nuclear Overhauser effect spectroscopy
PAGE	polyacrylamide gel electrophoresis
ppm	parts per million
TFO	triplex-forming oligonucleotide
T_m	Melting temperature
TOF	time-of-flight
Tris	tris(hydroxymethyl)aminomethane
UV	ultraviolet
Vis	visible

Contents

Chapter 1.

General introduction

1-1. Programmable self-assembled DNA structures

A DNA molecule is one of the biopolymers, which serves as a common carrier of genetic information in organisms. A deoxyribonucleotide, which is a monomer of DNA strands, consists of nucleobase, deoxyribose, and phosphoric acid (Figure 1-1a). Adenine (**A**), thymine (**T**), guanine (**G**), and cytosine (**C**) are canonical DNA bases in the biological systems. A typical structural feature is that two DNA strands form a double-stranded structure in a sequence-specific manner. The hybridization behaviors are caused by Watson–Crick-type base pairing between **A** and **T** as well as **G** and **C** through the complementary hydrogen bonding (Figure 1-1b). As for the size of a common right-handed DNA duplex (B-form DNA), the diameter is approximately 2 nm and the helical pitch with ca. 10 base pairs is approximately 3 nm (Figure 1-1c). The DNA chemical and enzymatic synthetic methods have been well established so that we can use natural DNAs with desired length and sequences.

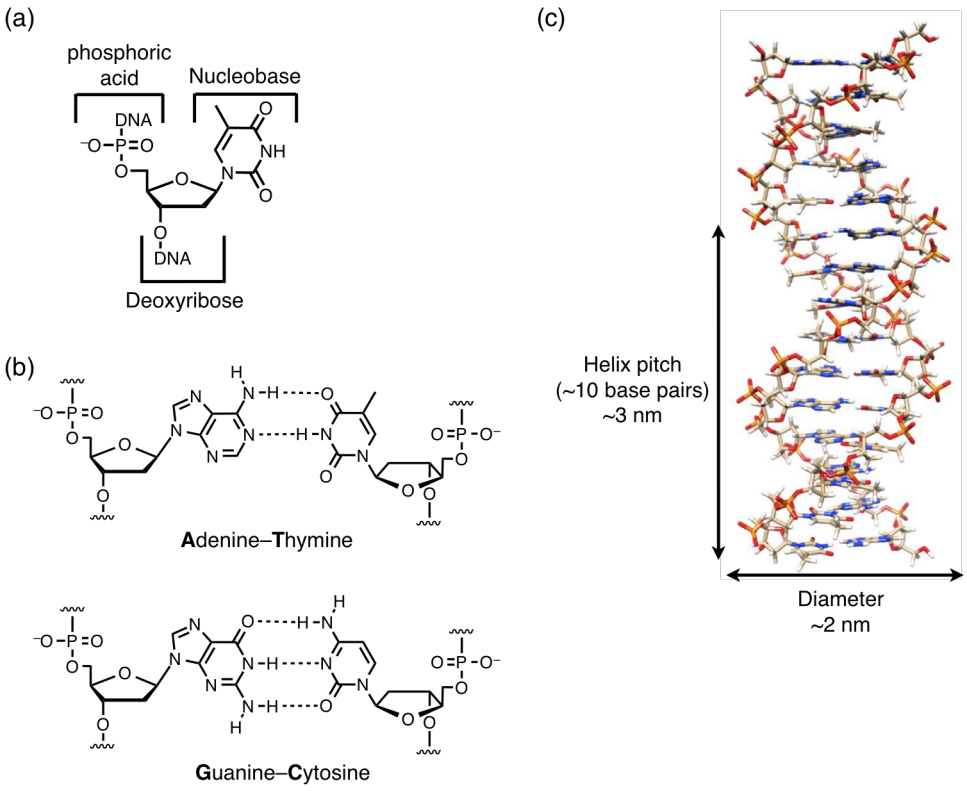

Figure 1-1. DNA structures. (a) Chemical structures of deoxyribonucleotide consisting of phosphoric acid, deoxyribose and nucleobase. (b) Chemical structures of Watson–Crick-type **A**–**T** and **G**–**C** base pairs. (c) The size of a common right-handed B-form DNA duplex.

Based on the above properties, DNA molecules have been extensively used for nanomaterials. The DNA-based nanostructures are spontaneously formed from various designed DNA strands. One of the most successful DNA nanomaterials is DNA origami developed by Rothemund (Figure 1-2a).[1] The fine two-dimensional structures are folded by attaching a large number of short DNA strands on a long DNA strand, in which the resulting DNA origami structure and the components can be designed by utilizing computer. DNA origami has been employed as a molecular template to align the large molecules such as enzymes[2,3] and nanoparticles[4–6]. In addition, some groups have constructed discrete DNA polyhedrons such as a cubic (Figure 1-2b)[7,8] and a tetrahedral structures (Figure 1-2c)[9]. The self-assembled DNA nanostructures confer a well-defined nano-space to encapsulate appropriate molecules. For instance, Krishnan et al. have reported the encapsulation of a quantum dot inside DNA icosahedra and the cellar uptake of the host-guest complex for bioimaging (Figure 1-3a).[10] Encapsulation of proteins have been also achieved by the sequence design (Figure 1-3b).[11,12]

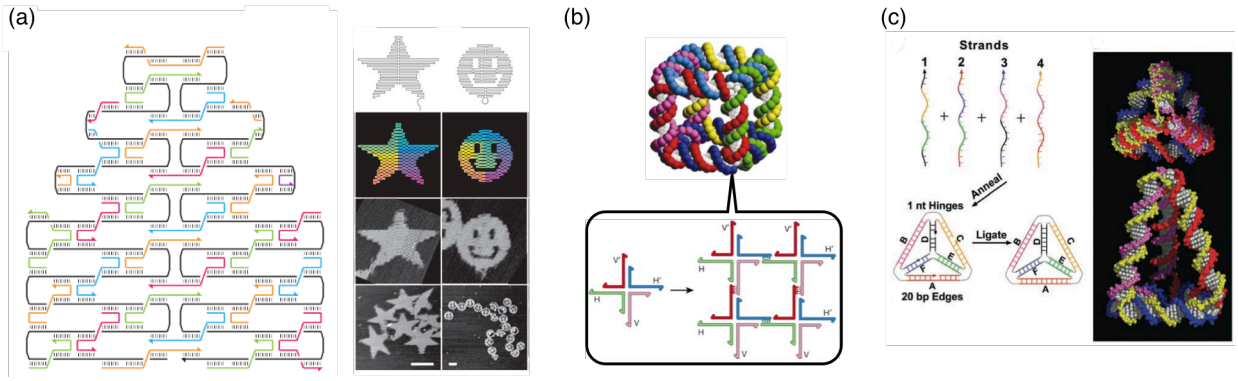

Figure 1-2. DNA nanoarchitectures. (a) DNA origami structures. Reproduced from ref. [1]. Copyright 2006 Nature Publishing Group. (b) DNA cubic nanostructure. Reproduced from ref. [8]. Copyright 2003 Nature Publishing Group. (c) DNA tetrahedron. Reproduced from ref. [9]. Copyright 2005 American Association for the Advancement of Science.

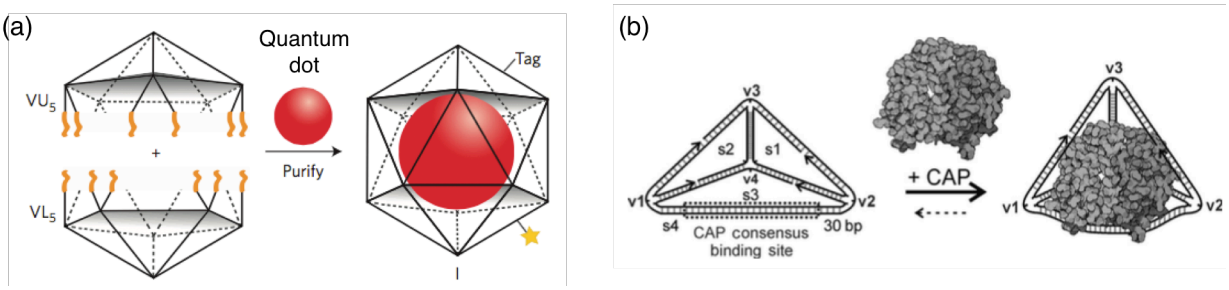

Figure 1-3. Encapsulation of large molecules inside the DNA polyhedrons possessing a well-defined nano-space. (a) Encapsulation of a quantum dot inside the DNA icosahedra. Reproduced from ref. [10]. Copyright 2016 Nature Publishing Group. (b) Encapsulation of catabolite activator protein (CAP) through the DNA sequence-specific binding. Reproduced from ref. [12]. Copyright 2013 Wiley-VCH.

A non-enzymatic toehold-mediated DNA strand exchange/displacement reaction is a key technology to dynamically control the self-assembled DNA structures. The toehold-mediated strand displacement confers thermodynamically stable DNA structures through DNA hybridization at toehold region and branch migration steps (Figure 1-4a).[13] These reactions have served as motive powers of DNA-based computing based on multi-input logic gates (Figure 1-4b)[13,14] and dynamic structural conversion of nanoarchitectures such as DNA switching system (Figure 1-4c)[15] and opening of a DNA box with a lid (Figure 1-4d)[16].

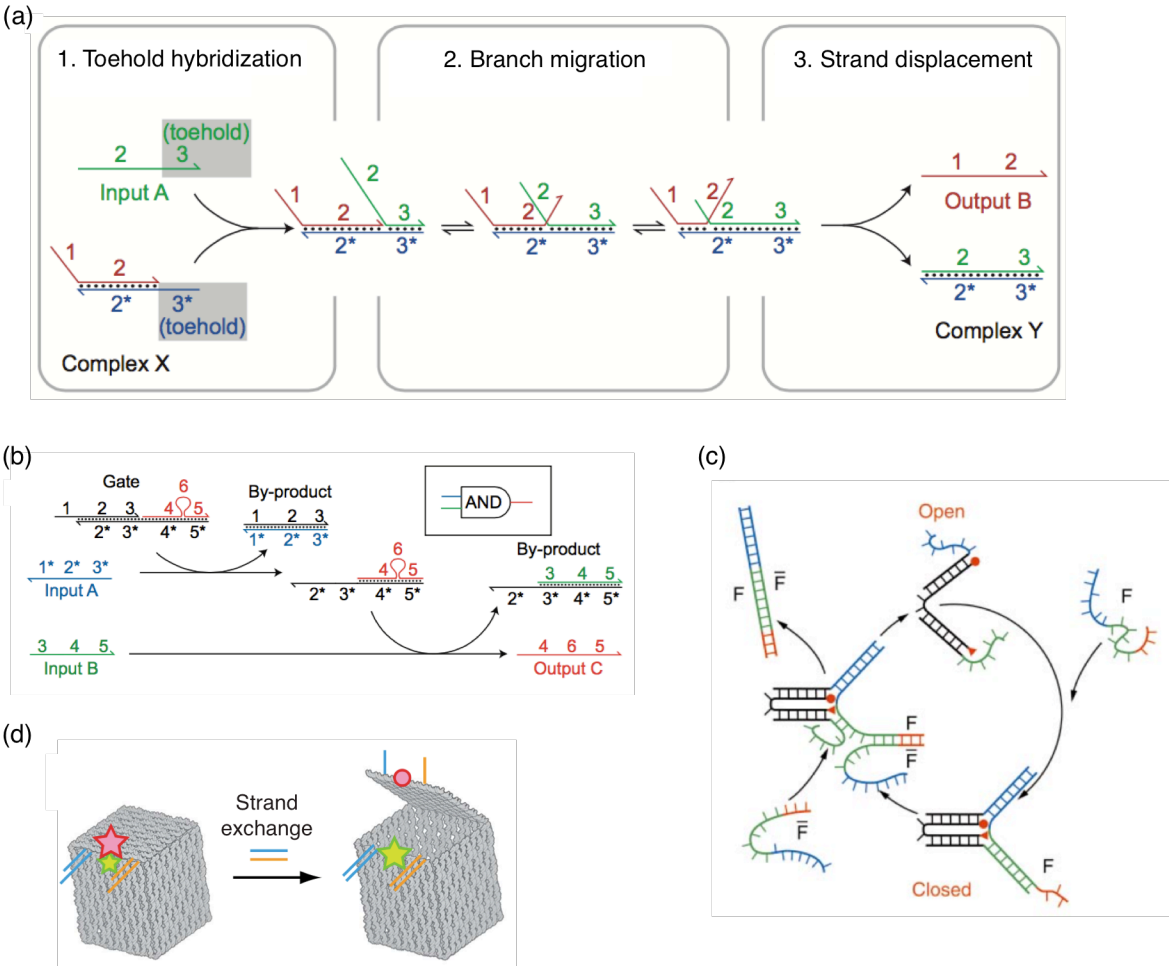

Figure 1-4. Dynamic DNA systems based on the DNA strand exchange/displacement reactions. (a) The strand displacement reaction proceeds through the toehold hybridization and branch migration steps. Reproduced from ref. [13]. Copyright 2011 Nature Publishing Group. (b) A DNA logic gate. Reproduced from ref. [13]. Copyright 2011 Nature Publishing Group. (c) DNA switch. Reproduced from ref. [15]. Copyright 2000 Nature Publishing Group. (d) Opening of a DNA box. Reproduced from ref. [16]. Copyright 2009 Nature Publishing Group.

DNA strands also form a triple-stranded and other higher-order structures in a sequence-specific manner. Formation of the higher-order structures not only develops unique nano-fabrication but also controls biorelevant functions. Triplex-forming oligonucleotides (TFOs) bind to a target region on endogenous DNA duplexes through the formation of base triplets such as **T**•**A**–**T** and $\mathbf{C}^{+}$•**G**–**C**. The formation of a triplex possibly inhibits the access of DNA-binding proteins such as RNA polymerases to the target regions (Figure 1-5). Thus, TFOs have been extensively applied for gene manipulation methods and antigene reagents.[17,18]

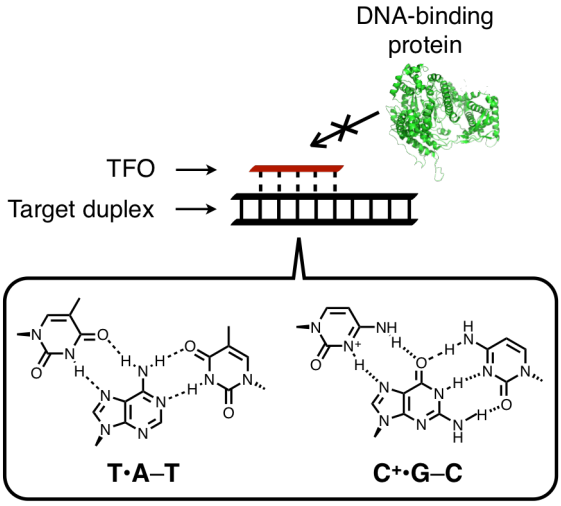

Figure 1-5. Schematic representation of the inhibition of the access of DNA-binding proteins to the target DNA duplexes mediated by the formation of the triple-stranded DNA.

The programmable self-assembly of DNA strands confers unique structures and functions. Thus, DNA molecules are powerful molecular foundations in many fields such as materials science and biology.

1-2. Stimuli-responsive DNAs

A number of stimuli-responsive DNAs have been developed, in which the DNA self-assembly can be controlled by small molecules, light, pH, and metal ions. Such stimuli-driven assembly allows sensing specific environments and to achieve the structural and functional regulation at a desired DNA region with precise control of the timing.

Natural DNA strands adopt some higher-order structures which are formed by external stimuli. A parallel triple-stranded DNA containing $\mathbf{C}^+ \cdot \mathbf{G}$–$\mathbf{C}$ base triplets ($\mathbf{C}^+$ is protonated **C**) and i-motif through the stacking of $\mathbf{C}^+$–**C** base pairs are formed and dissociated in response to pH (Figure 1-6a, b). pH sensors were developed by utilizing these pH-sensitive DNAs.[19] Guanine-rich DNA strands are folded into a G-quadruplex which is stabilized by K^+ ions put between Guanine-quartet structures (Figure 1-6c). The folding occurs only at high concentrations of K^+ ions. A G-quadruplex–hemin complex catalyzes oxidation of substrates such as luminol and NADH with hydrogen peroxide. Thus, many types of sensors and catalyst have been developed by using G-quadruplex as the building block.[20–23]

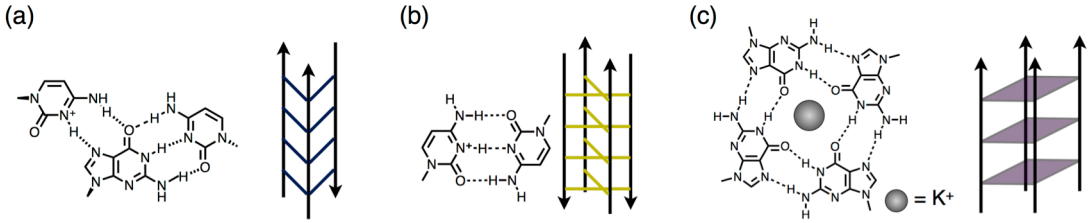

Figure 1-6. Stimuli-responsive self-assembly of natural DNA strands. (a) A pH-responsive parallel triple-stranded DNA. (b) A pH-responsive i-motif. (c) A K^+-responsive G-quadruplex.

Besides natural DNA systems, synthetic stimuli-responsive DNAs have been developed by chemical modification of DNA molecules. Artificial DNAs can be rationally designed and synthesized for desired structures and functions. Asanuma, Komiyama et al. have established versatile photo-responsive DNA strands containing azobenzene moieties through threoninol linkers (Figure 1-7a).[24] The thermal stability of duplexes and triplexes including azobenzene-containing DNA strands are reversibly regulated by photo-irradiation through the *trans-cis* isomerization. The

photo-regulation has been utilized for gene regulation and DNA nano-machines.[25,26] As another photo-responsive DNAs, artificial DNA strands functionalized by photo-cleavable linkers and protecting groups have been developed and applied for optogenetics (Figure 1-7b).[27–29]

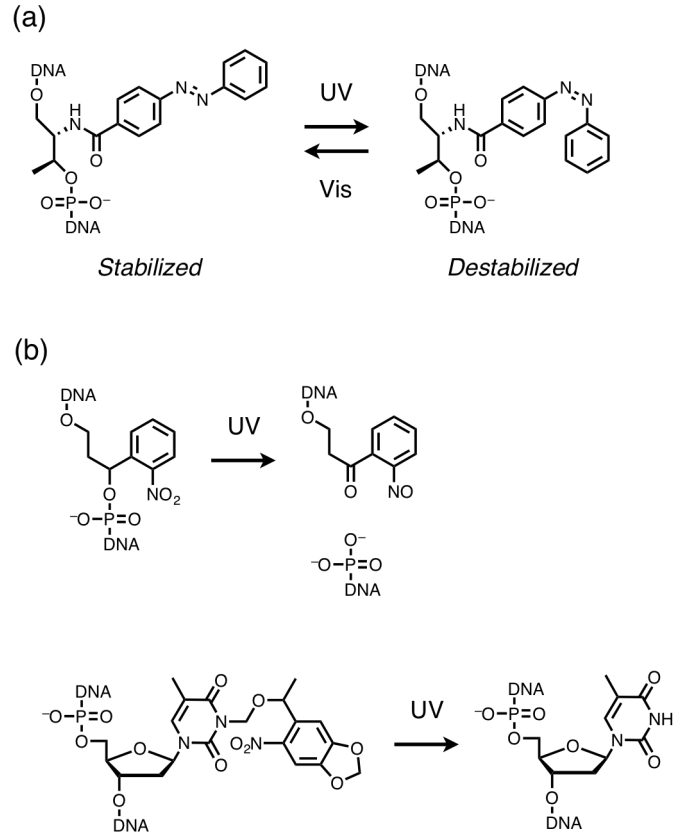

Figure 1-7. Photo-responsive artificial DNAs. (a) *Trans-cis* isomerization of Azobenzene moiety modified on DNA through the threoninol linker.[24] (b) DNA strands modified by photo-cleavable functionalities.[27,28]

Metal-responsive DNAs have been constructed by modification of metal ligands at the phosphodiester linkage and the sugar moiety of DNA strands. DNA duplexes modified by chelating ligands, that is, terpyridine (tpy) and/or diphenyl-phenanthroline (dpp), were thermally stabilized by the metal complexation (Figure 1-8a).[30] In addition, artificial DNA strands containing two tpy ligands were demonstrated to regulate DNA conformation and allosteric DNAzyme activity in response to first transition metal ions (Figure 1-8b).[31] The metal-mediated stabilization and metal-mediated structural conversion were also demonstrated for other higher-order structures such as 3-way junction (Figure 1-8c)[32,33] and quadruplex DNAs (Figure 1-8d)[34]. In addition, a number of metal complex-type DNAs have been developed by using ligand-bearing nucleobases, which

form metal-mediated base pairs instead of natural hydrogen-bonded base pairs.[35] Although details are mentioned in the next section, the metal-mediated base pairing confers the thermal stabilization,[35–37] DNA structural conversion,[38–40] and metal arrangement along the DNA helical scaffold[41–44].

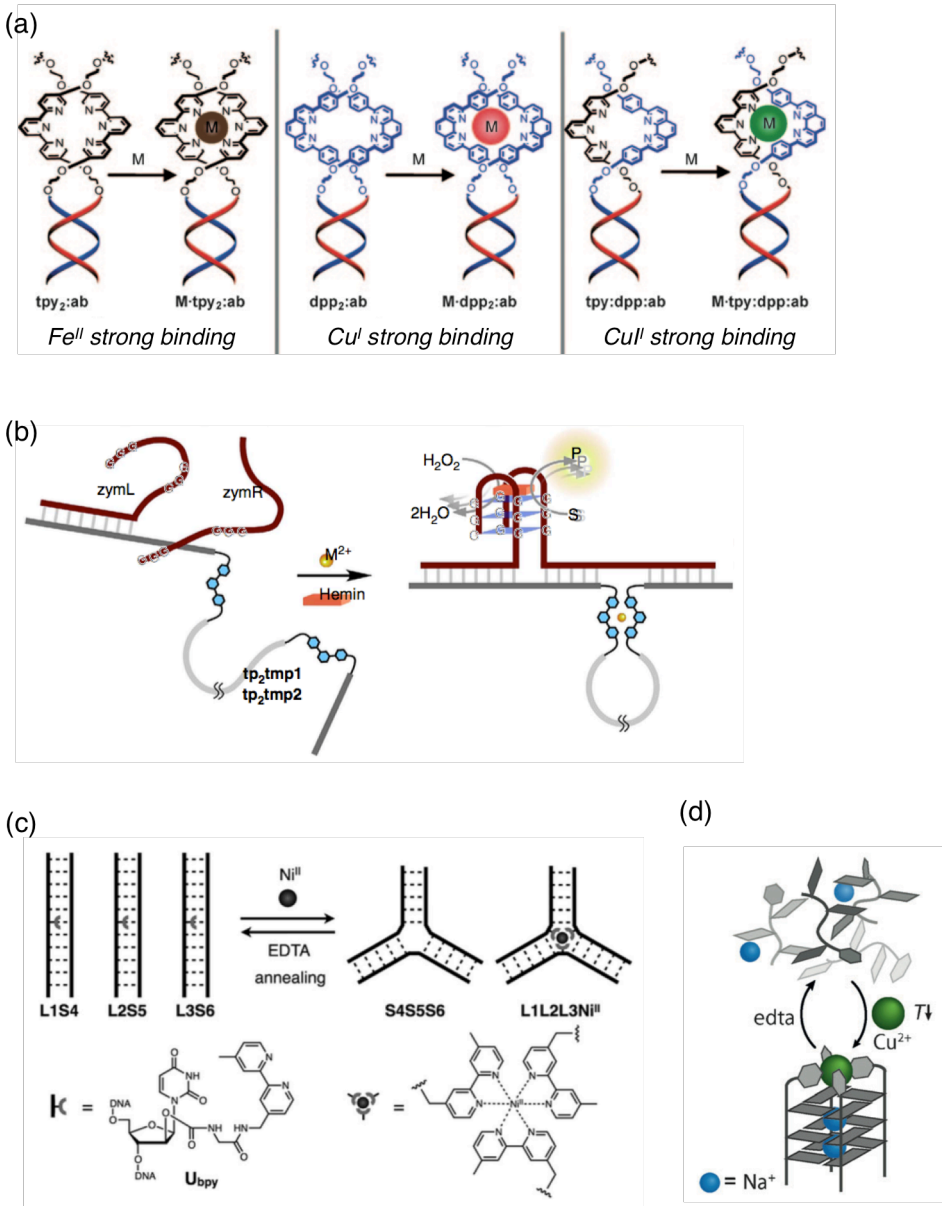

Figure 1-8. Metal-responsive artificial DNAs. (a) DNA duplexes modified by the terpyridine (tpy) and/or diphenyl-phenanthroline (dpp) ligands were stabilized by the specific metal ions. Reproduced from ref. [30]. Copyright 2009 Wiley-VCH. (b) Allosteric DNAzymes based on the tpy-modified artificial DNA strands. Reproduced from ref. [31]. Copyright 2015 Nature Publishing Group. (c) Stabilization and structural conversion of a DNA 3-way junction containing three bipyridine derivatives at the core. Reproduced from ref. [33]. Copyright 2016 The Royal Society of Chemistry. (d) A pyridine-modified G-quadruplex was reversibly stabilized by addition and removal of the transition metal ion. Reproduced from ref. [34]. Copyright 2013 Wiley-VCH.

1-3. Metal-mediated nucleobase pairing

Our group has firstly developed "artificial metallo-DNA" which includes unnatural metal-mediated base pairs instead of natural hydrogen-bonded base pairs (Figure 1-9a).[36,45] The metal-mediated base pair firstly reported consists of a 2:1 complex of ligand-type nucleobases with a metal ion. The formation of metal-mediated base pair normally stabilizes the resulting DNA duplexes in response to a specific metal ion (Figure 1-9b).[35–37] DNA secondary structures are also

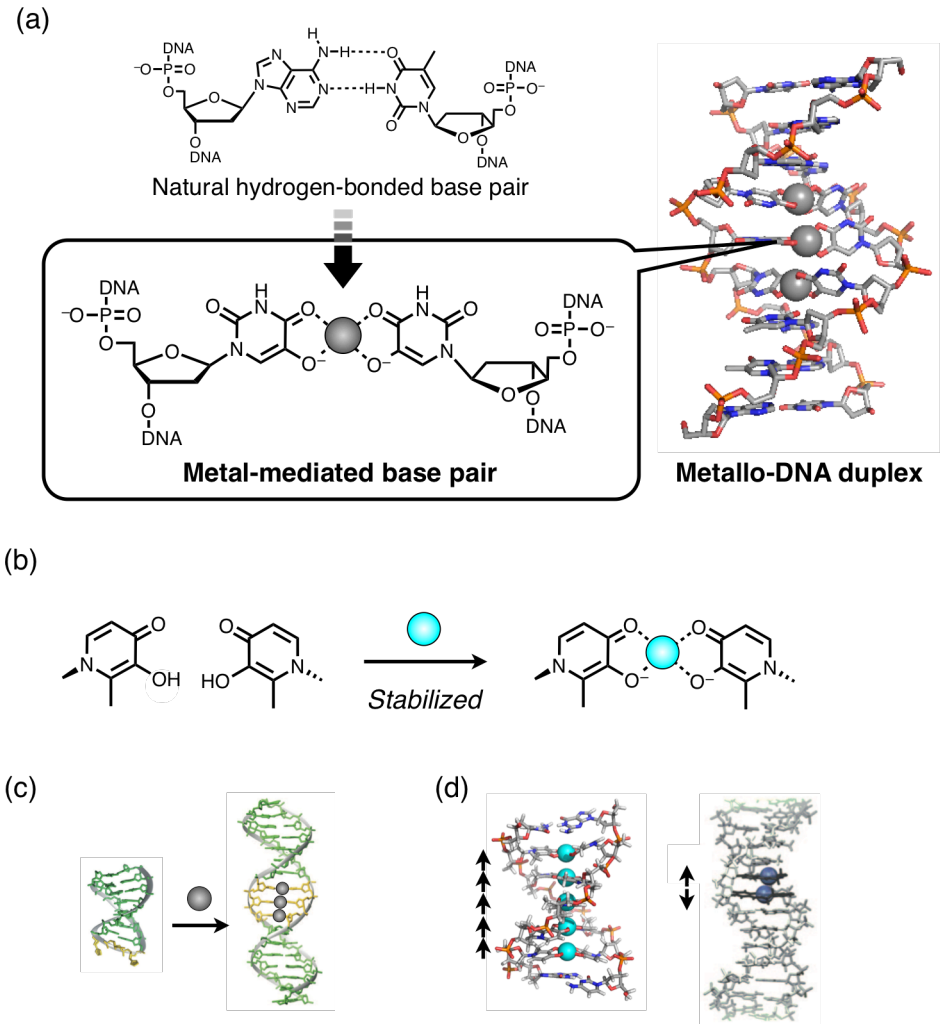

Figure 1-9. Artificial metallo-DNA duplexes. (a) Schematic representation of the metallo-DNA duplex containing the metal-mediated base pairs instead of the natural hydrogen-bonded base pairs. (b) The DNA duplexes are stabilized through the metal-mediated base pairing [e.g. **H**–Cu^{II}–**H** (**H** = hydroxypyridone-type nucleobase)].[36] (c) The metal-responsive structural conversion occurred with the formation of the Ag^{I}-mediated base pairs. Reproduced from ref. [40]. Copyright 2010 Nature Publishing Group. (d) The introduction of multiple metal-mediated base pairs confers metal arrangements and induces physical properties such as spin-spin interaction. Reproduced from refs. [41,44]. Copyright 2003 American Association for the Advancement of Science (left) and 2010 Wiley-VCH (right).

regulated by metal coordination (Figure 1-9c).[38–40] In addition, the introduction of multiple metal-mediated base pairs allows metal arrangement along the DNA helical scaffold to provide unique physical properties such as magnetic interaction (Figure 1-9d).[41–44] Thus, the development of metal-mediated base pairs has impacted wide fields such as nucleic acid chemistry, materials science, and biology.

As for natural DNA bases, thymine (**T**) and cytosine (**C**) are known to act as a monodentate metal ligand to form an Hg^{II}-[38,46–48] and Ag^{I}-mediated base pair[49], respectively (Figure 1-10). Since natural DNA strands can be easily synthesized by the chemical and enzymatic methods, the pyrimidine-based metallo-base pairs have been applied for many applications such as DNA-based nano-machines[50], metal sensors[51], and logic gates[52].

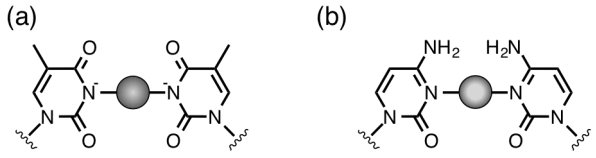

Figure 1-10. Chemical structures of the pyrimidine-based metal-mediated base pairs. (a) **T**–Hg^{II}–**T** base pair. (c) **C**–Ag^{I}–**C** base pair.

Many types of the fully artificial ligand-bearing nucleobases have been designed and synthesized, since our group has reported the first metal-mediated base pair with an *o*-phenylene diamine-type nucleobase in 1999.[45] Then, Schultz et al. reported a DNA duplex which includes a Ni^{II}-mediated base pair with a monodentate pyridine nucleobase and a tridentate pyridine-2,6-dicarboxylate-type nucleobase.[53] Our group further developed achieved more efficient duplex stabilization using **H**–Cu^{II}–**H** (**H** = hydroxypyridone-type nucleobase) base pairing (Figure 1-8b).[36] The metallo-DNA duplex containing Cu^{II}-mediated base pairs was thermally more stable than a natural duplex in which the metal-mediated base pair was replaced by an **A**–**T** base pair. In another systems, other metal ions such as Ag^{I} ion have been utilized for the metal-mediated base pairs based on the ligand designablity of the fully artificial ligand-bearing nucleobases.[39,40] Taken all together, the synthetic ligand-bearing nucleobases have expanded the chemical and physical functions of the metallo-DNA duplexes.

1-4. Bifacial nucleobases

The "bifacial" nucleobase has two recognition sites to bind to two different natural nucleobases simultaneously. Lehn firstly reported an artificial "bifacial" nucleobase which recognizes two different nucleobases at the orthogonal hydrogen donor/acceptor sites through hydrogen bonding.[54] MacLaughlin et al. demonstrated that peptide nucleic acid (PNA) oligomers possessing bifacial nucleobases selectively recognize matched/mismatched base pairs to form triple-stranded structures (Figure 1-11a).[55,56] Tor et al. synthesized other bifacial DNA bases that orthogonally form Watson–Crick-type base pairs with **T** and **A** nucleobases inside DNA duplexes (Figure 1-11b).[57] Based on the hybridized or switchable base-pairing behaviors, the bifacial nucleobases would allow us to construct gene sensors and supramolecular assembled structures.

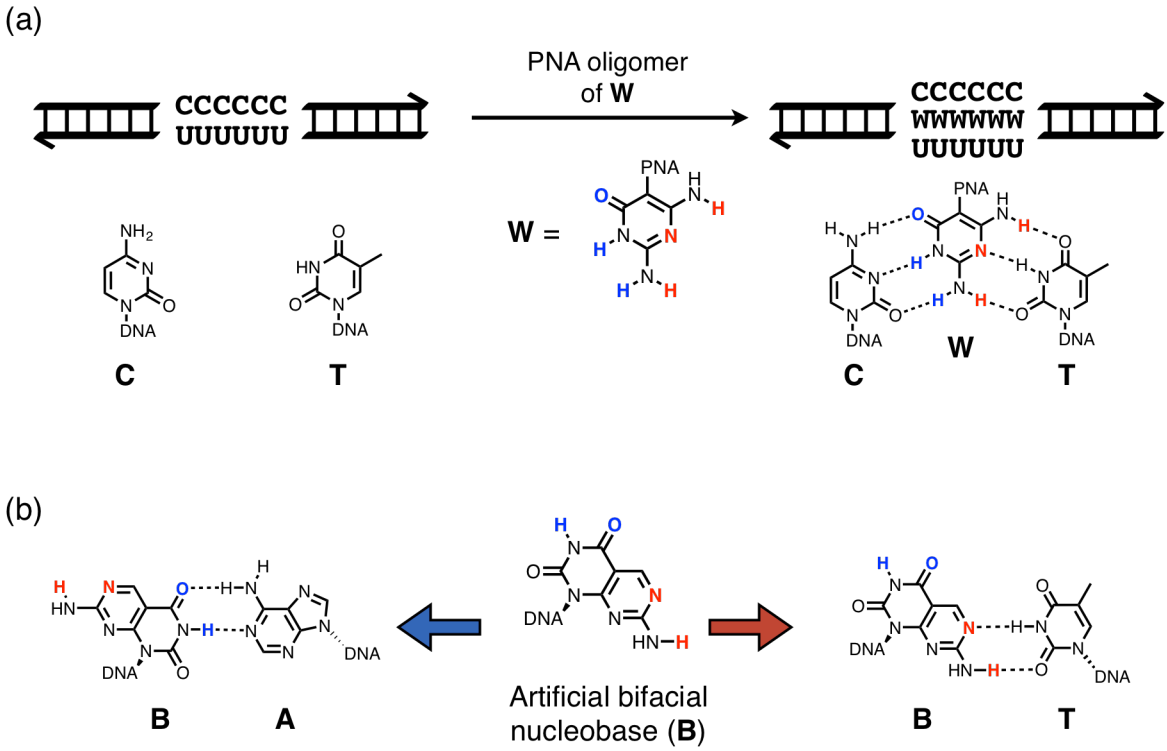

Figure 1-11. Schematic representation of bifacial nucleobase pairing. (a) A PNA oligomer with bifacial nucleobases (**W**) simultaneously forms two base pairs to form a triplex.[55] (b) A bifacial DNA base (**B**) separately forms two different base pairs with **A** and **T**.[57]

1-5. The aim of this study

Bifacial nucleobases, which have two recognition sites for two different nucleobases, are expected to separately form two different base pairs or simultaneously form two different base pairs to bridge two nucleobases. This unique pairing pattern can be applied to external stimuli-responsive molecular switching systems.

This study aimed to develop a "metal-responsive bifacial DNA base pairing" based on a 5-hydroxyuracil ($\mathbf{U}^{\mathbf{OH}}$) nucleobase. This nucleobase has both a hydrogen bonding site and a metal

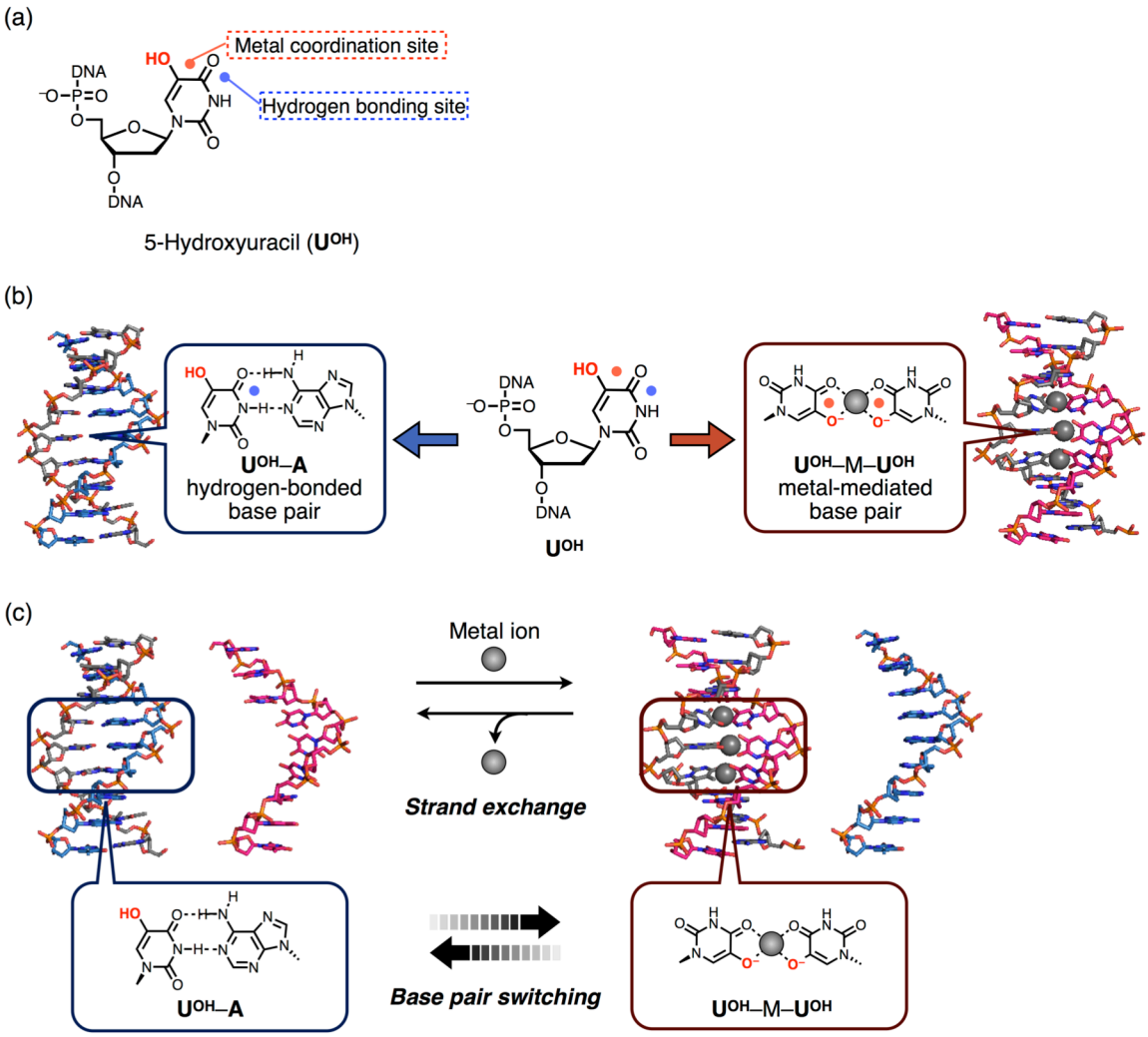

Figure 1-12. Schematic representation of a metal-responsive bifacial DNA base pairing of 5-hydroxyuracil ($\mathbf{U}^{\mathbf{OH}}$) nucleobases. (a) $\mathbf{U}^{\mathbf{OH}}$ nucleobase possesses both the hydrogen bonding and metal coordination sites. (b) $\mathbf{U}^{\mathbf{OH}}$ nucleobases may form both a hydrogen-bonded base pair ($\mathbf{U}^{\mathbf{OH}}$–**A**; **A** = adenine) and a metal-mediated base pair ($\mathbf{U}^{\mathbf{OH}}$–M–$\mathbf{U}^{\mathbf{OH}}$; M = metal ion). (c) Metal-responsive DNA strand exchange reactions through base pair switching of $\mathbf{U}^{\mathbf{OH}}$ nucleobase.

coordination site as difference faces (Figure 1-12a). Thus, $\mathbf{U^{OH}}$ nucleobases may form both a hydrogen-bonded base pair ($\mathbf{U^{OH}}$–**A**; **A** = adenine) and a metal-mediated base pair ($\mathbf{U^{OH}}$–M–$\mathbf{U^{OH}}$; M = metal ion) (Figure 1-12b). The metal complexation of $\mathbf{U^{OH}}$ nucleobases possibly alters the base pair preference inside DNA duplexes; the $\mathbf{U^{OH}}$–M–$\mathbf{U^{OH}}$ and $\mathbf{U^{OH}}$–**A** base pairs are selectively formed with and without metal ions, respectively. Such metal-responsive regulation of the base pair preference would contribute to the development of dynamic DNA strand exchange reactions which generate thermodynamically stable DNA duplexes (Figure 1-12c). In contrast to general DNA strand exchange/displacement reactions, the $\mathbf{U^{OH}}$-based strand exchange reactions can reversibly proceed without any additional DNA strands.

Chapter **2** describes the design and synthesis of novel metallo-DNA duplexes based on metal-mediated base pairing of 5-hydroxyuracil ($\mathbf{U^{OH}}$) designed as a metal-responsive bifacial nucleobase.

Chapter **3** discusses the control of DNA hybridization preference based on the metal-responsive bifacial base-pairing behaviors of $\mathbf{U^{OH}}$ nucleobases.

Chapter **4** demonstrates the reversible metal-responsive DNA strand exchange reactions by utilizing $\mathbf{U^{OH}}$ nucleobases.

Chapter **5** describes the metal-assisted regulation of the binding behaviors of triplex-forming oligonucleotides bearing $\mathbf{U^{OH}}$ nucleobases to target double-stranded DNAs.

1-6. References

[1] P. W. K. Rothemund, *Nature* **2006,** *440,* 297–302.

[2] J. Fu, M. Liu, Y. Liu, N. W. Woodbury, H. Yan, *J. Am. Chem. Soc.* **2012**, *134*, 5516−5519.

[3] E. Nakata, F. F. Liew, C. Uwatoko, S. Kiyonaka, Y. Mori, Y. Katsuda, M. Endo, H. Sugiyama, T. Morii, *Angew. Chem. Int. Ed.* **2012**, *51*, 2421–2424.

[4] A. Kuzyk, R. Schreiber, Z. Fan, G. Pardatscher, E.-M. Roller, A. Högele, F. C. Simmel, A. O. Govorov, T. Liedl, *Nature* **2012**, *483*, 311–314.

[5] B. Ding, Z. Deng, H. Yan, S. Cabrini, R. N. Zuckermann, J. Bokor, *J. Am. Chem. Soc.* **2010**, *132*, 3248−3249.

[6] A. M. Hung, C. M. Micheel, L. D. Bozano, L. W. Osterbur, G. M. Wallraff, J. N. Cha, *Nat. Nanotechnol.* **2010**, *5*, 121–126.

[7] J. Chen, N. C. Seeman, *Nature* **1991**, *350*, 631–633.

[8] N. C. Seeman, *Nature* **2003**, *421*, 427–431.

[9] R. P. Goodman, I. A. T. Schaap, C. F. Tardin, C. M. Erben, R. M. Berry, C. F. Schmidt, A. J. Turberfield, *Science* **2005**, *310*, 1661–1665.

[10] D. Bhatia, S. Arumugam, M. Nasilowski, H. Joshi, C Wunder, V. Chambon, V. Prakash, C. Grazon, B. Nadal, P. K. Maiti, L. Johannes, B. Dubertret, Y. Krishnan, *Nat. Nanotechnol.* **2016**, *11*, 1112–1119.

[11] C. M. Erben, R. P. Goodman, A. J. Turberfield, *Angew. Chem. Int. Ed.* **2006**, *118*, 7414–7417.

[12] R. Crawford, C. M. Erben, J. Periz, L. M. Hall, T. Brown, A. J. Turberfield, A. N. Kapanidis, *Angew. Chem. Int. Ed.* **2013**, *52*, 2284 –2288.

[13] D. Y. Zhang, G. Seelig, *Nat. Chem.* **2011**, 3, 103–113.

[14] G. Seelig, D. Soloveichik, D. Y. Zhang, E. Winfree, *Science* **2006**, *314*, 1585–1588.

[15] B. Yurke, A. J. Turberfield, A. P. Mills Jr., F. C. Simmel, J. L. Neumann, *Nature* **2000**,

406, 605–608.

[16] E. S. Andersen, M. Dong, M. M. Nielsen, K. Jahn, R. Subramani, W. Mamdouh, M. M. Golas, B. Sander, H. Stark, C. L. P. Oliveira, J. S. Pedersen, V. Birkedal, F. Besenbacher, K. V. Gothelf, J. Kjems, *Nature* **2009**, *459*, 73–76.

[17] L. J. Maher III, B. Word, P. B. Dervan, *Science* **1989**, *245*, 725–730.

[18] L. J. Maher III, *Biochemistry* **1992**, *31*, 7587–7594.

[19] A. Amodio, B. Zhao, A. Porchetta, A. Idili, M. Castronovo, C. Fan, F. Ricci, *J. Am. Chem. Soc.* **2014**, *136*, 16469–16472.

[20] E. Golub, R. Freeman, I. Willner, *Angew. Chem. Int. Ed.* **2011**, *50*, 11710–11714.

[21] T. Li, S. Dong, E. Wang, *Anal. Chem.* **2009**, *81,* 2144–2149.

[22] D.-M. Kong, L.-L. Cai, H.-X. Shen, *Analyst* **2010**, *135*, 1253–1258.

[23] T. Li, E. Wang, S. Dong, *Chem. Commun.* **2008**, 3654–3656.

[24] H. Asanuma, T. Takarada, T. Yoshida, D. Tamaru, X. Liang, M. Komiyama, *Angew. Chem. Int. Ed.* **2001**, *40*, 2671–2673.

[25] M. Liu, H. Asanuma, M. Komiyama, *J. Am. Chem. Soc.* **2006**, *128*, 1009–1015.

[26] X. Liang, H. Nishioka, N. Takenaka, H. Asanuma, *ChemBioChem* **2008**, *9*, 702–705.

[27] P. Ordoukhanian, J.-S. Taylor, *Bioconjugate Chem.* **2000**, *11*, 94−103.

[28] C. M. Connelly, R. Uprety, J. Hemphill, A. Deiters, *Mol. BioSyst.* **2012**, *8*, 2987–2993.

[29] J. Hemphill, Q. Liu, R. Uprety, S. Samanta, M. Tsang, R. L. Juliano, A. Deiters, *J. Am. Chem. Soc.* **2015**, *137*, 3656−3662.

[30] H. Yang, A. Z. Rys, C. K. McLaughlin, H. F. Sleiman, *Angew. Chem. Int. Ed.* **2009**, *48*, 9919–9923.

[31] T. Ihara, H. Ohura, C. Shirahama, T. Furuzono, H. Shimada, H. Matsuura, Y. Kitamura, *Nat. Commun.* **2015**, *6*, 6640.

[32] J.-L. H. A. Duprey, Y. Takezawa, M. Shionoya, *Angew. Chem. Int. Ed.* **2013**, *52*, 1212–1216.

[33] Y. Takezawa, S. Yoneda, J.-L. H. A. Duprey, T. Nakama, M. Shionoya, *Chem*. *Sci*. **2016**, *7*, 3006–3010.

[34] D. M. Engelhard, R. Pievo, G. H. Clever, *Angew*. *Chem*. *Int*. *Ed*. **2013**, *52*, 12843–12847.

[35] G. H. Clever, C. Kaul, T. Carell, *Angew*. *Chem*. *Int*. *Ed*. **2007**, *46*, 6226–6236.

[36] T. Tanaka, A. Tengeiji, T. Kato, N. Toyama, M. Shiro, M. Shionoya, *J*. *Am*. *Chem*. *Soc*. **2002**, *124*, 12494–12498.

[37] G. H. Clever, K. Polborn, T. Carell, *Angew*. *Chem*. *Int*. *Ed*. **2005**, *44*, 7204–7208.

[38] Z. Kuklenyik, L. G. Marzilli, *Inorg*. *Chem*. **1996**, *35*, 5654–5662.

[39] D. Böhme, N. Düpre, D. A. Megger, J Müller, *Inorg*. *Chem*. **2007**, *46*, 10114–10119.

[40] S. Johannsen, N. Megger, D. Böhme, R. K. O. Sigel, J. Müller, *Nat*. *Chem*. **2010**, *2*, 229–234.

[41] K. Tanaka, A. Tengeiji, T. Kato, N. Toyama, M. Shionoya, *Science* **2003**, *299*, 1212–1213.

[42] K. Tanaka, G. H. Clever, Y. Takezawa, Y. Yamada, C. Kaul, M. Shionoya, T. Carell, *Nat*. *Nanotechnol*. **2006**, *1*, 190–194.

[43] G. H. Clever, T. Carell, *Angew*. *Chem*. *Int*. *Ed*. **2007**, *46*, 250–253.

[44] G. H. Clever, S. J. Reitmeier, T. Carell, O. Schiemann, *Angew*. *Chem*. *Int*. *Ed*. **2010**, *122*, 5047–5049.

[45] K. Tanaka, M. Shionoya, *J. Org. Chem.* **1999,** *64,* 5002–5003.

[46] S. Katz, *Biochim*. *Biophys*. *Acta* **1963**, *68*, 240–253.

[47] Y. Miyake, H. Togashi, M. Tashiro, H. Yamaguchi, S. Oda, M. Kudo, Y. Tanaka, Y. Kondo, R. Sawa, T. Fujimoto, T. Machinami, A. Ono, *J*. *Am*. *Chem*. *Soc*. **2006**, *128*, 2172–2173.

[48] J. Kondo, T. Yamada, C. Hirose, I. Okamoto, Y. Tanaka, A. Ono, *Angew*. *Chem*. *Int*. *Ed*. **2014**, *53*, 2385–2388.

[49] A. Ono, S. Cao, H. Togashi, M. Tashiro, T. Fujimoto, T. Machinami, S. Oda, Y. Miyake, I. Okamoto, Y. Tanaka, *Chem*. *Commun*. **2008**, *44*, 4825–4827.

[50] J. M. Thomas, H.-Z. Yu, D. Sen, *J. Am. Chem. Soc.* **2012**, *134*, 13738–13748.

[51] J. Liu, Y. Lu, *Angew*. *Chem*. *Int*. *Ed*. **2007**, *46*, 7587–7590.

[52] N. Kanayama, T. Takarada, M. Fujita, M. Maeda, *Chem*. *Eur*. *J*. **2013**, *19*, 10794–10798.

[53] E. Meggers, P. L. Holland, W. B. Tolman, F. E. Romesberg, P. G. Schultz, *J. Am. Chem. Soc.* **2000**, *122*, 10714–10715.

[54] N. Branda, G. Kurz, J.-M. Lehn, *Chem*. *Commun*. **1996**, *32*, 2443–2444.

[55] D. L. Chen, M. Meena, S. K. Sharma, L. W. McLaughlin, *J. Am. Chem. Soc*. **2004**, *126*, 70–71.

[56] H. Chen, M. Meena, L. W. McLaughlin, *J. Am. Chem. Soc*. **2008**, *130*, 13190–13191.

[57] D. Shin, Y. Tor, *J. Am. Chem. Soc*. **2011**, *133*, 6926–6929.

Chapter 2.

Metal-mediated DNA base pairing of 5-hydroxyuracil nucleobases

2-1. Introduction

As shown in the section **1-3**, a metal-mediated base pair consists of two ligand-bearing nucleobases and a metal ion. This artificial base pairing stabilizes the resulting DNA duplex in response to a specific metal ion.[1–6] The metal-responsive base-pairing behavior possibly leads to changes in DNA secondary structures.[7-9] Moreover, introduction of multiple metal-mediated base pairs conferred metal arrays inside DNA helical scaffolds in a way that the number and the sequence of the metal ions can be controlled.[10-13] The precise metal assemblies caused spin-spin interactions between their *d*-electrons.[10,13] These metal-related DNA functions would contribute to the construction of DNA-based nanomaterials.

In this work, a 5-modified uracil was designed as a new class of ligand-modified nucleobases (Figure 2-1). The functionality at the 5 position and the carbonyl group at the 4-position were expected to serve as a bidentate metal ligand (Figure 2-1a). By changing the substituent at the 5-position, the affinity of the ligand-bearing nucleobase for metal ions would be altered based on the hard-soft acid-base (HSAB) theory (Figure 2-1b). This modulable design would encourage us to utilize many types of metal ions to construct metal-mediated base pairs. Compared with the fully artificial ligand-bearing nucleosides, these 5-modified uracil nucleosides can be readily synthesized

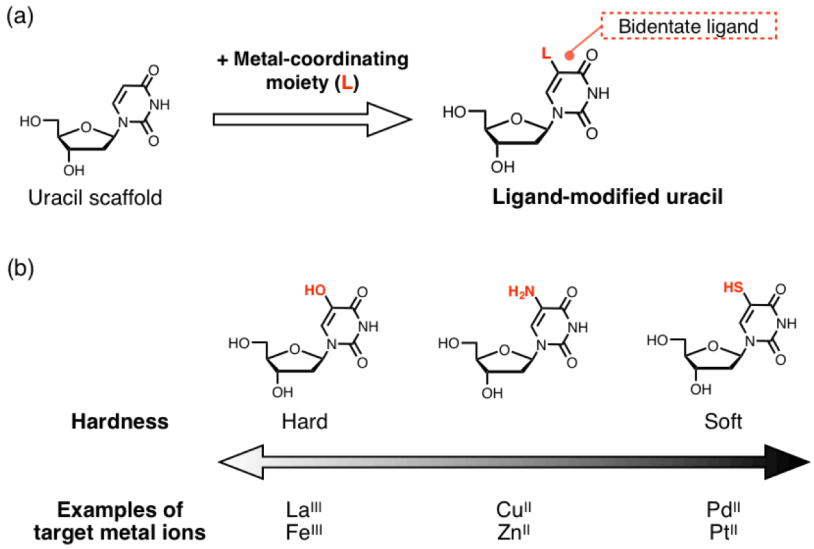

Figure 2-1. Chemical structures of 5-modified ligand-bearing nucleobases. (a) The carbonyl group at the 4-position and the 5-substituent (e.g. hydroxyl group) can serve as a bidentate metal ligand. (b) Expected metal binding affinity of the 5-modified ligand-bearing nucleobases.

from commercially available uracil deoxynucleoside derivatives.[14–16]

As a first step, I chose 5-hydroxyuracil ($\mathbf{U}^{\mathbf{OH}}$) as a ligand-bearing nucleobase (Figure 2-2a). The $\mathbf{U}^{\mathbf{OH}}$ nucleobase possesses a hard *O*,*O*-bidentate donor, which is suitable to coordinate hard metal ions. Homogeneous base pairing of $\mathbf{U}^{\mathbf{OH}}$ nucleobases was expected to form a metal-mediated base pair ($\mathbf{U}^{\mathbf{OH}}$–M–$\mathbf{U}^{\mathbf{OH}}$; M = metal ion) inside DNA duplexes (Figure 2-2b). In this section, I describe the development of the metal-mediated base pairs of $\mathbf{U}^{\mathbf{OH}}$ nucleobases with relatively hard metal ions; the first transition metal ions including Zn^{II} and rare-earth metal ions. In addition, metal alignment is possible by incorporation of multiple $\mathbf{U}^{\mathbf{OH}}$–M–$\mathbf{U}^{\mathbf{OH}}$ base pairs into a DNA duplex (Figure 2-2c).

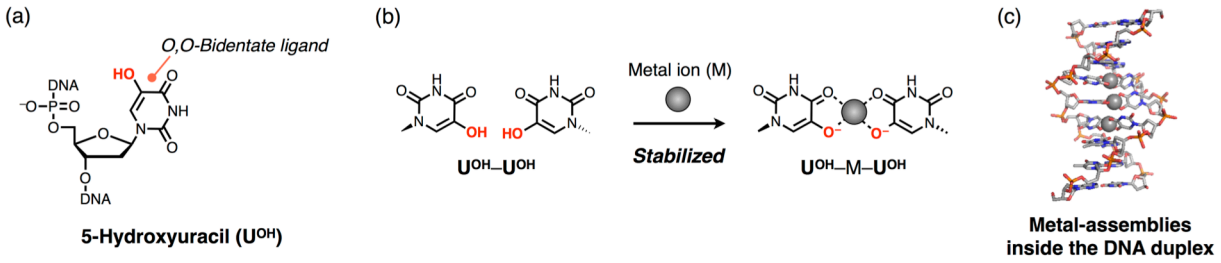

Figure 2-2. 5-Hydroxyuracil ($\mathbf{U}^{\mathbf{OH}}$) as a novel ligand-bearing nucleobase to achieve the thermal stabilization and the assemblies of metal ions. (a) Chemical structure of $\mathbf{U}^{\mathbf{OH}}$ nucleobase inside a DNA strand. (b) Metal-responsive thermal stabilization of DNA duplexes through metal-mediated base pairing ($\mathbf{U}^{\mathbf{OH}}$–M–$\mathbf{U}^{\mathbf{OH}}$; M = metal ion). (c) Metal assembly inside DNA duplexes through the incorporation of the multiple metal-mediated base pairs.

2-2. Design and synthesis of DNA duplexes containing homogeneous base pairs of 5-hydroxyuracil nucleobases

I designed and synthesized DNA strands containing $\mathbf{U}^{\mathbf{OH}}$ nucleobases. According to the literatures,[16,17] a phosphoramidite derivative of the $\mathbf{U}^{\mathbf{OH}}$ nucleoside, which is utilized for the solid-phase DNA synthesis, was synthesized by only 4 steps from 2′-deoxyuridine (Scheme 2-1). Using the $\mathbf{U}^{\mathbf{OH}}$ monomer, DNA strands **1**–**4** were synthesized by an automated DNA synthesizer (Table 2-1). Each coupling yield of $\mathbf{U}^{\mathbf{OH}}$ monomers was over 99%, which was comparable to that of natural nucleosides. DNA strands **1** and **2** form a double-stranded DNA **1·2** including three $\mathbf{U}^{\mathbf{OH}}$–$\mathbf{U}^{\mathbf{OH}}$ base pairs. Because the two $\mathbf{U}^{\mathbf{OH}}$ nucleobases face each other within a DNA duplex, it was expected that one appropriate metal ion can bind to the $\mathbf{U}^{\mathbf{OH}}$ nucleobases to form a metal-mediated $\mathbf{U}^{\mathbf{OH}}$–M–$\mathbf{U}^{\mathbf{OH}}$ base pair. In other words, the DNA duplex **1·2** would form a metallo-DNA structure containing three $\mathbf{U}^{\mathbf{OH}}$–M–$\mathbf{U}^{\mathbf{OH}}$ base pairs. The other strands **3** and **4** also form a duplex **3·4**, which were used for NMR analysis. A natural DNA duplex **1T·2T**, in which three $\mathbf{U}^{\mathbf{OH}}$ nucleobases were replaced by the canonical thymine (**T**) nucleobases, was also prepared for control experiments.

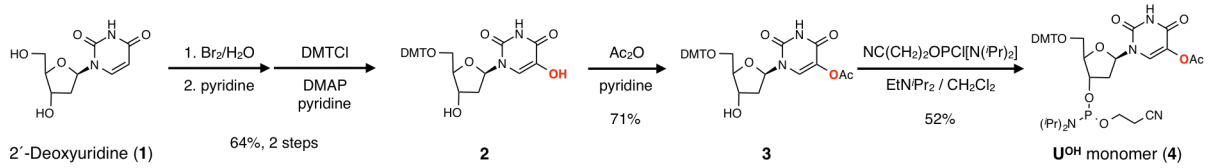

Scheme 2-1. Synthetic route of a $\mathbf{U}^{\mathbf{OH}}$ monomer for the solid-phase DNA synthesis.[16,17]

Table 2-1. Sequences of DNA strands used in this section.

Name	Sequence (5′ to 3′)
1	CAC ATT $\mathbf{U}^{\mathbf{OH}}\mathbf{U}^{\mathbf{OH}}\mathbf{U}^{\mathbf{OH}}$ GTT GTA
2	TAC AAC $\mathbf{U}^{\mathbf{OH}}\mathbf{U}^{\mathbf{OH}}\mathbf{U}^{\mathbf{OH}}$ AAT GTG
1T	CAC ATT **TTT** GTT GTA
2T	TAC AAC **TTT** AAT GTG
3 (for NMR)	GCT AGT $\mathbf{U}^{\mathbf{OH}}\mathbf{U}^{\mathbf{OH}}\mathbf{U}^{\mathbf{OH}}$ GAG TCC
4 (for NMR)	GGA CTC $\mathbf{U}^{\mathbf{OH}}\mathbf{U}^{\mathbf{OH}}\mathbf{U}^{\mathbf{OH}}$ ACT AGC

2-3. Duplex stabilization based on the metal-mediated base pairing of 5-hydroxyuracil nucleobases

To develop the metal-mediated base pairs of $\mathbf{U}^{\mathbf{OH}}$ nucleobases, I investigated complexation with various kinds of metal ions shown in Figure 2-3. Based on the hard-soft acid-base (HSAB) theory, the $\mathbf{U}^{\mathbf{OH}}$ nucleobase tends to favorably interact with relatively hard metal ions; the first transition ions, Zn^{II} and rare-earth metal ions.

3	4	5	6	7	8	9	10	11	12
Sc^{III}	Ti	V	Cr	**Mn^{II}**	**Fe^{II}**	**Co^{II}**	**Ni^{II}**	**Cu^{II}**	**Zn^{II}**
Y^{III}	Zr	Nb	Mo	Tc	Ru	Rh	Pd	Ag	Cd
★	Hf	Ta	W	Re	Os	Ir	Pt	Au	Hg

★	**La^{III}**	**Ce^{III}**	**Pr^{III}**	**Nd^{III}**	Pm	**Sm^{III}**	**Eu^{III}**	**Gd^{III}**	**Tb^{III}**	**Dy^{III}**	**Ho^{III}**	**Er^{III}**	**Tm^{III}**	**Yb^{III}**	**Lu^{III}**

Figure 2-3. Transition metal ions, group 12 elements, and lanthanide metal ions. 22 kinds of metal ions examined in this study are described in bold style.

To find suitable metal ions for the metal-mediated base pairing of $\mathbf{U}^{\mathbf{OH}}$ nucleobases, duplex melting experiments were carried out. The thermal stability of DNA duplex **1·2** containing three $\mathbf{U}^{\mathbf{OH}}$–$\mathbf{U}^{\mathbf{OH}}$ base pairs was evaluated in the absence or in the presence of metal ions. In general, the formation of metal-mediated base pairs enhances the thermal stability of DNA duplexes because two strands are additionally crosslinked through metal coordination bonding. Figure 2-4 shows the melting curves of DNA duplex **1·2** in the absence or in the presence of the metal ions. The increase in the UV absorption with increasing temperatures is due to the dissociation of double-stranded DNA into single strands. The inflection point of the sigmoidal curve is defined as the melting temperature (T_m) of a DNA duplex. When a DNA duplex is thermally stabilized, its melting curve is shifted to the right side and the T_m value is increased. In the presence of most of the transition metal ions (Mn^{II}–Cu^{II}) and Ce^{III} ions, no stabilization of duplex **1·2** was observed. In contrast, upon addition of Zn^{II} or rare-earth metal ions (Y^{III}, Gd^{III}, Tb^{III} etc.) except for Ce^{III} ion, their melting curves were shifted to the right side compared to the curve in the absence of metal ions (Figure 2-4).

The observed stabilization effects strongly suggested that the metal-mediated base pairs, $\mathbf{U}^{\mathbf{OH}}$–M–$\mathbf{U}^{\mathbf{OH}}$ (M = Zn^{II}, rare-earth metal ions), were formed inside the DNA duplex.

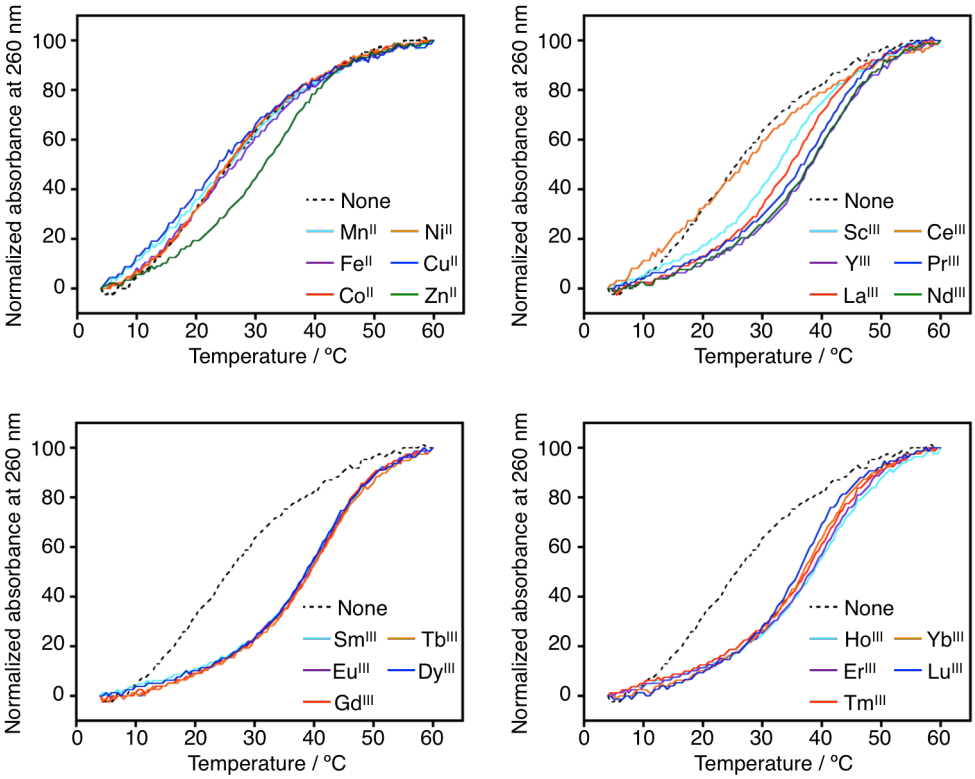

Figure 2-4. Melting curves of DNA duplex **1·2**, containing three $\mathbf{U}^{\mathbf{OH}}$–$\mathbf{U}^{\mathbf{OH}}$ base pairs, in the absence and in the presence of various metal ions. [duplex] = 2 μM, [metal ion]/[duplex] = 0 (dashed lines), 3 (solid lines) in 10 mM HEPES-NaOH buffer (pH 8.0), 100 mM NaCl, 0.2 °C/min.

The difference in the stabilization effect of metal ions may be mainly explained by two factors, that is, Lewis acidity and redox activity. The $\mathbf{U}^{\mathbf{OH}}$ nucleobase is a "hard" metal ligand according to the HSAB theory. Lanthanide ions are generally harder than divalent first transition metals.[18] Thus, the affinity of lanthanide ions to $\mathbf{U}^{\mathbf{OH}}$ nucleobase is possibly higher than the other metal ions. In addition, Cu^{II} and Ce^{III} ions with high redox activity did not show significant stabilization effects. The redox active metal ions often decompose $\mathbf{U}^{\mathbf{OH}}$ nucleobases in a manner similar to naturally occurring pyrimidine oxidation.[19,20]

Considering that typical lanthanide complexes have high coordination numbers such as 8 and 9, other ligands such as water molecules and neighboring nucleobases were likely to coordinate to the lanthanide ions of the $\mathbf{U}^{\mathbf{OH}}$–M–$\mathbf{U}^{\mathbf{OH}}$ base pairs.

In general, metal complexes of smaller lanthanide ions show relatively higher stability constants.[21] The T_m values of duplex **1·2** with or without 3 equivalents of Y^{III} and lanthanide ions as well as their ionic radii are summarized in Table 2-2. The stabilization effects of medium sized Nd^{III}–Ho^{III} and Y^{III} ions were higher than those of larger La^{III}–Pr^{III} ions and those of smaller Er^{III}–Lu^{III} ions. This relationship can be partially explained by the pK_a values of water molecules bound to lanthanide ions, in which a negatively charged hydroxide ion shows a larger affinity to lanthanide ions than a neutral water molecule. That is, smaller lanthanide ions show lower pK_a values. As the melting experiments were carried out at pH 8.0 near the pK_a values of the bound water molecules (ca. 8–9), in the case of the smaller lanthanide ions, the concentration of the bound hydroxide ions is increased and consequently the hydroxide ions significantly compete with deprotonated $\mathbf{U^{OH}}$ nucleobases in the metal complexation process. This reduces the apparent binding affinity at pH 8.0 of deprotonated $\mathbf{U^{OH}}$ nucleobase to the smaller lanthanide ions.

Table 2-2. Melting temperatures (T_m) of DNA duplex **1·2** and chemical properties of lanthanide ions.

Sample	T_m / °C[a]	Ionic radius / Å[b]	pK_a[c]
Metal-free	22.8 ± 0.9	–	–
La^{III}	39.2 ± 0.3	1.03	9.33
Pr^{III}	38.7 ± 0.4	0.990	8.82
Nd^{III}	39.6 ± 0.0	0.983	8.70
Sm^{III}	42.8 ± 1.2	0.958	8.61
Eu^{III}	41.1 ± 1.8	0.947	8.59
Gd^{III}	41.1 ± 1.2	0.938	8.62
Tb^{III}	41.2 ± 2.3	0.923	8.43
Dy^{III}	40.3 ± 1.6	0.912	8.37
Ho^{III}	43.1 ± 1.8	0.901	8.31
Y^{III}	40.5 ± 1.0	0.900	8.61
Er^{III}	40.2 ± 1.5	0.890	8.26
Tm^{III}	40.9 ± 0.6	0.880	8.19
Yb^{III}	40.0 ± 0.8	0.868	8.19
Lu^{III}	36.8 ± 0.6	0.861	8.17

[a]Melting temperatures (T_m) were determined as the temperature at the inflection point of melting curves, and average of at least 2 runs with standard deviation was shown. [b]Effective ionic radii of lanthanide ions when the coordination number is assumed to be 6.[22] [c]pK_a values of water molecules bound to lanthanide ions.[18,23]

The melting curves of duplex **1·2** in the presence of Zn^{II} and lanthanide ions showed a wider step than those of natural duplexes. In general, a metal coordination bond is thermodynamically more stable than a hydrogen bond. Thus, the terminal hydrogen-bonded base pairs within the metallo-DNA duplex should be firstly dissociated because the central metal complexes serve as the foundation to strongly maintain the hybridized structure. In other words, as all the base pairs were not simultaneously dissociated, the melting curves showed the slow transition.

Control experiments were also conducted with a natural DNA duplex **1T·2T**, in which all the $\mathbf{U^{OH}}$–$\mathbf{U^{OH}}$ base pairs were replaced by mismatched thymine–thymine (**T**–**T**) base pairs. **T** nucleobase has the same chemical structure as $\mathbf{U^{OH}}$ nucleobase except the functionality at the 5 position (Figure 2-5). The melting curve of duplex **1T·2T** was hardly changed upon addition of any metal ions (Figure 2-6). These results suggest that the metal-mediated stabilization was induced by metal coordination of $\mathbf{U^{OH}}$ nucleobases.

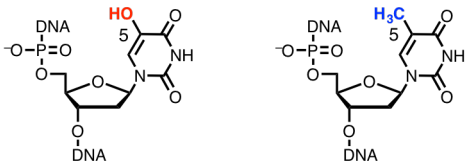

5-Hydroxyuracil (U^{OH}) **Thymine (T)**

Figure 2-5. Chemical structures of 5-hydroxyuracil ($\mathbf{U^{OH}}$) and thymine (**T**).

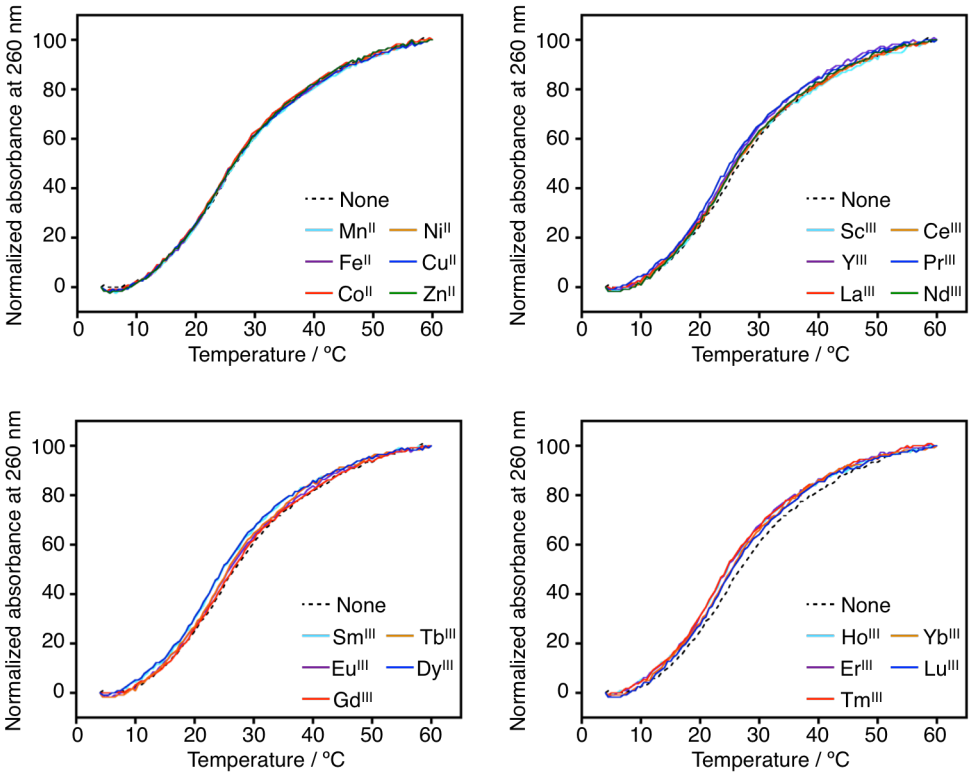

Figure 2-6. Melting curves of DNA duplex **1T·2T**, containing three **T–T** base pairs, in the absence and in the presence of various metal ions. [duplex] = 2 μM, [metal salt]/[duplex] = 0 (dashed lines), 3 (solid lines) in 10 mM HEPES-NaOH buffer (pH 8.0), 100 mM NaCl, 0.2 °C/min.

2-4. Quantitative metal assemblies templated by DNA duplexes containing 5-hydroxyuracils

Next, I estimated the stoichiometry of metal complexation and the structure of the metal complex of DNA duplex **1·2**. As the DNA duplex **1·2** contains three consecutive $\mathbf{U^{OH}}$–$\mathbf{U^{OH}}$ base pairs, it was expected that three metal-mediated base pairs ($\mathbf{U^{OH}}$–M–$\mathbf{U^{OH}}$; M = Zn^{II}, Y^{III}, Gd^{III} etc.) were formed inside the duplex structure. In other words, three metal ions are likely to be assembled within the DNA helical scaffold. The results shown in the section **2-3** suggested that three $\mathbf{U^{OH}}$–M–$\mathbf{U^{OH}}$ base pairs were formed inside the DNA duplex **1·2**.

In this section, the stoichiometry of the metal complexation with the DNA duplex **1·2** was investigated by melting analysis, UV absorption-based titration experiment, and electrospray ionization time-of-flight (ESI-TOF) mass spectrometry. As the Gd^{III} complex of duplex **1·2** is one of the most thermally stable complexes, Gd^{III} ion was chosen as a representative.

Figure 2-7 shows the melting curves of DNA duplex **1·2** in the absence or in the presence of various amounts of Gd^{III} ions. The melting curve was gradually shifted to the right side with increasing amounts of Gd^{III} ions. The largest thermal stabilization was observed when 3 equivalents of Gd^{III} ions were added against the duplex. This stoichiometry suggests that three $\mathbf{U^{OH}}$–Gd^{III}–$\mathbf{U^{OH}}$ base pairs were quantitatively formed within the DNA duplex **1·2**.

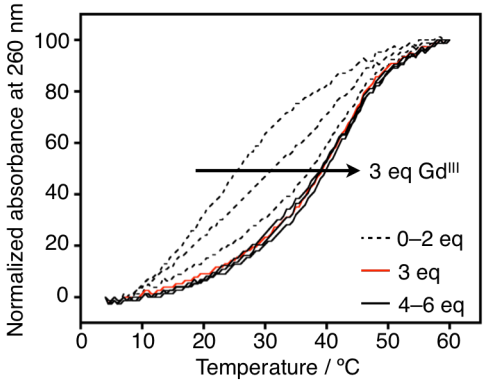

Figure 2-7. Melting curves of DNA duplex **1·2** in the presence of various amounts of Gd^{III} ions. [duplex] = 2 μM, [$GdCl_3$]/[duplex] = 0, 1, 2 (black, dashed lines), 3 (red, solid line), 4, 5, 6 (black, solid lines) in 10 mM HEPES-NaOH buffer (pH 8.0), 100 mM NaCl, 0.2 °C/min.

To investigate the metal complexation behaviors in more detail, UV absorption-based titration (Figure 2-8a, b) and Job's plot analysis (Figure 2-9) were carried out. In the titration experiment, a UV absorption band newly appeared around 310 nm, which is derived from the deprotonation of the 5-OH groups of the $\mathbf{U^{OH}}$ nucleobases with the metal coordination (Figure 2-8c).[24] These spectra varied linearly until 3 equivalents of Gd^{III} ions were added (Figure 2-8b). Job's plot (Figure 2-9) showed an inflection point at $[Gd^{III}]/([\text{duplex } \mathbf{1{\cdot}2}] + [Gd^{III}]) = 0.75$, that is, $[\text{duplex } \mathbf{1{\cdot}2}]/[Gd^{III}] = 1{:}3$. Both results strongly suggest that three Gd^{III} ions quantitatively bound to the DNA duplex **1·2** to form a trinuclear Gd^{III} complex $\mathbf{1{\cdot}2{\cdot}Gd^{III}_3}$.

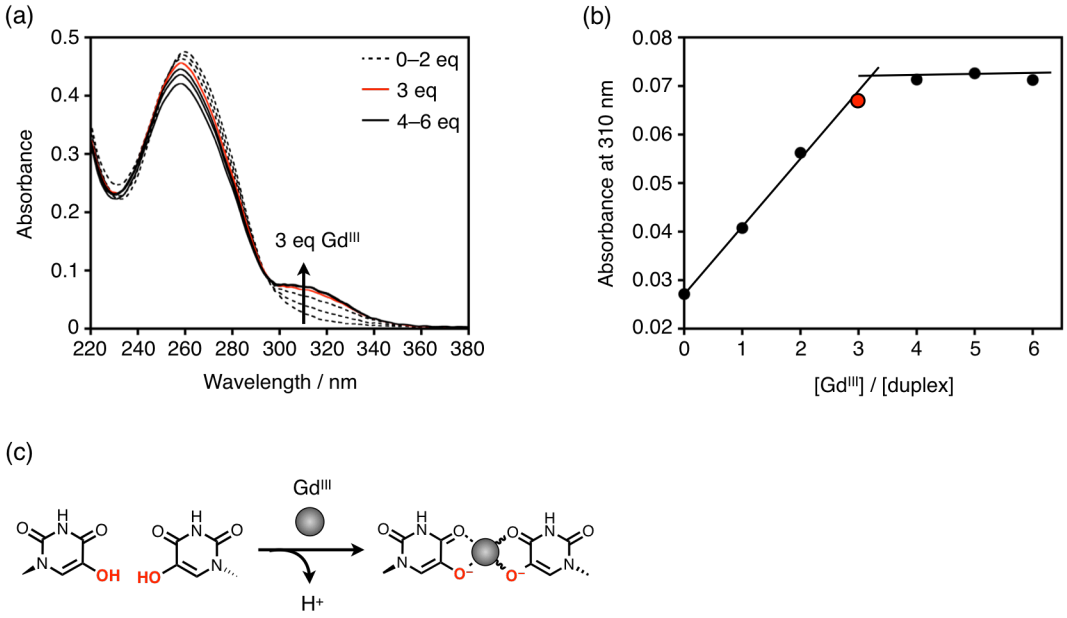

Figure 2-8. UV absorption spectra of DNA duplex **1·2** in the presence of various amounts of Gd^{III} ions. (a, b) [Duplex **1·2**] = 2 μM, $[GdCl_3]$/[Duplex **1·2**] = 0, 1, 2 (black, dashed lines), 3 (red, solid line), 4, 5, 6 (black, solid lines) in 10 mM HEPES-NaOH buffer (pH 8.0), 100 mM NaCl, *l* = 1.0 cm, 5 °C. (c) Schematic representation of the deprotonation process accompanied with the Gd^{III} complexation of $\mathbf{U^{OH}}$ nucleobases.

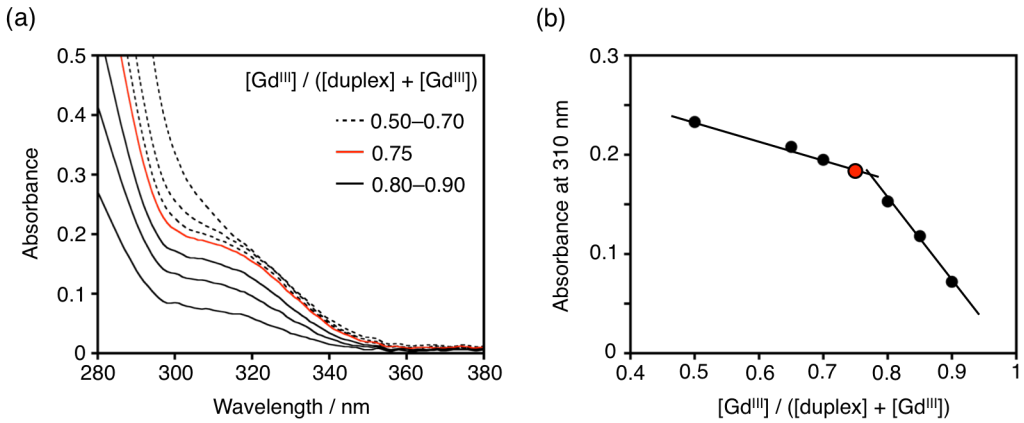

Figure 2-9. Job's plot analysis based on UV absorption spectra for the complexation of DNA duplex **1·2** with Gd^{III} ions. [Duplex **1·2**] + [$GdCl_3$] = 200 μM, [$GdCl_3$]/([Duplex **1·2**] + [$GdCl_3$]) = 0.50, 0.65, 0.70 (black, dashed lines), 0.75 (red, solid line), 0.80, 0.85, 0.90 (black, solid lines) in 10 mM HEPES-NaOH buffer (pH 8.0), 100 mM NaCl, *l* = 0.1 cm, rt.

Control experiments were also conducted by using a natural DNA duplex **1T·2T**, in which all $\mathbf{U}^{\mathbf{OH}}$–$\mathbf{U}^{\mathbf{OH}}$ base pairs were replaced by mismatched thymine–thymine (**T**–**T**) base pairs. The UV absorption of duplex **1T·2T** was hardly changed upon addition of Gd^{III} ions (Figure 2-10). This result suggests that the spectral changes of the $\mathbf{U}^{\mathbf{OH}}$-containing DNA duplex resulted from the binding of deprotonated $\mathbf{U}^{\mathbf{OH}}$ nucleobase to Gd^{III} ions.

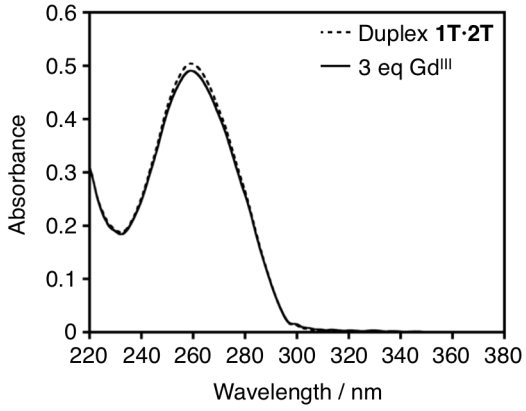

Figure 2-10. UV absorption spectra of DNA duplex **1T·2T** in the absence and in the presence of 3 equivalents of Gd^{III} ions. [duplex] = 2 μM, [$GdCl_3$]/[duplex] = 0 (dashed line), 3 (solid line) in 10 mM HEPES-NaOH buffer (pH 8.0), 100 mM NaCl, *l* = 1.0 cm, 5 °C.

Furthermore, ESI-TOF mass analysis was carried out to confirm the formation of the trinuclear Gd^{III} complex with duplex **1·2** (**1·2·Gd$^{III}_3$**) (Figure 2-11). The main peak was assigned to the trinuclear Gd^{III} complex **1·2·Gd$^{III}_3$** (found: 1368.77 (z = 7); calcd for [**1·2** + 3Gd –16H]$^{7-}$: 1368.73). This result indicates that three **U^{OH}**–Gd^{III}–**U^{OH}** base pairs were formed inside the DNA duplex **1·2**.

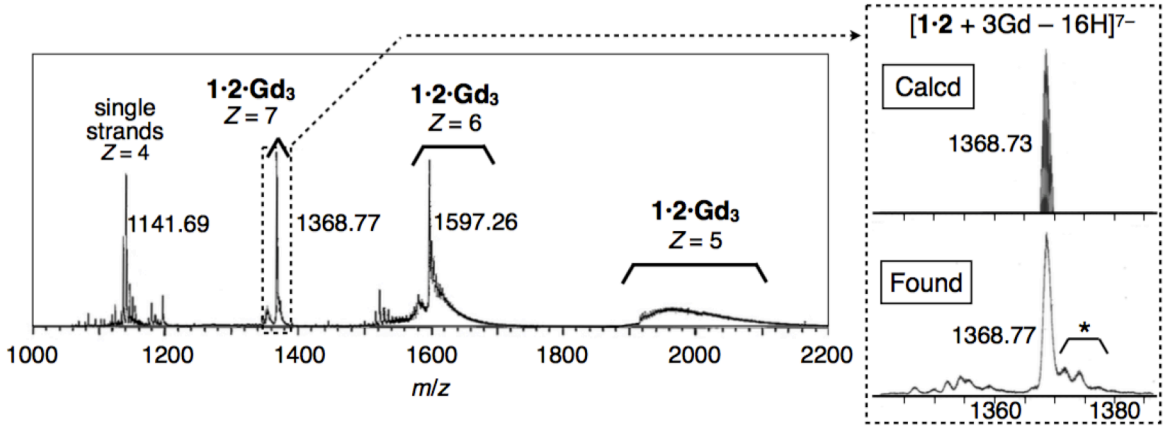

Figure 2-11. An ESI-TOF mass spectrum of DNA duplex **1·2** with 3 equivalents of Gd^{III} ions. M (**1·2·Gd$^{III}_3$**) = $C_{290}H_{355}N_{100}O_{188}P_{28}Gd_3$. [duplex] = 20 μM, [$GdCl_3$]/[duplex] = 3 in 20 mM NH_4OAc aqueous solution (pH 8.0). Negative mode; desolvation temperature, 20 °C; source temperature, 20 °C. Signals with an asterisk (*) are ascribable to the sodium and/or ammonium adducts.

All of melting analysis, UV absorption-based titration, Job's plot, and ESI-TOF mass studies revealed that three Gd^{III} ions were quantitatively assembled inside the DNA duplex containing three **U^{OH}**–**U^{OH}** base pairs. Lanthanide ions usually have high coordination numbers such as 8 and 9. Therefore, in addition to **U^{OH}**–**U^{OH}** base pairs, other ligands such as neighboring nucleobases[25,26] and water molecules[27] could bind to these three Gd^{III} ions inside the DNA duplex (Figure 2-12).

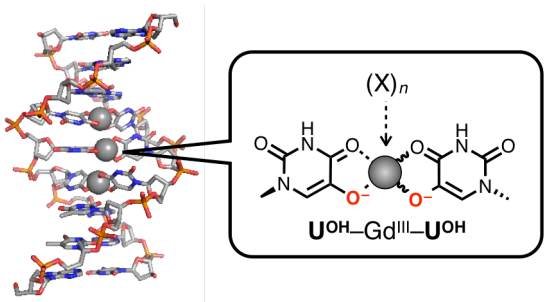

Figure 2-12. A possible structure of the trinuclear Gd^{III}-DNA complex **1·2·Gd$^{III}_3$** and the **U^{OH}**–Gd^{III}–**U^{OH}** base pairs. $(X)_n$ describes other external ligands such as neighboring nucleobases and water molecules.

Next, I discuss the DNA structure of the trinuclear Gd^{III} complex **1·2·Gd$^{III}_3$**. To investigate whether the Gd^{III}-DNA complex remains the typical right-handed helical structure (B-form structure), circular dichroic (CD) spectra were measured for the DNA duplex **1·2** in the absence or in the presence of 3 equivalents of Gd^{III} ions. In both cases, a positive Cotton effect around 260–280 nm and a negative one around 250 nm were observed. These Cotton effects clearly indicate the typical B-form DNA duplex.[28] The CD intensity around 280 nm decreased upon addition of Gd^{III} ions (Figure 2-13). Considering that the changes in the UV absorption around 280 nm was not significant, the phenomenon can be assigned to partial unwinding of the DNA structure induced by the formation of **U^{OH}**–Gd^{III}–**U^{OH}** base pairs.

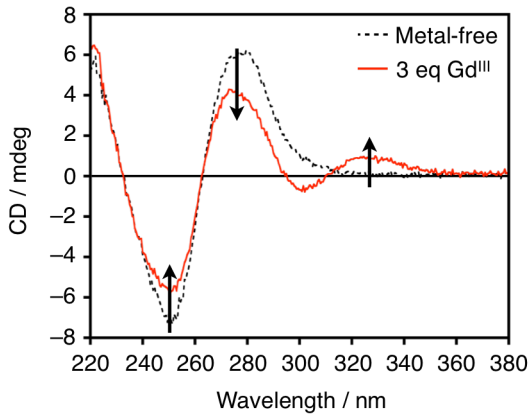

Figure 2-13. CD spectra of the DNA duplex **1·2** in the absence and in the presence of 3 equivalents of Gd^{III} ions. [duplex] = 2 μM, [$GdCl_3$]/[duplex] = 0 (black, dashed line), 3 (red, solid line) in 10 mM HEPES-NaOH buffer (pH 8.0), 100 mM NaCl, *l* = 1.0 cm, 5 °C.

NMR studies were also conducted to investigate the effect of Gd^{III} complexation on the DNA structure. To this end, more stable DNA duplex **3·4** (Table 2-1), which contains three **U^{OH}**–**U^{OH}** base pairs, was prepared. The Gd^{III} ion employed normally causes neighboring ^{1}H NMR signals to be broadened and disappear due to the paramagnetic relaxation enhancement.[29] Therefore, diamagnetic Y^{III}, whose complexes generally have almost the same coordination structures as Gd^{III} complexes, was used. Melting experiment (Figure 2-14), UV absorption study (Figure 2-15), and ESI-TOF mass analysis (Figure 2-16) confirmed that the DNA duplex **3·4** formed a trinuclear Y^{III} complex **3·4·Y$^{III}_3$** in a manner similar to the trinuclear Gd^{III} complex **1·2·Gd$^{III}_3$**. CD study (Figure 2-17) also indicated that the Y^{III} complex **3·4·Y$^{III}_3$** had the B-form DNA structure as was the case

for the Gd^{III} complex **1·2·Gd^{III}_3**.

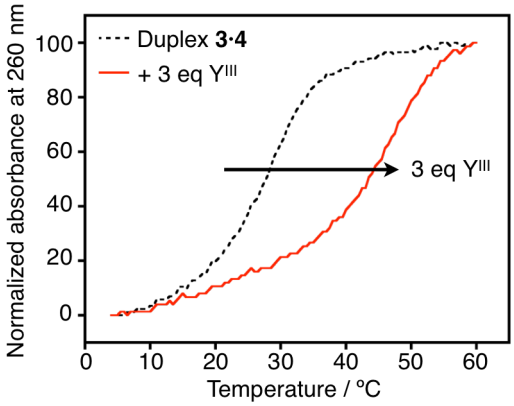

Figure 2-14. Melting curves of DNA duplex **3·4** in the absence and in the presence of 3 equivalents of Y^{III} ions. [duplex] = 2 μM, [YCl_3]/[duplex] = 0 (black, dashed line), 3 (red, solid line) in 10 mM HEPES-NaOH buffer (pH 8.0), 100 mM NaCl, 0.2 °C/min.

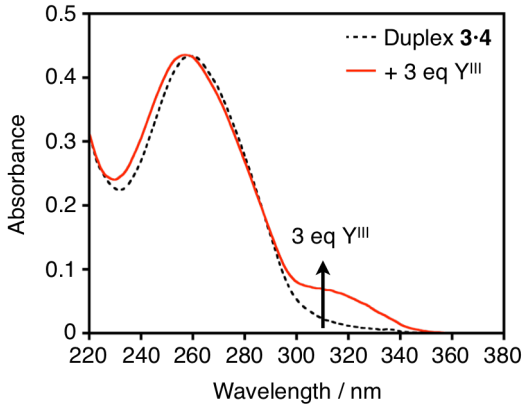

Figure 2-15. UV absorption spectra of DNA duplex **3·4** in the absence and in the presence of 3 equivalents of Y^{III} ions. [duplex] = 2 μM, [YCl_3]/[duplex] = 0 (black, dashed line), 3 (red, solid line) in 10 mM HEPES-NaOH buffer (pH 8.0), 100 mM NaCl, *l* = 1.0 cm, 5 °C.

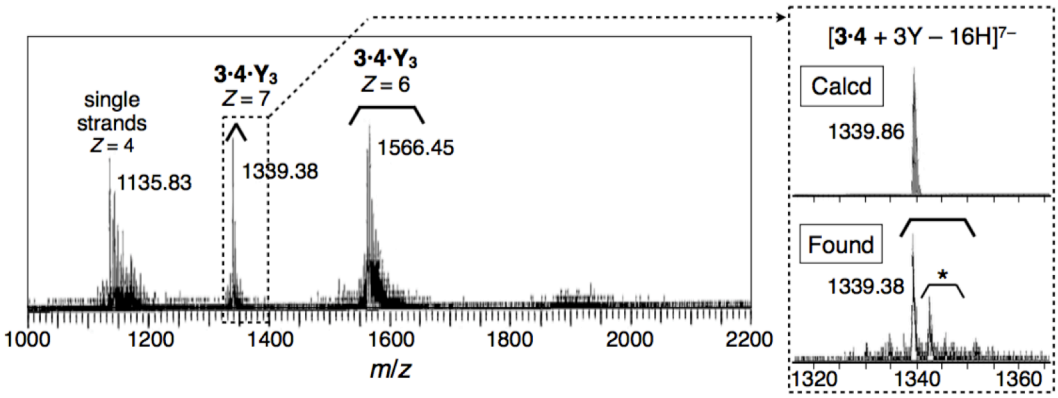

Figure 2-16. An ESI-TOF mass spectrum of DNA duplex **3·4** with 3 equivalents of Y^{III} ions. (**3·4·Y^{III}_3**) = $C_{287}H_{352}N_{103}O_{188}P_{28}Y_3$. [duplex] = 20 μM, [$YCl_3$]/[duplex] = 3 in 20 mM NH_4OAc aqueous solution (pH 8.0). Negative mode; desolvation temperature, 20 °C; source temperature, 20 °C. Signals with an asterisk (*) are ascribable to the sodium and/or ammonium adducts.

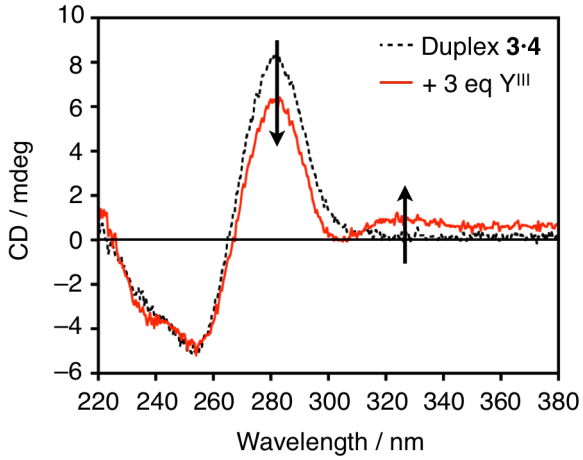

Figure 2-17. CD spectra of DNA duplex **3·4** in the absence and in the presence of 3 equivalents of Y^{III} ions. [duplex] = 2 μM, [YCl_3]/[duplex] = 0 (black, dashed line), 3 (red, solid line) in 10 mM HEPES-NaOH buffer (pH 8.0), 100 mM NaCl, *l* = 1.0 cm, 5 °C.

^{1}H and NOESY NMR spectroscopies were conducted for the metal-free duplex **3·4** and its trinuclear Y^{III} complex. Signals were assigned based on nuclear Overhauser enhancement (NOE) correlation between H1′(i–1)–H6/H8(i)–H1′(i) signals in the absence of Y^{III} ion (Figure 2-18a–d). As a result, some of the peaks around 7 ppm were assigned to the H6 of the $\mathbf{U^{OH}}$ nucleobases (Figure 2-18e). Upon addition of 3 equivalents of Y^{III} ions, the $\mathbf{U^{OH}}$-H6 signals disappeared while only a slight change was observed with other signals. These results indicate that the deprotonated $\mathbf{U^{OH}}$ nucleobases bind to Y^{III} ions.

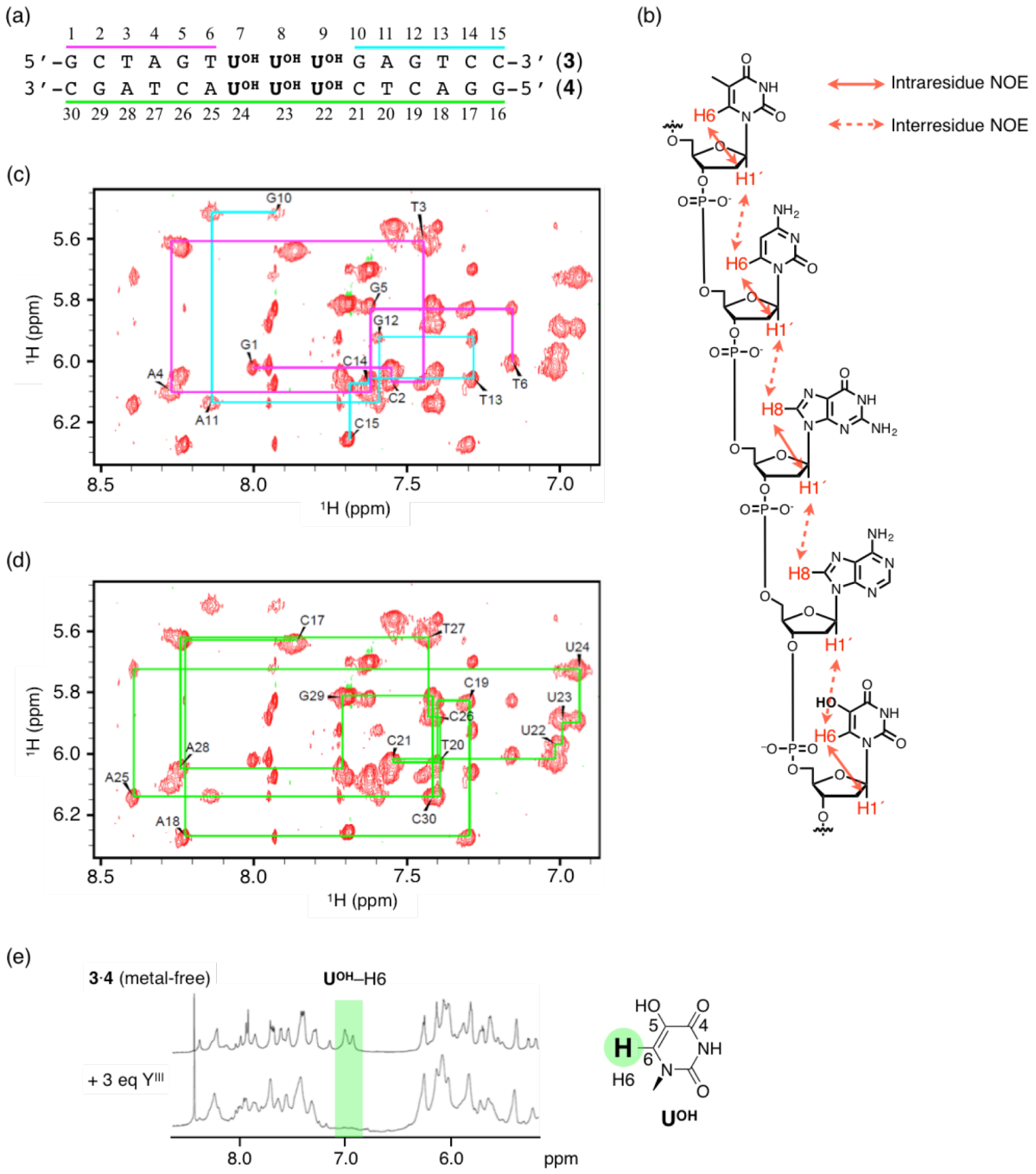

Figure 2-18. NOESY (c, d) and ^{1}H NMR (e, 600 MHz, D_2O) spectra of DNA duplex **3·4** in the absence and in the presence of 3 equivalents of Y^{III} ions. [duplex] = 400 μM, [YCl_3]/[duplex] = 0, 3, in 10 mM [D_{18}]HEPES-NaOH buffer (pH 7.0), 30 mM NaCl, 15 °C. (a) The sequence and numbering of the DNA duplex **3·4**. (b) Schematic representation of the consecutive assignments of NMR signals based on the intraresidue and interresidue NOE signals between H1′(i–1)–H6/H8(i)–H1′(i).

Furthermore, the conformation of the terminal regions of **3·4·Y^{III}_3** was analyzed based on

DQF-COSY and NOESY spectra. In general, when a DNA duplex adopts a B-form structure, the sugar moieties prefer $C_{2'\text{-}endo}$ conformation (Figure 2-19a). To classify the sugar conformation of the trinuclear Y^{III} complex **3·4·Y^{III}_3**, the intensity of COSY and NOE signals around the sugar moieties were evaluated as shown in Figure 2-19. The sugar pucker conformation was determined by the dihedral torsion angles based on the *J*-coupling constants in DQF-COSY (Table 2-3). This analysis indicated that the sugar pucker of the terminal regions was $C_{2'\text{-}endo}$. The H-H distances, calculated from the NOE intensity, were consistent with those of $C_{2'\text{-}endo}$ conformation (Table 2-4). Therefore, it was concluded that the terminal regions of the trinuclear complex **3·4·Y^{III}_3** maintained the

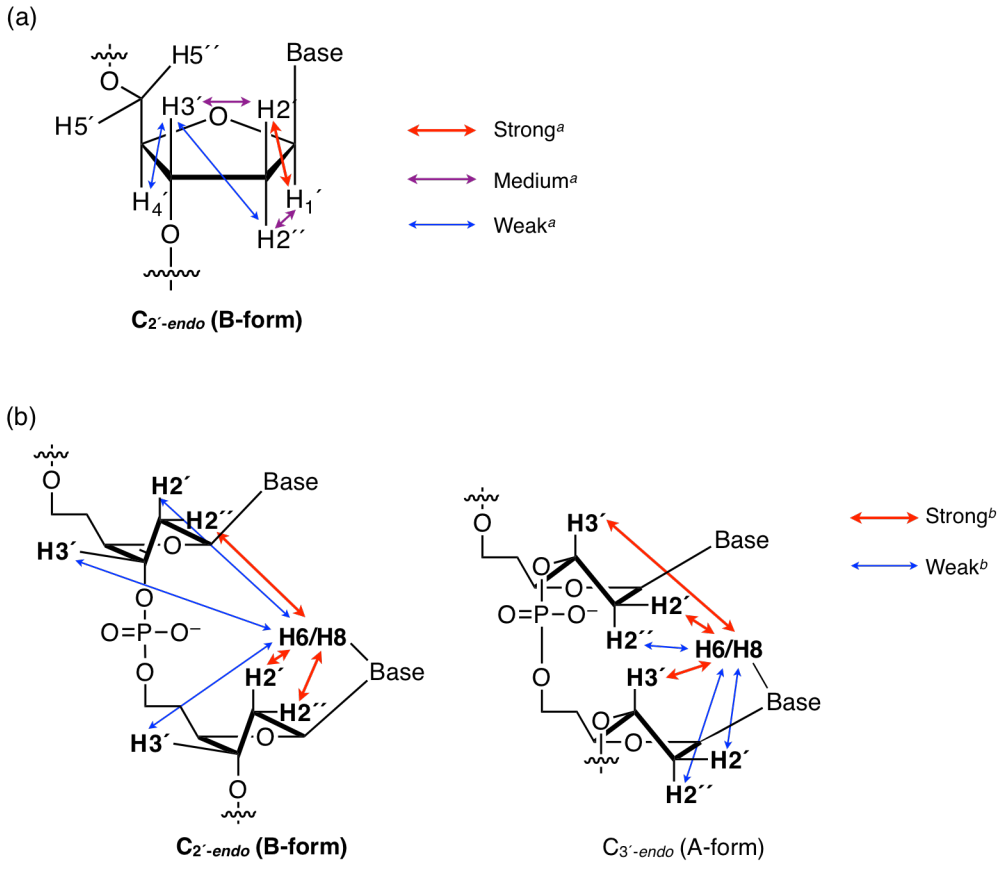

Figure 2-19. Relationship between NOESY/COSY signals and the sugar pucker. (a) $C_{2'\text{-}endo}$ (B-form) and $C_{3'\text{-}endo}$ (A-form) conformation of sugar moieties. The sugar pucker is determined from NOE intensity. (b) Characteristic *J*-coupling constants in the $C_{2'\text{-}endo}$ (B-form) sugar pucker are analyzed by (DQF-)COSY spectrometry. [a]*J*-coupling constant, estimated from the dihedral torsion angle, is related to the intensity based on the Karplus equation. [b]NOE intensity, in which the nearer distance between protons is, the stronger the intensity is.

right-handed B-form DNA duplex. This result was exactly coincident with the observation of CD analysis.

Table 2-3 Sugar pucker conformations of the trinuclear Y^{III} complex **3·4·Y_3**.

	H1′-H2′	H2″-H3′	H3′-H4′	Sugar pucker
G1	s	H_2O	H_2O	$C_{2'\text{-}endo}$ [a]
C2	s	n. a.	n. a.	$C_{2'\text{-}endo}$ [a]
C14	s	n. o.	w	$C_{2'\text{-}endo}$
C15	s	n. o.	m	$C_{2'\text{-}endo}$
G16	s	H_2O	H_2O	$C_{2'\text{-}endo}$ [a]
G17	s	n. o.	n. o.	$C_{2'\text{-}endo}$
A18	s - m	n. o.	n. o.	$C_{2'\text{-}endo}$
G29	s	n. o.	n. o.	$C_{2'\text{-}endo}$
C30	s	m	s	$O_{4'\text{-}endo}$

s, strong; m, medium; w, weak; n. o., not observed; H_2O, can not estimated due to overlapping with water signal; n. a., not assigned. [a]Sugar pucker conformations were deduced on the basis of the strong H1′-H2′ correlation peak.

Table 2-4 Interproton distances (Å) calculated by NOE signals for the trinuclear Y^{III} complex of duplex **3·4** (**3·4·Y_3**).

	Intraresidue		
	H2′-H6/H8	H2″-H6/H8	H3′-H6/H8
G1	3.08	3.58	4.11
C2	o. l.	2.87	n. a.
C14	2.60	3.02	3.81
C15	2.37	n. a.	2.77
G16	o. l.	3.59	n. a.
G17	3.02	3.43	4.10
A18	2.54	2.98	3.24
G29	o. l.	3.30	3.94
C30	2.48	2.56	4.45
	Interresidue		
	H2′(i-1)-H6/H8(i)	H2″(i-1)-H6/H8(i)	H3′(i-1)-H6/H8(i)
G1-C2	3.44	2.96	4.34
C2-T3	o. l.	o. l.	n. a.
C14-C15	o. l.	o. l.	4.25
G16-G17	3.62	2.72	n. a.
G17-A18	3.07	2.78	4.02
G29-C30	o. l.	2.96	3.94

o. l., Interproton distances could not be obtained due to overlapping with other signals; n. a., not assigned. Intraresidue H2'-H6/H8, H2"-H6/H8, and H3'-H6/H8 distances for $C_{2'\text{-}endo}$ are 2.0-2.5 Å, 3.0-3.5, and 4.0-5.0 Å, respectively, while for $C_{3'\text{-}endo}$, they are 3.5-4.0, 4.0-4.5, and 2.5-3.0 Å, respectively.[30] Interresidue H2'-H6/H8, H2"-H6/H8, and H3'-H6/H8 distances for $C_{2'\text{-}endo}$ are 3.8-4.0, 2.1-2.2, and 4.6 Å, respectively, while for $C_{3'\text{-}endo}$, they are 2.0-2.1, 3.7-3.9, and 3.0-3.1 Å, respectively.[30]

All the results from the spectroscopic analyses indicate that lanthanide ions such as Gd^{III} and Y^{III} ions are quantitatively assembled inside the DNA helical scaffold with $\mathbf{U^{OH}}$–$\mathbf{U^{OH}}$ base pairs. A limited number of examples of self-assembled helicates containing polymetallic lanthanide ions have been reported by utilizing linear metal ligands.[31–33] It is rather difficult to control the number and structured of assembled lanthanide ions. Thus, the paired $\mathbf{U^{OH}}$–$\mathbf{U^{OH}}$-containing DNA duplexes are excellent molecular templates for one-dimensional lanthanide array.

2-5. Cooperative assemblies of Gd^{III} ions inside the DNA duplex

Next, I performed mechanistic study of assembly of three Gd^{III} ions inside the DNA duplex **1·2**, containing three $\mathbf{U^{OH}}$–$\mathbf{U^{OH}}$ base pairs. There are two possible processes. One is a "stepwise" complexation mechanism (Scheme 2-2a) and the other is a "cooperative" complexation mechanism (Scheme 2-2b). In the stepwise mechanism, mononuclear and dinuclear Gd^{III} complexes with the DNA duplex including three $\mathbf{U^{OH}}$–$\mathbf{U^{OH}}$ base pairs (**1·2·Gd^{III}** and **1·2·Gd$^{III}_2$**, respectively) are formed as intermediates, whereas, in the cooperative process, only a metal-free DNA duplex and a fully metallated trinuclear Gd^{III} complex **1·2·Gd$^{III}_3$** exist.

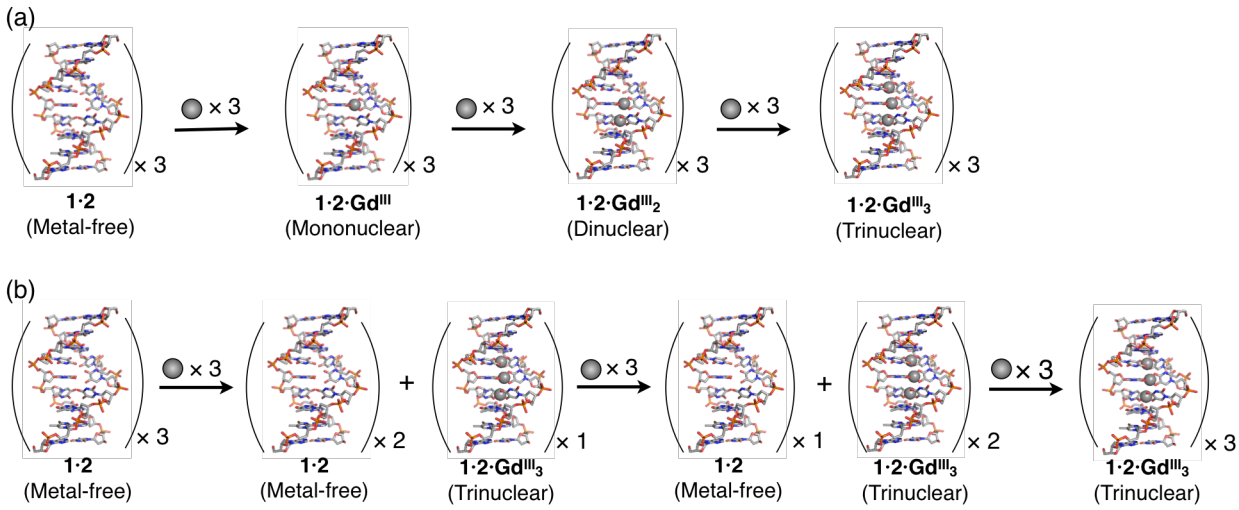

Scheme 2-2. Two possible mechanisms of the quantitative complexation of DNA duplexes containing three $\mathbf{U^{OH}}$–$\mathbf{U^{OH}}$ base pairs with three Gd^{III} ions. (a) A "stepwise" complexation mechanism. (b) a "cooperative" complexation mechanism.

In the section **2-4**, the trinuclear Gd^{III} complex of duplex **1·2** (**1·2·Gd$^{III}_3$**) was observed by ESI-TOF mass spectrometry. To confirm the existence of mononuclear and/or dinuclear Gd^{III} complexes, ESI-TOF mass analysis was carried out for DNA duplex **1·2** in the presence of 1 or 2 equivalents of Gd^{III} ion(s). As the result of addition of 1 or 2 equivalents of Gd^{III}, the existence of a trinuclear Gd^{III} complex was clearly confirmed but any signals derived from mononuclear and dinuclear Gd^{III} complexes were not detected (Figures 2-20a, b). These results suggest that the Gd^{III} complex of duplex **1·2** was formed through a "cooperative" complexation process as shown in

Scheme 2-2b.

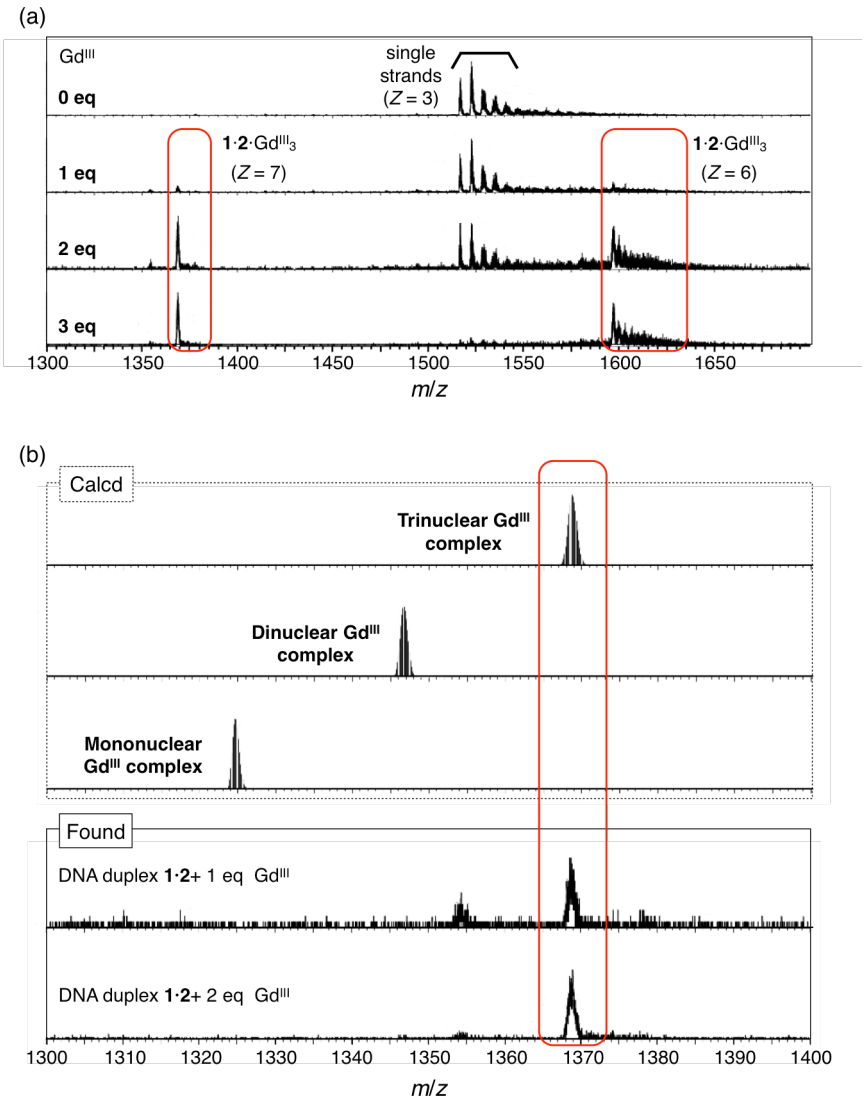

Figure 2-20. ESI-TOF mass spectra of DNA duplex **1·2** with 0, 1, 2, and 3 equivalents of Gd^{III} ions. (mononuclear complex **1·2·Gd^{III}**) = $C_{290}H_{361}N_{100}O_{188}P_{28}Gd$, (dinuclear complex **1·2·Gd$^{III}_2$**) = $C_{290}H_{358}N_{100}O_{188}P_{28}Gd_2$, (trinuclear complex **1·2·Gd$^{III}_3$**) = $C_{290}H_{355}N_{100}O_{188}P_{28}Gd_3$. [duplex] = 20 μM, [$GdCl_3$]/[duplex] = 0, 1, 2, 3 in 20 mM NH_4OAc aqueous solution (pH 8.0). Negative mode; desolvation temperature, 20 °C; source temperature, 20 °C. (a) Whole spectra. (b) Enlarged spectra in the presence of 1 and 2 equivalents of Gd^{III} ions.

To investigate the process of the metal assembly in more detail, duplex melting experiments were conducted. I assumed that the Gd^{III} complexation of duplex **1·2** would proceed through the "cooperative" complexation mechanism. In this case, there are only two species, the metal-free

duplex **1·2** and the trinuclear Gd^{III} complex **1·2·Gd$^{III}_3$** are formed in the presence of less than 3 equivalents of Gd^{III} ions. That is, melting curves in the presence of 1 and 2 equivalents of Gd^{III} ions can be described as weighted averages of the melting curves of metal-free duplex **1·2** and trinuclear complex **1·2·Gd$^{III}_3$** according to the following equation,

$$Abs = [(Abs_{1\cdot2}) \times (3 - X) + (Abs_{1\cdot2\cdot Gd3}) \times X] / 3$$

where $Abs_{1\cdot2}$ and $Abs_{1\cdot2\cdot Gd3}$ represent the absorption at 260 nm of metal-duplex **1·2** and that of trinuclear Gd^{III} complex **1·2·Gd$^{III}_3$**, respectively, and X is the number of equivalent of Gd^{III}. Figure 2-21 compares the calculated curves with the experimental curves with 1 and 2 equivalents of Gd^{III} ions. The experimental curves were well agreed with the calculated curves. These results further support the fact that the Gd^{III} assembly proceeds through the "cooperative" complexation mechanism (Scheme 2-2b).

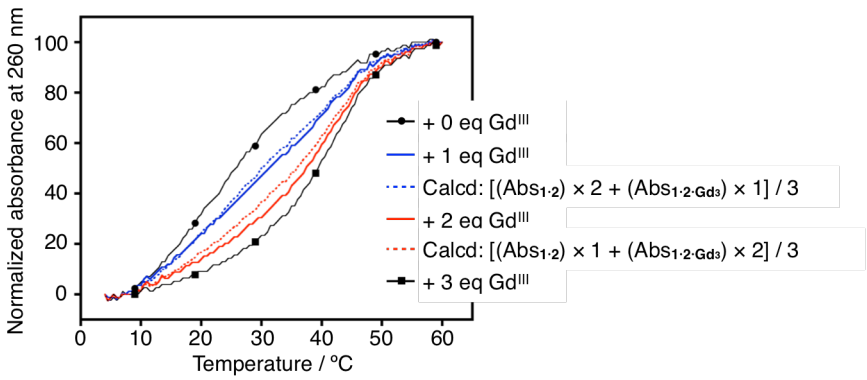

Figure 2-21. Experimental melting curves (solid lines) and calculated curves based on the weighted average (dashed lines) in the Gd^{III} complexation of DNA duplex **1·2**. [duplex] = 2 μM, [$GdCl_3$]/[duplex] = 0 (black, filled circle, solid line), 1 (blue, solid line), 2 (red, solid line), 3 (black, filled square, solid line) in 10 mM HEPES-NaOH buffer (pH 8.0), 100 mM NaCl, 0.2 °C/min. The calculated absorption at each temperature was obtained from the following equation: $[(Abs_{1\cdot2}) \times (3 - X) + (Abs_{1\cdot2\cdot Gd3}) \times X] / 3$; $Abs_{1\cdot2}$ = absorption at 260 nm of the metal-duplex **1·2**, $Abs_{1\cdot2\cdot Gd3}$ = absorption at 260 nm of the trinuclear Gd^{III} complex **1·2·Gd$^{III}_3$**, X = the number of equivalent of Gd^{III}.

The cooperative complexation behaviors have been also observed in other metallo-DNA duplexes. Müller et al. have found that consecutive two **Im**–**Im** base pairs (**Im** = imidazole-type nucleobase) cooperatively coordinate to two Ag^I ions inside a DNA duplex.[34] In this case, the first Ag^I binding confers pre-organized geometry of the second Ag^I-binding site based on the enthalpic

effects. The $\mathbf{U^{OH}}$–$\mathbf{U^{OH}}$ base pairs possibly undergo cooperative Gd^{III} assembly in an enthalpic-driven manner similar to the previous example. The cooperative complexation behaviors of metallo-DNA duplexes would allow switching systems in response to metal ions.

2-6. Summary

I successfully developed 5-hydroxyuracil ($\mathbf{U}^{\mathbf{OH}}$) as the novel ligand-bearing DNA base. The consecutive three $\mathbf{U}^{\mathbf{OH}}$–M–$\mathbf{U}^{\mathbf{OH}}$ (M = Zn^{II}, Sc^{III}, Y^{III}, trivalent lanthanide ions except Pm^{III} and Ce^{III}) base pairs were formed inside the DNA duplexes. The metal-mediated base pairing thermally stabilized the resulting duplex. The stabilization effects would allow us to dynamically control DNA secondary structures and DNA-based nanoarchitectures.

In addition to the stabilization effects, lanthanide ions were precisely assembled along the DNA helical axis. Lanthanide complexes are known to exhibit catalytic activity, luminescence, and magnetism. Thus, the $\mathbf{U}^{\mathbf{OH}}$-based lanthanide-assembled DNAs are expected to induce the unique chemical and physical properties such as asymmetric catalysis and circularly polarized luminescence.

2-7. Experimental section

DNA synthesis

DNA oligonucleotides containing 5-hydroxyuracil ($\mathbf{U}^{\mathbf{OH}}$) nucleobases were synthesized on an Applied Biosystems 394 DNA synthesizer on a 1-μmol scale in a DMTr-on mode with ultramild deprotection phosphoramidites and reagents (Glen Research). A phosphoramidite derivative of $\mathbf{U}^{\mathbf{OH}}$ deoxyribonucleoside, in which the 5-OH group was protected by an acetyl group, was synthesized from 2′-deoxyuridine on a reported protocol.[16,17] The DNA synthesis was carried out according to the standard procedure except for an extended coupling time (15 min). The products were deprotected using 28% NH_3 aqueous solution at room temperature for 2–3 h. The oligonucleotides were firstly purified and detritylated using a PolyPak II cartridge (Glen Research) and further purified by reverse phase HPLC (Waters XBridge C18 column, 0.1 M TEAA (pH 7.0)/MeCN gradient, 60 °C). All DNA strands were identified by ESI-TOF mass spectrometry. Unmodified oligonucleotides purified by HPLC were purchased from Japan Bio Services and used without further purification. The amount of the oligomers was determined based on the UV absorbance at 260 nm. The molar extinction coefficients (ε_{260}) of the oligonucleotides were calculated by the nearest-neighbor method (ε_{260} = 4,590 for the $\mathbf{U}^{\mathbf{OH}}$ nucleoside).

Characterization of the DNA strands possessing $\mathbf{U}^{\mathbf{OH}}$ nucleosides

ODN1. HPLC retention time: 10.5 min (gradient: 5%A (0 min), 8%A (30 min)). ESI-MS: *m*/*z* cacld for $[C_{145}H_{183}N_{47}O_{96}P_{14} - 7H]^{7-}$: 649.4; found: 649.5. $\varepsilon_{260} = 1.29 \times 10^5\ M^{-1}\ cm^{-1}$.

ODN2. HPLC retention time: 9.9 min (gradient: 5%A (0 min), 7%A (30 min)). ESI-MS: *m*/*z* cacld for $[C_{145}H_{181}N_{53}O_{92}P_{14} - 7H]^{7-}$: 652.0; found: 652.0. $\varepsilon_{260} = 1.36 \times 10^5\ M^{-1}\ cm^{-1}$.

ODN3. HPLC retention time: 15.4 min (gradient: 4%A (0 min), 6%A (40 min)). ESI-MS: *m*/*z* cacld for $[C_{144}H_{181}N_{51}O_{95}P_{14} - 8H]^{8-}$: 571.3; found: 571.4. $\varepsilon_{260} = 1.27 \times 10^5\ M^{-1}\ cm^{-1}$.

ODN4. HPLC retention time: 14.8 min (gradient: 4%A (0 min), 5%A (20 min)). ESI-MS: *m*/*z* cacld for $[C_{143}H_{180}N_{52}O_{93}P_{14} - 8H]^{8-}$: 567.5; found: 567.4. $\varepsilon_{260} = 1.27 \times 10^5\ M^{-1}\ cm^{-1}$.

Metal sources

Metal sources were purchased from Wako Pure Chemical Industries [$MnCl_2 \cdot 4H_2O$ (99% purity), $FeCl_2 \cdot 4H_2O$ (99.9%), $CoCl_2 \cdot 6H_2O$ (99.5%), $NiCl_2 \cdot 6H_2O$ (99.9%), $CuCl_2 \cdot 2H_2O$ (99.9%)], Kishida Chemical Co. [$CeCl_3 \cdot 7H_2O$ (99%), $SmCl_3 \cdot 6H_2O$ (99.9%)], Mitsuwa Chemicals Co. [$ScCl_3 \cdot 6H_2O$ (99.9%), $PrCl_3 \cdot 7H_2O$ (99.9%), $HoCl_3 \cdot 6H_2O$ (99.9%), $TmCl_3 \cdot 6H_2O$ (99.9%)], Soekawa Chemical Co. [$ZnSO_4 \cdot 7H_2O$ (99.9%), $LaCl_3 \cdot 7H_2O$ (99.5%), $EuCl_3 \cdot 6H_2O$ (99.9%), $GdCl_3 \cdot 6H_2O$ (99.9%), $TbCl_3 \cdot 6H_2O$ (99.9%), $YbCl_3 \cdot 6H_2O$ (99.9%)], Junsei Chemical Co. [$ErCl_3 \cdot 6H_2O$ (99.9%)], and Aldrich [$YCl_3 \cdot 6H_2O$ (99.99%), $NdCl_3 \cdot 6H_2O$ (99.9%), $DyCl_3 \cdot 6H_2O$ (99.9%), $LuCl_3 \cdot 6H_2O$ (99.99%)].

Sample preparation

All samples for the spectroscopic studies were prepared by mixing DNA strands (2 μM) in 10 mM HEPES-NaOH buffer (pH 8.0) containing 100 mM NaCl, unless otherwise noted. After addition of metal ions, the solutions were heated at 85 °C and cooled slowly to 4 °C at the rate of –1.0 °C/min.

Melting analysis

Absorbance at 260 nm was recorded on a UV-1700 spectrophotometer (Shimadzu) equipped with a TMSPC-8 temperature controller while the temperature was raised from 4 °C to 60 °C at the rate of 0.2 °C/min. A drop of mineral oil was laid on the sample to prevent evaporation. Normalized absorbance shown in the Figures were calculated as follows:

$$\textit{Normalized Absorbance at 260 nm} = \{Abs_{260}(t\ ^\circ\mathrm{C}) - Abs_{260}(4\ ^\circ\mathrm{C})\}/\{Abs_{260}(60\ ^\circ\mathrm{C}) - Abs_{260}(4\ ^\circ\mathrm{C})\} \times 100.$$

The melting temperatures (T_m) were determined as an inflection point of a melting curve using a T_m analysis software LabSolutions (Shimadzu) with a 17-point adaptive smoothing program. Average T_m values of at least 2 runs.

UV spectra

UV spectra were recorded on a Hitachi U-3500 spectrophotometer with a path length of 1.0 cm at 5 °C. For a Job's plot analysis, UV spectra were recorded on NanoDrop2000 (ThermoScientific) with a path length of 1.0 mm at room temperature.

CD spectra

CD spectra were recorded on a JASCO J-820 spectropolarimeter with 10-time accumulation using a path length of 1.0 cm at 5 °C.

Mass spectra

Electrospray ionization-time-of-flight (ESI-TOF) mass spectra were recorded on a Waters Micromass LCT premier. The samples were prepared in 20 mM NH_4OAc buffer (pH 8.0) and annealed just before the measurements (from 85 °C to 4 °C, –1.0 °C/min).

NMR structural analysis

After the measurement of the metal-free DNA, 3 equivalents of Y^{III} ions were added to the sample, which was subsequently annealed. NMR spectra, NOESY, TOCSY, and DQF-COSY were recorded with a Bruker AVANCEIIIHD600 spectrometer equipped with a cryoprobe. Resonance assignment for a finger print region was carried out using standard methods, as described for other nucleic acids.[35] The assignment was accomplished for almost all residues in the absence of Y^{III} ions. In the presence of Y^{III} ions, the assignments were obtained for the residues of both terminal regions, G1, C2, T3, C14, C15, G16, G17, A18, G29, and C30. Interproton distances were calculated from a NOESY spectrum with a mixing time of 80 ms, using the cytidine H5-H6 distance as a reference.

2-8. References

[1] E. Meggers, P. L. Holland, W. B. Tolman, F. E. Romesberg, P. G. Schultz, *J. Am. Chem. Soc.* **2000**, *122,* 10714–10715.

[2] T. Tanaka, A. Tengeiji, T. Kato, N. Toyama, M. Shiro, M. Shionoya, *J. Am. Chem. Soc.* **2002**, *124*, 12494–12498.

[3] G. H. Clever, K. Polborn, T. Carell, *Angew. Chem. Int. Ed.* **2005**, *44*, 7204–7208.

[4] C. Switzer, S. Sinha, P. H. Kim, B. D. Heuberger, *Angew. Chem. Int. Ed.* **2005**, *44*, 1529–1532.

[5] Y. Miyake, H. Togashi, M. Tashiro, H. Yamaguchi, S. Oda, M. Kudo, Y. Tanaka, Y. Kondo, R. Sawa, T. Fujimoto, T. Machinami, A. Ono, *J. Am. Chem. Soc.* **2006**, *128*, 2172–2173.

[6] A. Ono, S. Cao, H. Togashi, M. Tashiro, T. Fujimoto, T. Machinami, S. Oda, Y. Miyake, I. Okamoto, Y. Tanaka, *Chem. Commun.* **2008**, *44*, 4825–4827.

[7] Z. Kuklenyik, L. G. Marzilli, *Inorg. Chem.* **1996**, *35*, 5654–5662.

[8] D. Böhme, N. Düpre, D. A. Megger, J Müller, *Inorg. Chem.* **2007**, *46*, 10114–10119.

[9] S. Johannsen, N. Megger, D. Böhme, R. K. O. Sigel, J. Müller, *Nat. Chem.* **2010**, *2*, 229–234.

[10] K. Tanaka, A. Tengeiji, T. Kato, N. Toyama, M. Shionoya, *Science* **2003**, *299*, 1212–1213.

[11] K. Tanaka, G. H. Clever, Y. Takezawa, Y. Yamada, C. Kaul, M. Shionoya, T. Carell, *Nat. Nanotechnol.* **2006**, *1*, 190–194.

[12] G. H. Clever, T. Carell, *Angew. Chem. Int. Ed.* **2007**, *46*, 250–253.

[13] G. H. Clever, S. J. Reitmeier, T. Carell, O. Schiemann, *Angew. Chem. Int. Ed.* **2010**, *122*, 5047–5049.

[14] S. Gourdain, C. Petermann, D. Harakat, P. Clivio, *Nucleosides, Nucleotides Nucleic Acids* **2010**, *29*, 542–546.

[15] L. Szabo, I. Kalman, T, J. Bardos, *J. Org. Chem*. **1970**, *35*, 1434–1437.

[16] J. Fujimoto, L. Tran, L. C. Sowers, *Chem. Res. Toxicol*. **1997**, *10*, 1254–1258.

[17] M. L. Morningstar, D. A. Kreutzer, J. M. Essigmann, *Chem. Res. Toxicol*. **1997**, *10*, 1345–1350.

[18] C. F. Baes, R. E. Mesmer, *The hydrolysis of cations*, John Wiley & Sons, New York, **1976**.

[19] C. J. Borrows, J. G. Muller, *Chem. Rev*. **1998**, *98*, 1109–1151.

[20] J. Rivière, F. Bergeron, S. Tremblay, D. Gasparutto, J. Cadet, J. R. Wagner, *J. Am. Chem. Soc*. **2004**, *126*, 6548–6549.

[21] S. Cotton, *Lanthanide and actinide chemistry*, John Wiley & Sons, England, **2006**.

[22] Y. Q. Jia, *J. Solid State Chem*. **1991**, *95*, 184–187.

[23] 松本和子, *希土類元素の化学*, 朝倉書店, **2008**.

[24] C. J. La Francois, Y. H. Jang, T. Cagin, W. A. Goddard, L. C. Sowers, *Chem. Res. Toxicol*. **2000**, *13*, 462–470.

[25] S. Atwell, E. Meggers, G. Spraggon, P. G. Schultz, *J. Am. Chem. Soc*. **2001**, *123*, 12364–12367.

[26] S. S. Mallajosyula, S. K. Pati, *Angew. Chem. Int. Ed*. **2009**, *48*, 4977–4981.

[27] A. R. de Leon, A. O. Olatunde, J. R. Morrow, C. Achim, *Inorg. Chem*. **2012**, *51*, 12597–12599.

[28] M. Vorlíčková, I. Kejnovská, K. Bednářová, D. Renčiuk, J. Kypr, *Chirality* **2012**, *24*, 691–698.

[29] G. Otting, *Annu. Rev. Biophys*. **2010**. *39*, 387–405.

[30] K. Wüthrich, *NMR of Proteins and Nucleic Acids*, John Wiley & Sons, New York, **1986**.

[31] D. Imbert, M. Cantuel, J.-C. G. Bünzli, G. Bernardinelli, C. Piguet, *J. Am. Chem. Soc*. **2003**, *125*, 15698–15699.

[32] B. Wang, Z. Zang, H. Wang, W. Dou, X. Tang, W. Liu, Y. Shao, J. Ma, Y. Li, J. Zhou, *Angew. Chem. Int. Ed*. **2013**, *52*, 3756–3759.

[33] A. M. Johnson, M. C. Young, X. Zhang, R. R. Julian, R. J. Hooley, *J. Am. Chem. Soc.* **2013**, *135*, 17723–17726.

[34] K. Petrovec, B. J. Ravoob, J. Müller, *Chem. Commun.* **2012**, *48*, 11844–11846.

[35] T. Mashima, A. Matsugami, F. Nishikawa, S. Nishikawa, M. Katahira, *Nucleic Acids Res.* **2009**, *37*, 6249–6258.

Chapter 3.

Metal-mediated regulation of DNA hybridization preference using 5-hydroxyuracils

3-1. Introduction

Bifacial nucleobases have been developed toward construction of gene sensors and supramolecular architectures.[1–4] In this system, the bifacial base pairing can be possibly switchable by external stimuli, leading to dynamic regulation of DNA structures and functions. In this section, I discuss metal-responsive bifacial base-pairing behaviors of 5-hydroxyuracil ($\mathbf{U}^{\mathbf{OH}}$) nucleobase (Figure 3-1). In **chapter 2**, the thermal stabilization of DNA duplexes is described when the consecutive homogeneous $\mathbf{U}^{\mathbf{OH}}$–$\mathbf{U}^{\mathbf{OH}}$ base pairs are metal-mediated to form $\mathbf{U}^{\mathbf{OH}}$–M–$\mathbf{U}^{\mathbf{OH}}$ base pairs. A $\mathbf{U}^{\mathbf{OH}}$ nucleobase also forms a hydrogen-bonded base pair with a natural adenine (**A**) nucleobase ($\mathbf{U}^{\mathbf{OH}}$–**A**).[5,6] A $\mathbf{U}^{\mathbf{OH}}$–**A** base pair was expected to switch with a $\mathbf{U}^{\mathbf{OH}}$–M–$\mathbf{U}^{\mathbf{OH}}$ base pair through metal complexation. This base pair switching of $\mathbf{U}^{\mathbf{OH}}$ nucleobases would induce DNA strand exchange reactions (Figure 3-2). In this section, I report the thermal stability of DNA duplexes containing $\mathbf{U}^{\mathbf{OH}}$–**X** base pairs (**X** = $\mathbf{U}^{\mathbf{OH}}$ and natural nucleobases) in the absence and in the presence of metal ions to reveal the alteration of the DNA hybridization preference.

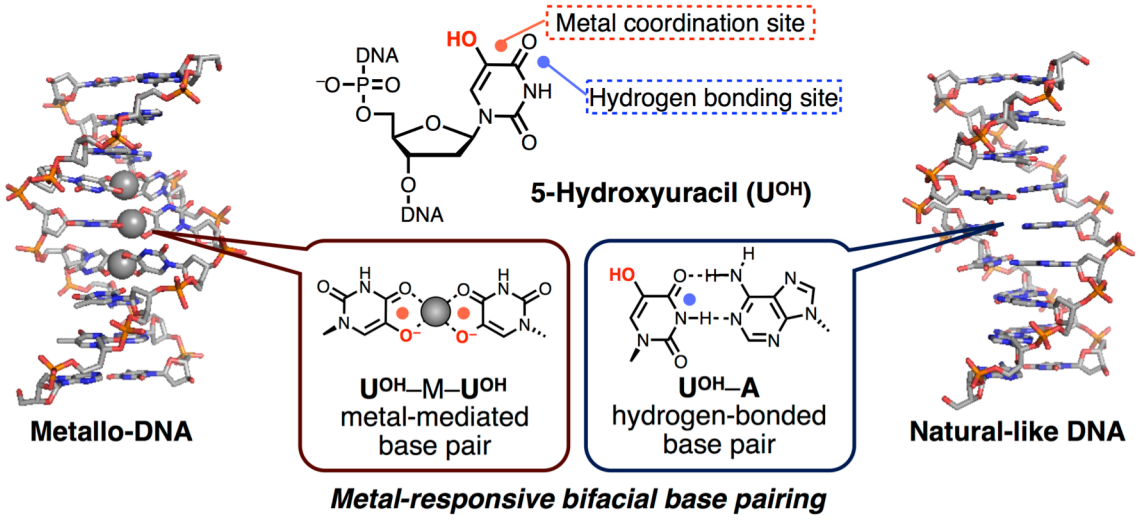

Figure 3-1. Schematic representation of the metal-responsive bifacial base pairing of 5-hydroxyuracil ($\mathbf{U}^{\mathbf{OH}}$) nucleobase. $\mathbf{U}^{\mathbf{OH}}$ nucleobases can form a metal-mediated base pair ($\mathbf{U}^{\mathbf{OH}}$–M–$\mathbf{U}^{\mathbf{OH}}$; M = Zn^{II}, Gd^{III} etc) and a hydrogen-bonded base pair ($\mathbf{U}^{\mathbf{OH}}$–**A**).

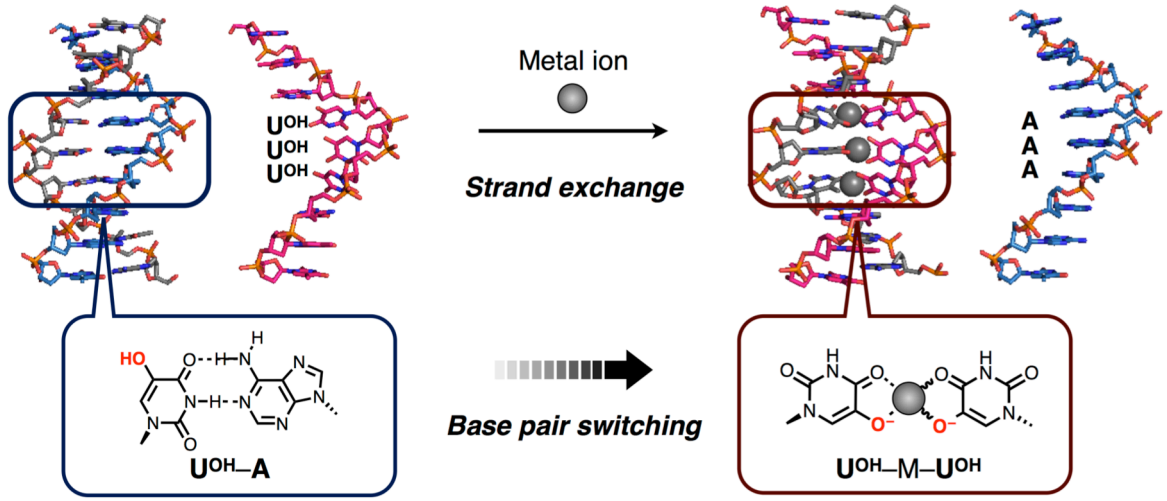

Figure 3-2. Schematic representation of the base pair switching and the metal-driven DNA strand exchange reaction utilizing $\mathbf{U^{OH}}$ nucleobases.

3-2. Destabilization effects of metal ions on 5-hydroxyuracil–adenine base pairs

I investigated the effects of metal ions on the thermal stability of a $\mathbf{U^{OH}}$–**A**-containing DNA duplex. First, a natural 15-mer DNA strand **2A** (Table 3-1), which fully hybridizes with the $\mathbf{U^{OH}}$-containing DNA strand **1** through the formation of Watson–Crick-type hydrogen-bonded base pairs including three $\mathbf{U^{OH}}$–**A** base pairs, was prepared. In section **2-3**, some lanthanide ions such as Gd^{III} were found to stabilize the $\mathbf{U^{OH}}$–$\mathbf{U^{OH}}$-containing DNA duplex **1·2** through the metal-mediated $\mathbf{U^{OH}}$–M–$\mathbf{U^{OH}}$ (M = Gd^{III} etc) base pairing. Hence, it was expected that Gd^{III} ion also affect the thermal stability of the $\mathbf{U^{OH}}$–**A**-containing DNA duplex **1·2A**.

Table 3-1. Sequences of DNA strands used in this section.

Name	Sequence (5′ to 3′)
1	CAC ATT $\mathbf{U^{OH}U^{OH}U^{OH}}$ GTT GTA
2	TAC AAC $\mathbf{U^{OH}U^{OH}U^{OH}}$ AAT GTG
1X (**X** = **A**, **T**, **G**, or **C**)	CAC ATT **XXX** GTT GTA
2X (**X** = **A**, **T**, **G**, or **C**)	TAC AAC **XXX** AAT GTG

The thermal stability of DNA duplex **1·2A** was evaluated by melting experiments. Figure 3-3 shows the melting curves of **1·2A** in the absence and in the presence of Gd^{III} ions. The melting

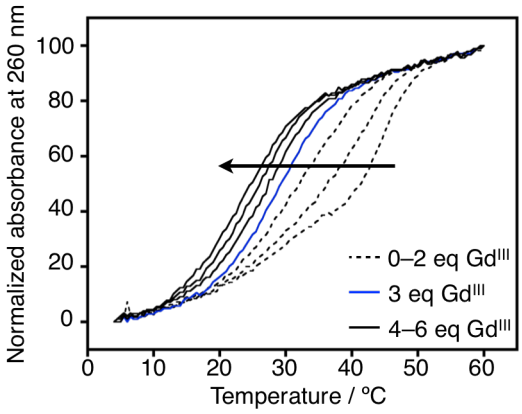

Figure 3-3. Melting curves of DNA duplex **1·2A** in the presence of 3 equivalents of Gd^{III} ions. [duplex] = 2 μM, [$GdCl_3$]/[duplex] = 0 (black, dashed lines), 3 (red, solid line) in 10 mM HEPES-NaOH buffer (pH 8.0), 100 mM NaCl, 0.2 °C/min.

curve was gradually shifted to the left side with increasing Gd^{III} ions. This observation indicates that the duplex **1·2A** was thermally destabilized. The addition of 3 equivalents of Gd^{III} ions decreased the melting temperature (T_m) of **1·2A** by 14 °C.

To confirm if the duplex destabilization was due to the binding of Gd^{III} ions to the $\mathbf{U^{OH}}$ nucleobases, UV absorption spectra were measured for the DNA duplex **1·2A**. Upon addition of 3 equivalents of Gd^{III} ions, a new absorption around 310 nm appeared (Figure 3-4a, b). This spectral change can be ascribable to the deprotonation of the 5-OH groups of $\mathbf{U^{OH}}$ nucleobases, which resulted from Gd^{III} binding (Figure 3-4c).[7]

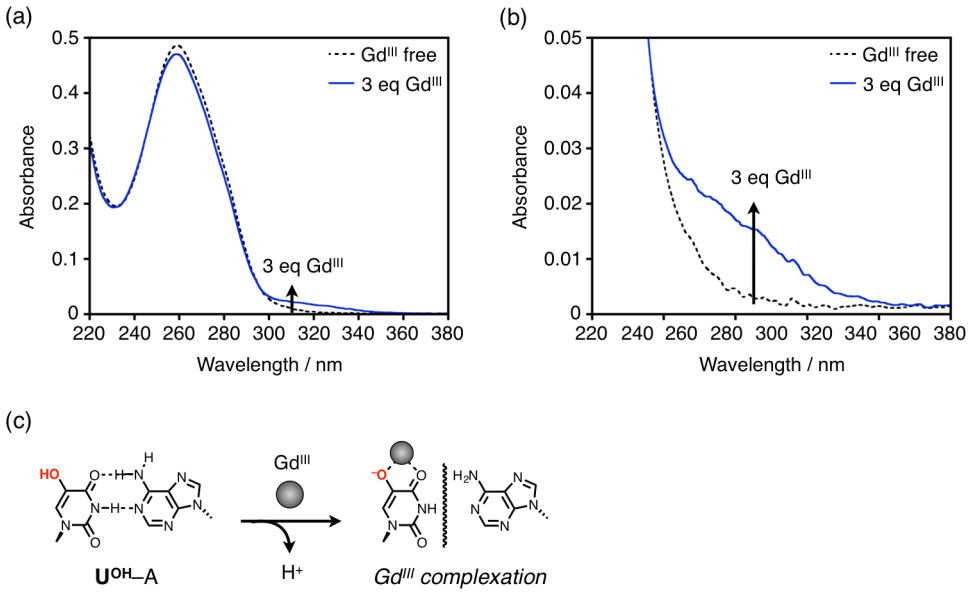

Figure 3-4. UV absorption spectra of the DNA duplex **1·2A** in the absence and in the presence of of Gd^{III} ions. (a, b) [duplex] = 2 μM, [$GdCl_3$]/[duplex] = 0 (black, dashed lines), 3 (blue, solid lines) in 10 mM HEPES-NaOH buffer (pH 8.0), 100 mM NaCl, *l* = 1.0 cm, 5 °C. (c) Schematic representation of the deprotonation events accompanied with the Gd^{III} complexation of $\mathbf{U^{OH}}$–**A** base pairs.

Subsequently, as a control experiment, a natural 15-mer DNA duplex **1T·2A** containing three **T**–**A** base pairs was used instead of that containing three $\mathbf{U^{OH}}$–**A** base pairs. The melting curves and the UV spectra of this duplex were not significantly changed when Gd^{III} ions were added (Figure 3-5). These results support that Gd^{III} ions selectively bound to the $\mathbf{U^{OH}}$–**A** base pair moieties and thermally destabilized the DNA duplex.

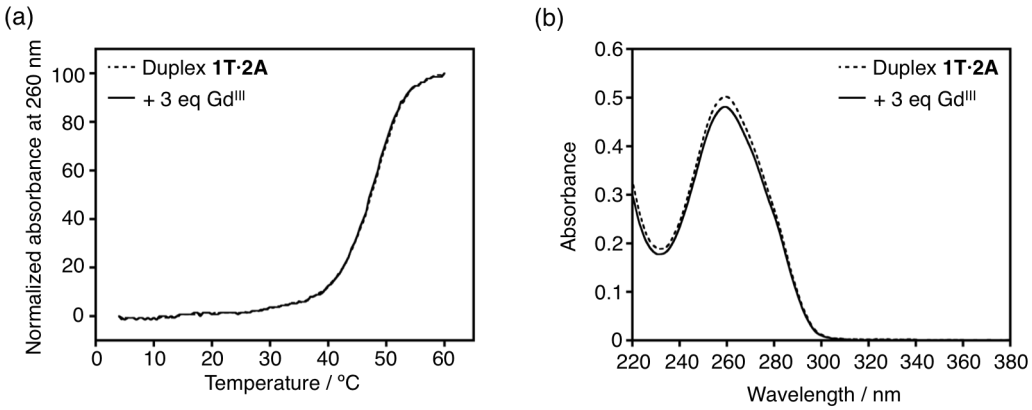

Figure 3-5. Melting curves (a) and UV absorption spectra (b) of DNA duplex **1T·2A** in the absence and in the presence of Gd^{III} ions. [duplex] = 2 μM, [$GdCl_3$]/[duplex] = 0 (dashed lines), 3 (solid line) in 10 mM HEPES-NaOH buffer (pH 8.0), 100 mM NaCl, 0.2 °C/min (a), *l* = 1.0 cm, 5 °C (b).

To investigate the destabilization effects in more detail, melting analyses were conducted for the DNA duplexes containing $\mathbf{U^{OH}}$–**X** (**X** = **T**, **G**, or **C**) mismatched base pairs. Their melting curves were scarcely changed by addition of Gd^{III} (Figure 3-6). These results suggest that the Gd^{III} complexation of $\mathbf{U^{OH}}$ nucleobases should weaken the hydrogen bonds between $\mathbf{U^{OH}}$ and **A** nucleobases.

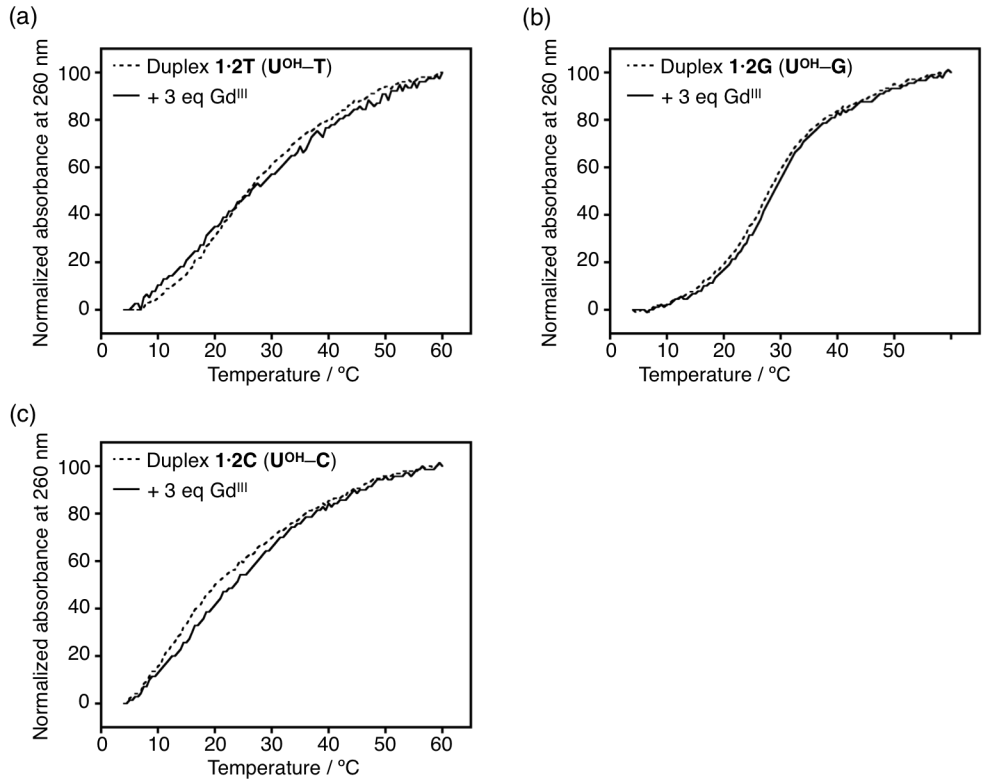

Figure 3-6. Melting curves of DNA duplex **1·2X** [**X** = **T** (a), **G** (b), **C** (c)], containing a mismatched base pair in the absence and in the presence of Gd^{III} ions. [duplex] = 2 μM, [$GdCl_3$]/[duplex] = 0 (dashed lines), 3 (solid line) in 10 mM HEPES-NaOH buffer (pH 8.0), 100 mM NaCl, 0.2 °C/min.

The destabilization effect is most likely to result from the weakened hydrogen bonds between $\mathbf{U}^{\mathbf{OH}}$ and **A** nucleobases. This derives from the fact that the bound Lewis-acidic Gd^{III} has an electron-withdrawing inductive effect on the tautomerism of the $\mathbf{U}^{\mathbf{OH}}$ nucleobase,[8,9] from the keto form to the enol form (Figure 3-7a). As the result, the hydrogen bonding pattern can be remarkably altered. In addition, the Gd^{III} ions allow intrastrand cross-linking between $\mathbf{U}^{\mathbf{OH}}$ nucleobases in a manner similar to the cisplatin complex with consecutive two guanine bases.[10,11] This metal-mediated bridging would unwind the DNA duplex structure and consequently decrease its thermal stability (Figure 3-7b).

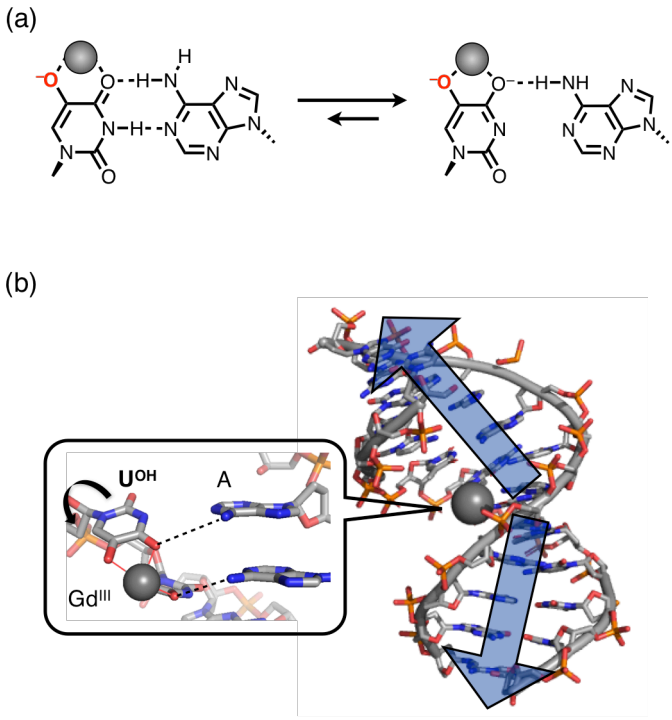

Figure 3-7. Possible mechanisms of the Gd^{III}-induced destabilization of a DNA duplex containing $\mathbf{U^{OH}}$–**A** base pairs. (a) Tautomerism of $\mathbf{U^{OH}}$ nucleobases altered by Gd^{III} binding. (b) Gd^{III}-mediated intrastrand crosslinking between two $\mathbf{U^{OH}}$ nucleobases.

In summary, it was found that the hydrogen-bonded 5-hydroxyuracil–adenine ($\mathbf{U^{OH}}$–**A**) base pairs were thermally destabilized by the Gd^{III} complexation with the $\mathbf{U^{OH}}$ nucleobases. This destabilization behavior is quite a contrast to stabilization effects due to the formation of $\mathbf{U^{OH}}$–Gd^{III}–$\mathbf{U^{OH}}$ base pairs. Both Gd^{III}-mediated stabilization of $\mathbf{U^{OH}}$–$\mathbf{U^{OH}}$ and Gd^{III}-mediated destabilization of $\mathbf{U^{OH}}$–**A** would alter the DNA hybridization preference of $\mathbf{U^{OH}}$-containing DNA strands.

3-3. Regulation of DNA hybridization preference through the metal complexation of 5-hydroxyuracil nucleobases

In sections **2-3** and **3-2**, it was demonstrated that the metal-mediated $\mathbf{U^{OH}}$–M–$\mathbf{U^{OH}}$ (M = Gd^{III} etc) base pairing thermally stabilizes the resulting DNA duplexes, while the metal complexation of hydrogen-bonded 5-hydroxyuracil–adenine ($\mathbf{U^{OH}}$–**A**) base pairs thermally destabilizes the duplex. Then, I examined the effects of Gd^{III} complexation on the DNA hybridization preference of $\mathbf{U^{OH}}$-containing DNA strands.

Figure 3-8 describes the melting temperatures (T_m) of five DNA duplexes, in which opposite three nucleobases against three $\mathbf{U^{OH}}$ bases of DNA strand **1** are $\mathbf{U^{OH}}$, adenine (**A**), thymine (**T**), guanine (**G**), and cytosine (**C**). In the absence of Gd^{III} ions, the $\mathbf{U^{OH}}$–**A**-containing DNA duplex **1·2A** was more stable than the other DNA duplexes (Figure 3-8, left). The T_m value of **1·2A** was higher than that of the $\mathbf{U^{OH}}$–$\mathbf{U^{OH}}$-containing duplex **1·2** by 22 °C. Thus, the $\mathbf{U^{OH}}$ nucleobases preferentially recognize **A** nucleobases through hydrogen bonding like a canonical **T**–**A** base pair. In the presence of 3 equivalents of Gd^{III} ions, the trinuclear Gd^{III} complex of duplex **1·2** (**1·2·**$\mathbf{Gd^{III}_3}$) showed the highest melting temperature (Figure 3-8, right). This is because both Gd^{III}-mediated stabilization of $\mathbf{U^{OH}}$–$\mathbf{U^{OH}}$ base pairs and Gd^{III}-mediated destabilization of $\mathbf{U^{OH}}$–**A** base pairs. The T_m value of **1·2·**$\mathbf{Gd^{III}_3}$ was higher than that of $\mathbf{U^{OH}}$–**A**-containing duplex **1·2A** by 10 °C. Thus, the DNA hybridization preference of $\mathbf{U^{OH}}$-containing DNA is switchable by addition of Gd^{III}.

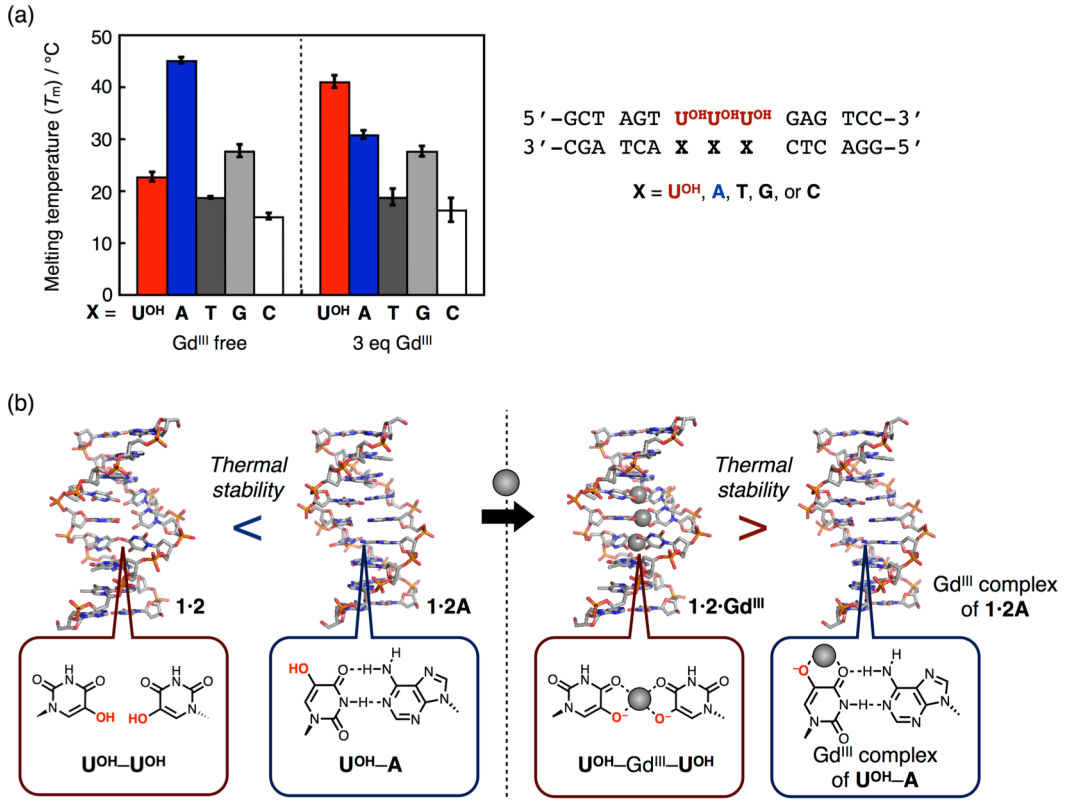

Figure 3-8. Investigation of DNA hybridization preference of the $\mathbf{U^{OH}}$-containing DNA strand. (a) Melting temperatures (T_m) of the DNA duplexes containing three $\mathbf{U^{OH}}$–**X** (**X** = $\mathbf{U^{OH}}$, **A**, **T**, **G**, or **C**) base pairs. [duplex] = 2 μM, [$GdCl_3$]/[duplex] = 0, 3 in 10 mM HEPES-NaOH buffer (pH 8.0), 100 mM NaCl. Error bars indicate the standard deviations. (b) Schematic representation of DNA hybridization preference of the $\mathbf{U^{OH}}$-containing DNA strand in the absence and in the presence of 3 equivalents of Gd^{III} ions.

In summary, I successfully demonstrated the regulation of hybridization preference of $\mathbf{U^{OH}}$-containing DNA strands through the metal-mediated stabilization of $\mathbf{U^{OH}}$–$\mathbf{U^{OH}}$ and metal-mediated destabilization of $\mathbf{U^{OH}}$–**A** base pairs. The unique bifacial base-pairing behaviors were expected to contribute to the development of DNA strand exchange reactions. As the general DNA strand exchange/displacement reactions have been utilized as a motive power of DNA-based dynamic nanoarchitectures,[12–14] the introduction of $\mathbf{U^{OH}}$ nucleobase into DNA strands would become a powerful tool for DNA nanotechnology.

3-4. pH dependence in the metal-mediated stabilization and destabilization effects

In sections **2-4** and **3-2**, UV absorption study revealed that the metal coordination of $\mathbf{U^{OH}}$ nucleobase is accompanied by the deprotonation of its 5-hydroxy group (Figure 3-9a). In the light of this finding, the concentration of proton (H^+), that is, pH is an important factor to determine the metal complexation behavior of $\mathbf{U^{OH}}$ nucleobase. The pK_a value of the 5-hydroxy group is approximately 7.7 (Figure 3-9b).[7] Thus, the pH dependence of the metal-mediated stabilization and destabilization was investigated around this pK_a value.

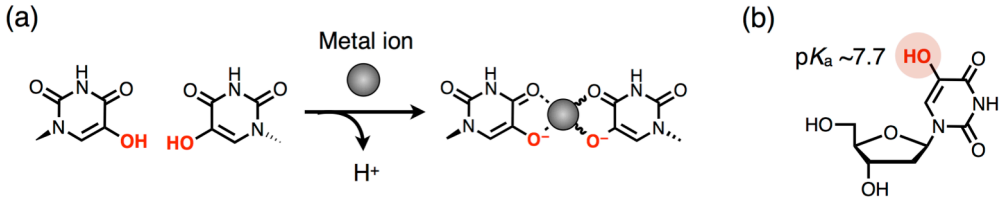

Figure 3-9. (a) Metal complexation of $\mathbf{U^{OH}}$ nucleobases accompanied by deprotonation of their 5-hydroxy groups. (b) The pK_a value of the 5-hydroxy group of $\mathbf{U^{OH}}$ is approximately 7.7.[6]

In section **2-3**, the melting experiments were conducted at pH 8.0. As the result, it was revealed that various lanthanide ions such as Gd^{III} and Zn^{II} ions thermally stabilized the 15-mer DNA duplex **1·2** containing three $\mathbf{U^{OH}}$–$\mathbf{U^{OH}}$ base pairs. Firstly, the pH dependence of the Gd^{III}-induced duplex stabilization was examined. Melting experiments were conducted for duplex **1·2** at pH 7.0 and 9.0. Under this condition, melting curves of duplex **1·2** were shifted to the right side upon addition of 3 equivalents of Gd^{III} ions. That is, melting temperatures (T_m) were raised by addition of Gd^{III} independent of pH (Figure 3-10). It was considered that as is well known, the apparent pK_a value of the 5-hydroxy group of $\mathbf{U^{OH}}$ nucleobase was lowered due to the relatively high Lewis-acidity of Gd^{III}.

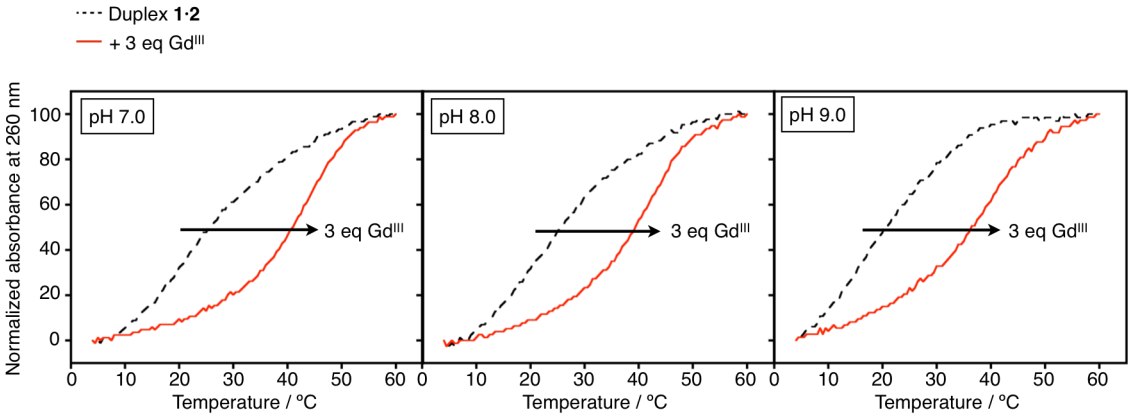

Figure 3-10. Melting curves of DNA duplex **1·2** in the absence and in the presence of 3 equivalents of Gd^{III} ions. [duplex] = 2 μM, [$GdCl_3$]/[duplex] = 0 (black, dashed lines), 3 (red, solid lines) in 10 mM HEPES-NaOH buffer (pH 7.0 or 8.0) or 10 mM CHES-NaOH buffer (pH 9.0), 100 mM NaCl, 0.2 °C/min.

Next, pH dependence of the Zn^{II}-mediated stabilization was examined because Zn^{II} ions largely differ from Gd^{III} ions in terms of Lewis acidity and the coordination number. The melting experiments were also carried out in the range from pH 7.0 to 9.0. The Zn^{II} addition resulted in the significant thermal stabilization of duplex **1·2** at pH 8.0 and 9.0, whereas no changes in the stability were observed at pH 7.0 (Figure 3-11). This is probably due to the weaker Lewis-acidity of Zn^{II} ions compared with that of Gd^{III}, that is, the apparent pK_a value of the 5-hydroxy group in the presence of Zn^{II} was not so lowered.

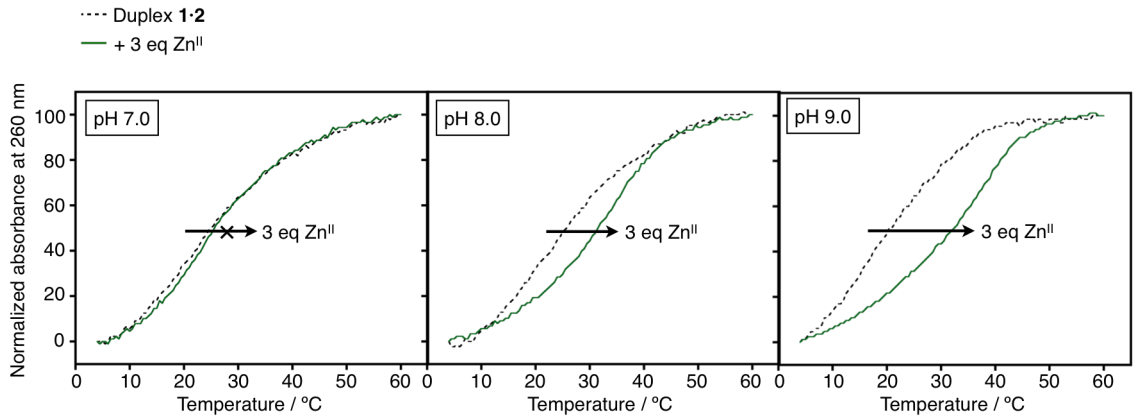

Figure 3-11. Melting curves of DNA duplex **1·2** in the absence and in the presence of 3 equivalents of Zn^{II} ions. [duplex] = 2 μM, [$ZnSO_4$]/[duplex] = 0 (black, dashed lines), 3 (green, solid lines) in 10 mM HEPES-NaOH buffer (pH 7.0 or 8.0) or 10 mM CHES-NaOH buffer (pH 9.0), 100 mM NaCl, 0.2 °C/min.

The pH dependence of Zn^{II} complexation of $\mathbf{U^{OH}}$ nucleobases was also confirmed by UV absorption spectroscopy in the range from pH 7.0 to 9.0. At pH 8.0 and 9.0, the UV absorption band around 310 nm, derived from the deprotonation of the 5-hydroxy groups of $\mathbf{U^{OH}}$ nucleobases, clearly appeared upon addition of Zn^{II} (Figure 3-12). In contrast to this, at pH 7.0, only a slight spectral change was observed (Figure 3-12). Thus, it was concluded that the Zn^{II} complexation of $\mathbf{U^{OH}}$ nucleobases took place only under basic pH conditions. Based on the melting analysis, the pH-dependent stabilization behaviors were ascribed to the type of metal ions with a different Lewis-acidity.

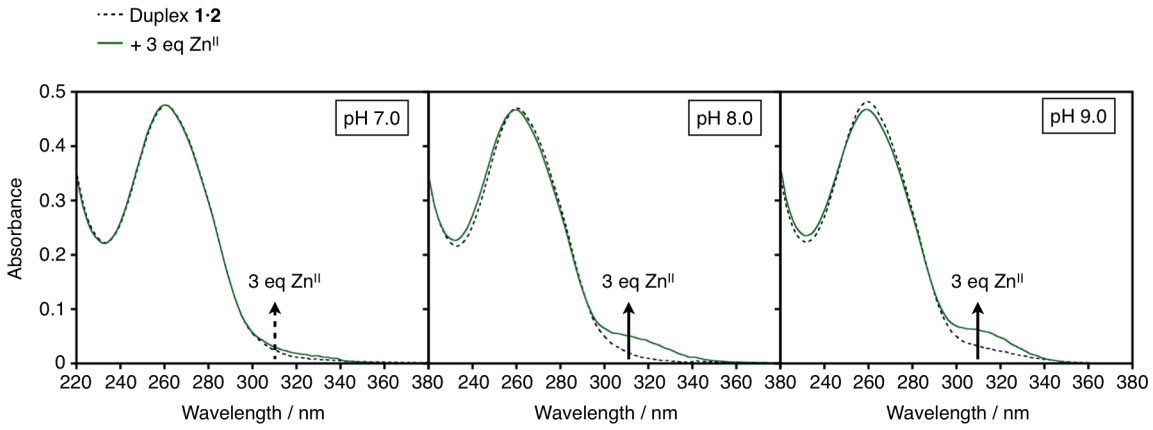

Figure 3-12. UV absorption spectra of DNA duplex **1·2** in the absence and in the presence of of Zn^{II} ions at different pH. [duplex] = 2 μM, [$ZnSO_4$]/[duplex] = 0 (black, dashed lines), 3 (green, solid lines) in 10 mM HEPES-NaOH buffer (pH 7.0 or 8.0) or CHES-NaOH buffer (pH 9.0), 100 mM NaCl, 5 °C.

In addition to the stabilization behaviors of $\mathbf{U^{OH}}$–$\mathbf{U^{OH}}$ base pairs, the pH dependence of the destabilization behavior of $\mathbf{U^{OH}}$–**A**-containing DNA duplex was examined. Melting analysis was conducted for duplex **1·2A**, which has three $\mathbf{U^{OH}}$–**A** base pairs, at pH 7.0–9.0. Figure 3-13 shows melting curves of duplex **1·2A** in the absence and in the presence of Zn^{II} ions. At pH 8.0 and 9.0, duplex **1·2A** was destabilized upon addition of 3 equivalents of Zn^{II} ions. In contrast, almost no spectral changes were observed at pH 7.0. As with the Zn^{II}-induced stabilization, this result indicates that the Zn^{II}-induced destabilization of $\mathbf{U^{OH}}$–**A** base pairs was also affected by pH.

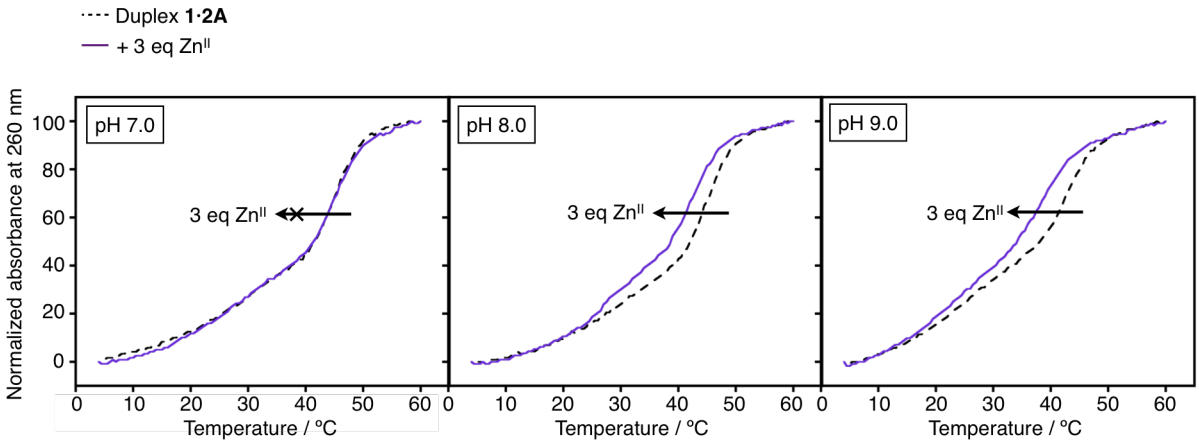

Figure 3-13. Melting curves of DNA duplex **1·2A** in the absence and in the presence of 3 equivalents of Zn^{II} ions. [duplex] = 2 μM, [$ZnSO_4$]/[duplex] = 0 (black, dashed lines), 3 (purple, solid lines) in 10 mM HEPES-NaOH buffer (pH 7.0 or 8.0) or 10 mM CHES-NaOH buffer (pH 9.0), 100 mM NaCl, 0.2 °C/min.

In section **3-3**, I mentioned that the Gd^{III} complexation of $\mathbf{U^{OH}}$ nucleobases adapts the DNA hybridization preference. Thus, it was expected that both the Zn^{II}-mediated stabilization and destabilization differently altered the DNA hybridization preference in a pH-dependent manner. Figure 3-14 indicates the difference in T_m values (ΔT_m) between the $\mathbf{U^{OH}}$–**A**-containing DNA duplex **1·2A** ($T_{m\mathbf{1\cdot 2A}}$) and the $\mathbf{U^{OH}}$–$\mathbf{U^{OH}}$-containing duplex **1·2** ($T_{m\mathbf{1\cdot 2}}$) in the range from pH 7.0 to 9.0. In the absence of metal ions, ΔT_m values were around +20 °C independent on pH. This result

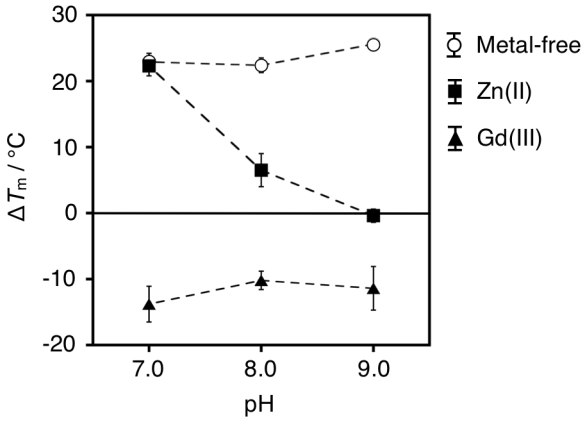

Figure 3-14. Difference of T_m values (ΔT_m) between the $\mathbf{U^{OH}}$–**A**-containing DNA duplex **1·2A** ($T_{m\mathbf{1\cdot 2A}}$) and the $\mathbf{U^{OH}}$–$\mathbf{U^{OH}}$-containing duplex **1·2** ($T_{m\mathbf{1\cdot 2}}$) in the absence and in the presence of Gd^{III} and Zn^{II} ions at several pH. [duplex] = 2 μM, [metal salt]/[duplex] = 0, 3 in 10 mM HEPES-NaOH buffer (pH 7.0 or 8.0) or 10 mM CHES-NaOH buffer (pH 9.0), 100 mM NaCl, 0.2 °C/min. Error bars indicate the standard deviations.

represents the duplex **1·2A** is more stable than the duplex **1·2** due to the hydrogen-bonded $\mathbf{U^{OH}}$–**A** base pairing. In contrast, upon addition of 3 equivalents of Gd^{III} ions, ΔT_m was negative. Duplex **1·2** with Gd^{III} ions is constantly more stable than duplex **1·2A** as the result of Gd^{III}-mediated stabilization of $\mathbf{U^{OH}}$–$\mathbf{U^{OH}}$ base pairs as well as destabilization of $\mathbf{U^{OH}}$–**A** base pairs. In the presence of Zn^{II} ions, ΔT_m values were largely changed depending on the pH values. Whereas the stability of duplex **1·2A** is higher than that of duplex **1·2** at pH 7.0 and 8.0, these T_m values are almost identical with each other at pH 9.0. This should be attributed to the pH-dependent stabilization of $\mathbf{U^{OH}}$–$\mathbf{U^{OH}}$ and the Zn^{II}-mediated destabilization of $\mathbf{U^{OH}}$–**A**.

It has been previously reported that some metal-mediated base pairs exhibit pH dependence. Ono et al. found that 5-cyano- and 5-halogen-substituted uracil nucleobases formed Ag^{I}-mediated homo base pairs. This base pairing stabilized DNA duplexes more effectively at higher pH.[15] Carell et al. demonstrated that a synthetic pyrazole-type ligand-bearing nucleobase conferred pH-dependent Cu^{II}-mediated base pairing.[16] Similarly to these examples, the $\mathbf{U^{OH}}$–Zn^{II}–$\mathbf{U^{OH}}$ base pairing stabilizes the resulting DNA duplex in a pH-dependent manner. It is worthy of note that the Zn^{II} complexation also destabilizes hydrogen-bonded $\mathbf{U^{OH}}$–**A** base pairs and thereby alters the hybridization preference only at basic pH. This dual-responsiveness by Zn^{II} and pH would help to construct pH-driven DNA nanomachines[17,18] and pH sensors[19] as well as logic gates[20–22].

3-5. Summary

I found that the DNA hybridization preference of $\mathbf{U}^{\mathbf{OH}}$-containing DNA strands can be controlled by the binding of Gd^{III} ions to $\mathbf{U}^{\mathbf{OH}}$ nucleobases (Figure 3-15a). These behaviors are due to the metal-mediated thermal stabilization of $\mathbf{U}^{\mathbf{OH}}$–$\mathbf{U}^{\mathbf{OH}}$ base pairs (Figure 3-15b) and the destabilization of $\mathbf{U}^{\mathbf{OH}}$–**A** base pairs (Figure 3-15c). Thus, the metal-responsive bifacial base-pairing behaviors of $\mathbf{U}^{\mathbf{OH}}$ nucleobase were successfully demonstrated. This unique ability of $\mathbf{U}^{\mathbf{OH}}$ nucleobase would induce DNA strand exchange reactions in response to Gd^{III} ions through base pair switching between $\mathbf{U}^{\mathbf{OH}}$–Gd^{III}–$\mathbf{U}^{\mathbf{OH}}$ and $\mathbf{U}^{\mathbf{OH}}$–**A** base pairs.

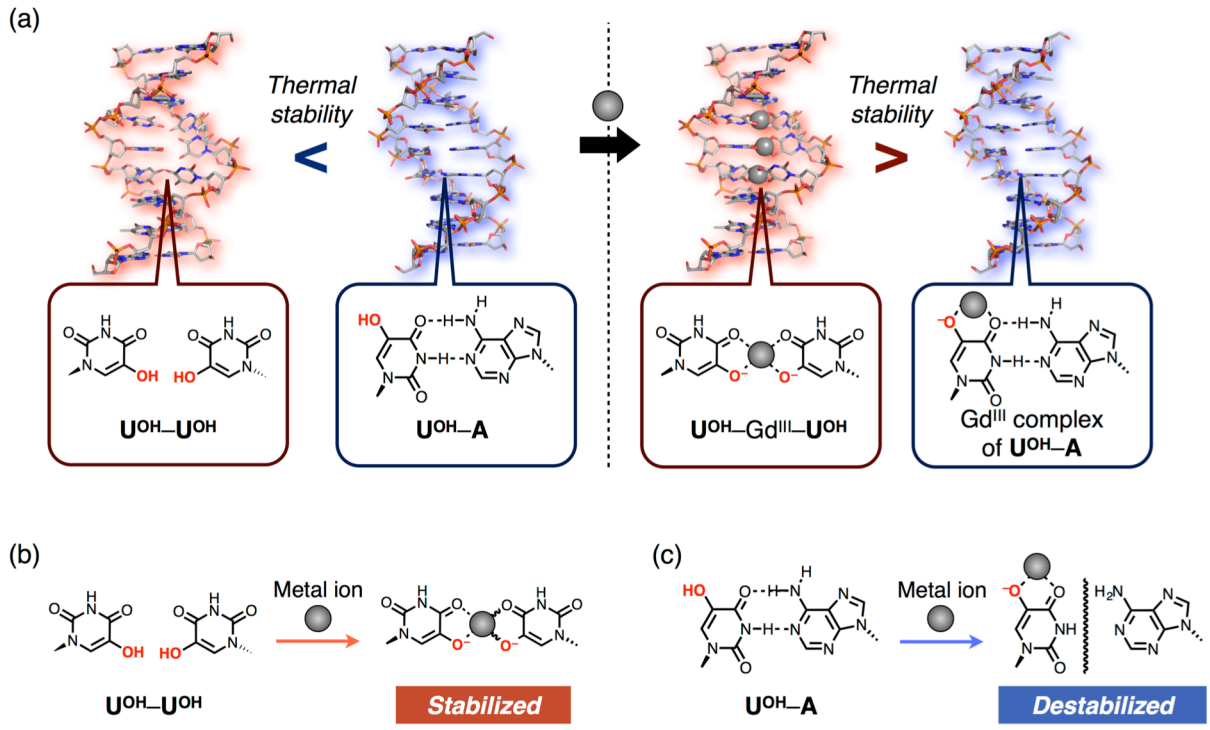

Figure 3-15. (a) Control of the DNA hybridization preference of $\mathbf{U}^{\mathbf{OH}}$-containing DNA strands. (b) The thermal DNA stabilization through $\mathbf{U}^{\mathbf{OH}}$–Gd^{III}–$\mathbf{U}^{\mathbf{OH}}$ base pairs. (c) The thermal destabilization of $\mathbf{U}^{\mathbf{OH}}$–**A** base pairs by the Gd^{III} binding.

Moreover, the Zn^{II}-specific pH dependence in the stabilization and the destabilization was demonstrated (Figure 3-16). This Zn^{II}-pH dual responsiveness would show promise in the development of DNA-based dynamic nanoarchitectures and logic gates.

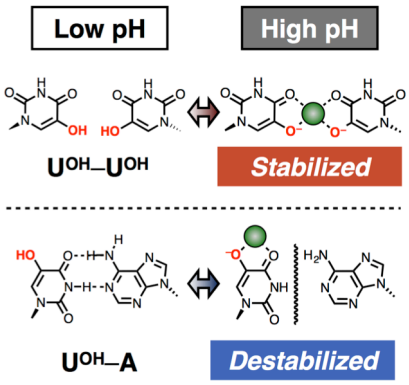

Figure 3-16. Schematic representation of the Zn^{II}-induced stabilization and destabilization in a pH-dependent manner.

3-6. Experimental section

Metal sources

Metal sources were purchased from Soekawa Chemical Co. [$ZnSO_4 \cdot 7H_2O$ (99.9%), $GdCl_3 \cdot 6H_2O$ (99.9%)].

Sample preparation

All samples for the spectroscopic studies were prepared by mixing the DNA strands (2 μM) in 10 mM HEPES-NaOH buffer (pH 7.0 or 8.0) or CHES-NaOH buffer (pH 9.0) containing 100 mM NaCl. After addition of metal ions, the solutions were heated to 85 °C and cooled to 4 °C at the rate of –1.0 °C/min.

Melting analysis

Absorbance at 260 nm was recorded on a UV-1700 spectrophotometer (Shimadzu) equipped with a TMSPC-8 temperature controller while the temperature was raised from 4 °C to 60 °C at the rate of 0.2 °C/min. A drop of mineral oil was laid on the sample to prevent the evaporation. Normalized absorbance shown in the Figures were calculated as follows:

$$\textit{Normalized Absorbance at 260 nm} = \{Abs_{260}(t\ ^\circ\mathrm{C}) - Abs_{260}(4\ ^\circ\mathrm{C})\}/\{Abs_{260}(60\ ^\circ\mathrm{C}) - Abs_{260}(4\ ^\circ\mathrm{C})\} \times 100$$

The melting temperatures (T_m) were determined as an inflection point of a melting curve using a T_m analysis software LabSolutions (Shimadzu) with a 17-point adaptive smoothing program. The T_m values are averages of at least 3 runs.

UV spectra

UV spectra were recorded on a Hitachi U-3500 spectrophotometer with a path length of 1.0 cm at 5 °C.

3-7. References

[1] N. Branda, G. Kurz, J.-M. Lehn, *Chem*. *Commun*. **1996**, *32*, 2443–2444.

[2] D. L. Chen, M. Meena, S. K. Sharma, L. W. McLaughlin, *J*. *Am*. *Chem*. *Soc*. **2004**, *126*, 70–71.

[3] H. Chen, M. Meena, L. W. McLaughlin, *J*. *Am*. *Chem*. *Soc*. **2008**, *130*, 13190–13191.

[4] D. Shin, Y. Tor, *J*. *Am*. *Chem*. *Soc*. **2011**, *133*, 6926–6929.

[5] V. Thiviyanathan, A. Somasunderam, D. E. Volk, D. G. Gorenstein, *Chem*. *Commun*. **2005**, *41*, 400–402.

[6] V.Thiviyanathan, A. Somasunderam, D. E. Volk, T. K. Hazra, S. Mitra, D. G. Gorenstein, *Biochem*. *Biophys*. *Res*. *Commun*. **2008**, *366*, 752–757.

[7] C. J. La Francois, Y. H. Jang, T. Cagin, W. A. Goddard, L. C. Sowers, *Chem*. *Res*. *Toxicol*. **2000**, *13*, 462–470.

[8] E. Kimura, H. Kitamura, T. Koike, M. Shiro, *J*. *Am*. *Chem*. *Soc*. **1997**, *119*, 10909–10919.

[9] B. Lippert, *Chem*. *Biodiversity* **2008**, *5*, 1455–1474.

[10] P. M. Takahara, A. C. Rosenzweig, C. A. Frederick, S. J. Lippard, *Nature* **1995**, 377, 649–652.

[11] N. Poklar, D. S. Pilch, S. J. Lippard, E. A. Redding, S. U. Dunham, K. J. Breslauer, *Proc*. *Natl*. *Acad*. *Sci*. *U*. *S*. *A*. **1996**, *93*, 7606–7611.

[12] B. Yurke, A. J. Turberfield, A. P. Mills Jr., F. C. Simmel, J. L. Neumann, *Nature* **2000**, *406*, 605–608.

[13] R. P. Goodman, M. Heilemann, S. Doose, C. M. Erben, A. N. Kapanidis, A. J. Turberfield, *Nat*. *Nanotechnol*. **2008**, *3*, 93–96.

[14] E. S. Andersen, M. Dong, M. M. Nielsen, K. Jahn, R. Subramani, W. Mamdouh, M. M. Golas, B. Sander, H. Stark, C. L. P. Oliveira, J. S. Pedersen, V. Birkedal, F. Besenbacher, K. V. Gothelf, J. Kjems, *Nature* **2009**, *459*, 73–76.

[15] I. Okamoto, K. Iwamoto, Y. Watanabe, Y. Miyake, A. Ono, *Angew*. *Chem*. *Int*. *Ed*. **2009**,

48, 1648–1651.

[16] M. Su, M. Tomás-Gamasa, T. Carell, *Chem*. *Sci*. **2015**, *6*, 632–638.

[17] E. Cheng, Y. Xing, P. Chen, Y. Yang, Y. Sun, D. Zhou, L. Xu, Q. Fan, D. Liu, *Angew*. *Chem*. *Int*. *Ed*. **2009**, *48*, 7660–7663.

[18] C. Wang, Y. Tao, F. Pu, J. Ren, X. Qua, *Soft*. *Matter*. **2011**, *7*, 10574–10576.

[19] A. Idili, A. Vallée-Bélisle, F. Ricci, *J*. *Am*. *Chem*. *Soc*. **2014**, *136*, 5836–5839.

[20] D. Miyoshi, M. Inoue, N. Sugimoto, *Angew*. *Chem*. *Int*. *Ed*. **2006**, *45*, 7716–7719.

[21] H. Liu, Y. Zhou, Y. Yang, W. Wang, L. Qu, C. Chen, D. Liu, D. Zhang, D. Zhu, *J. Phys. Chem. B* **2008**, *112*, 6893–6896.

[22] L. Xu, Y. Guo, J. Wang, L. Zhou, Y. Zhang, S. Hong, Z. Wang, J. Zhang, R. Pei, *Chem*. *Asian*. *J*. **2015**, *10*, 1126–1129.

Chapter 4.

Metal-driven DNA strand exchange reactions through base pair switching of 5-hydroxyuracils

4-1. Introduction

DNA strand exchange/displacement reactions are essential events not only in biological systems[1] but also in DNA-based nanotechnology.[2–6] Without the aid of recombinase enzymes, "toeholds" are usually required to promote DNA strand exchange reactions, in which the products are more thermally stable DNA duplexes.[6] In this system, an additional DNA strand is utilized to trigger the reaction. Recently, strand exchange reactions have been controlled by external stimuli such as small molecules[7], light[8,9], pH[10–12], and metal ions[11–13]. These stimuli-responsive exchange reactions have powerful potential as key technologies for DNA nanomachines, DNA-based drug delivery systems, and logic gates.[14,15]

In this section, I describe metal-responsive DNA strand exchange reactions based on the bifacial base-pairing behaviors of 5-hydroxyuracil ($\mathbf{U^{OH}}$) nucleobase (Figure 4-1). In section **3-3**, $\mathbf{U^{OH}}$ nucleobases were found to preferentially form $\mathbf{U^{OH}}$–**A** base pairs without Gd^{III} ions and $\mathbf{U^{OH}}$–Gd^{III}–$\mathbf{U^{OH}}$ base pairs with Gd^{III} ions. Thus, it was expected that strand exchange reaction proceeds through the base pair switching of $\mathbf{U^{OH}}$ nucleobases from $\mathbf{U^{OH}}$–**A** to $\mathbf{U^{OH}}$–Gd^{III}–$\mathbf{U^{OH}}$ base pairs upon addition of Gd^{III} ions. Moreover, the exchange reaction would proceed to the reverse direction by removal of Gd^{III} ions.

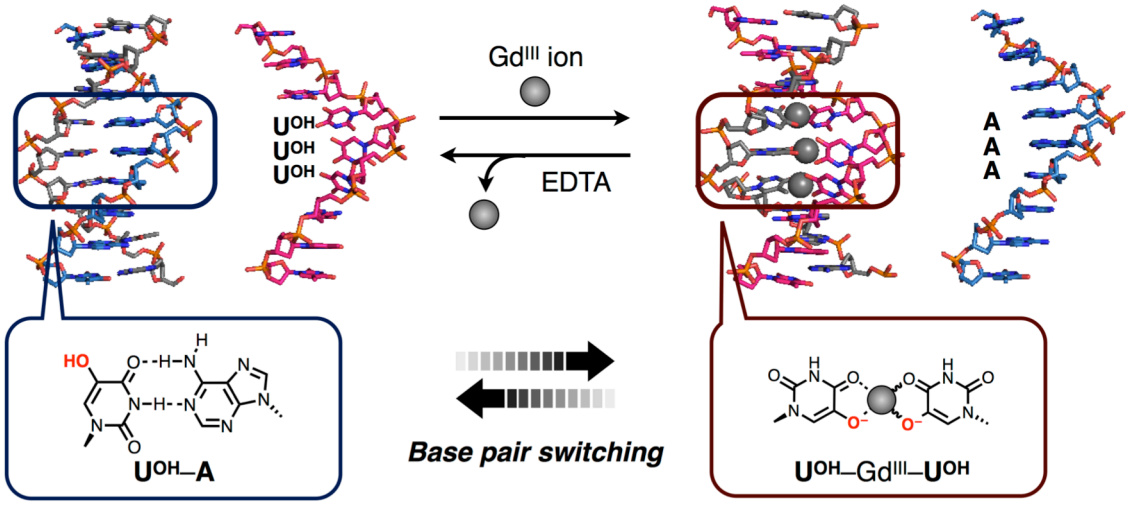

Figure 4-1. Schematic representation of DNA strand exchange reactions through the base pair switching of $\mathbf{U^{OH}}$ nucleobases between $\mathbf{U^{OH}}$–**A** and $\mathbf{U^{OH}}$–Gd^{III}–$\mathbf{U^{OH}}$ base pairs.

4-2. Effects of Gd^{III} ions on DNA hybridization patterns

To achieve metal-mediated DNA strand exchange reactions, I investigated DNA hybridization patterns in the absence and in the presence of Gd^{III} ions and subsequently optimized the conditions (Figure 4-2). First, the template DNA strand **1**, containing three $\mathbf{U^{OH}}$ nucleobases, and its complementary strands **2A** and **2** were utilized (Table 4-1). As described in **chapters 2** and **3**, the strand **1** hybridizes both with the strands **2A** and **2** through three hydrogen-bonded $\mathbf{U^{OH}}$–**A** and three metal-mediated $\mathbf{U^{OH}}$–Gd^{III}–$\mathbf{U^{OH}}$ base pairs, respectively (Figure 4-2a). Equimolar amounts of three DNA strands **1**, **2A**, and **2** were mixed in the absence and in the presence of Gd^{III} ions and then the reaction mixtures were annealed to form thermodynamically stable products (Figure 4-2b). The hybridization patterns were quantitatively analyzed.

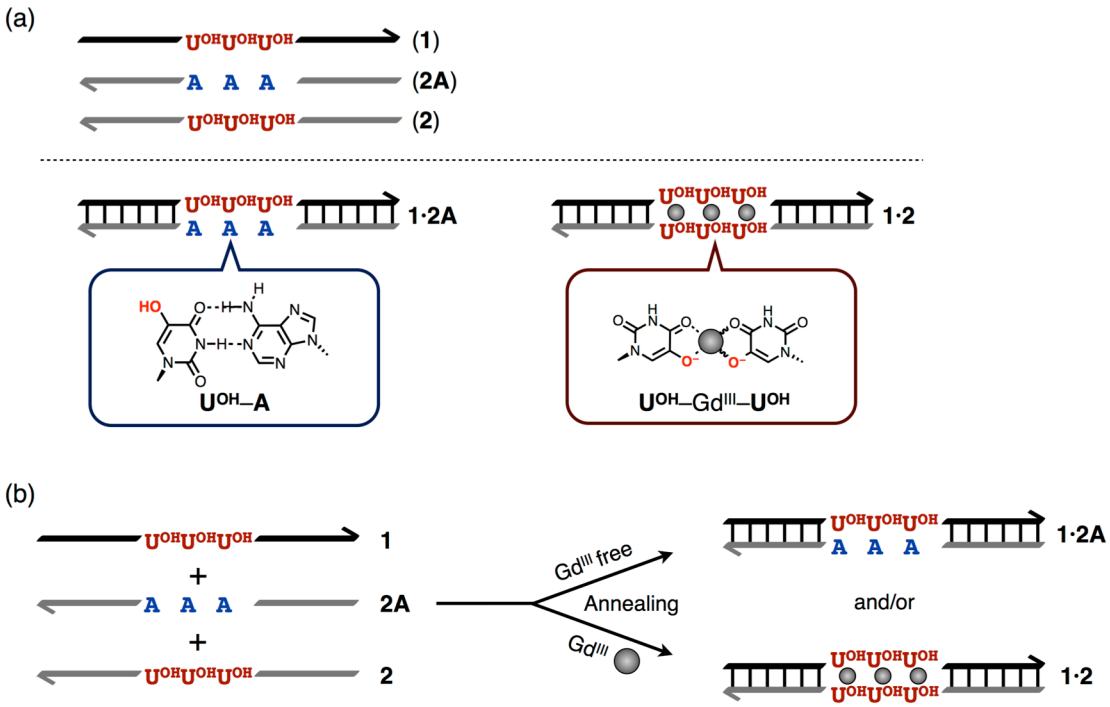

Figure 4-2. (a) The template DNA strand **1** and its complementary DNA strands **2A** and **2** used. The template strand **1** hybridizes with strands **2A** and **2** through the $\mathbf{U^{OH}}$–**A** and $\mathbf{U^{OH}}$–Gd^{III}–$\mathbf{U^{OH}}$ base pairs, respectively. (b) Schematic representation of DNA hybridization patterns of the template DNA strand **1**. The thermodynamically stable product(s), that is, DNA duplexes **1·2A** and/or **1·2**, were obtained through the annealing process.

Table 4-1. Sequences of DNA strands used.

Name	Sequence (5′ to 3′)
1	CAC ATT $\mathbf{U^{OH}U^{OH}U^{OH}}$ GTT GTA
2A	TAC AAC **AAA** AAT GTG
2A (labeled by 6-FAM)	FAM-TAC AAC **AAA** AAT GTG
2	TAC AAC $\mathbf{U^{OH}U^{OH}U^{OH}}$ AAT GTG
2 (labeled by 6-FAM)	FAM-TAC AAC $\mathbf{U^{OH}U^{OH}U^{OH}}$ AAT GTG
5	CAC ATT $\mathbf{U^{OH}U^{OH}U^{OH}U^{OH}}$ GTT GTA
6A	TAC AAC **AAAA** AAT GTG
6A (labeled by 6-FAM)	FAM-TAC AAC **AAAA** AAT GTG
6	TAC AAC $\mathbf{U^{OH}U^{OH}U^{OH}U^{OH}}$ AAT GTG
6T	TAC AAC **TTTT** AAT GTG

Native polyacrylamide gel electrophoresis (PAGE) was conducted to analyze the hybridization products. The 5′-terminal of DNA strand **2A** was labeled by 6-FAM as a fluorescence tag to detect the products on the gels. Mobility of the gel bands was compared with those of duplex **1·2A** and single strand **2A** to characterize the products. Based on the fluorescence intensity of these bands, the yields of single- and double-stranded DNAs were calculated. In the absence of Gd^{III} ions, the gel band indicated that the template strand **1** quantitatively hybridized with the strand **2A** through the hydrogen-bonded base pairing including $\mathbf{U^{OH}}$–**A** (Figure 4-3a, lane 3). In contrast, upon addition of 3 equivalents of Gd^{III} ions, the strand **2A** was ascribed to the double-stranded **1·2A** and

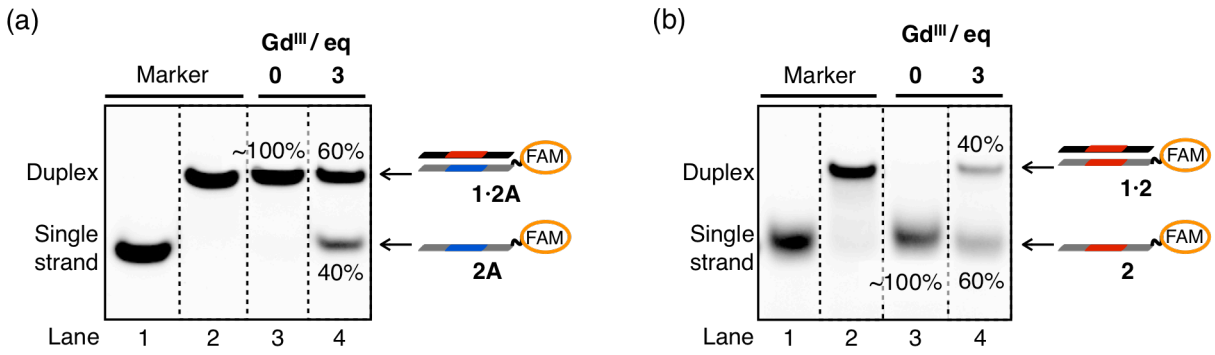

Figure 4-3. Native PAGE analysis to investigate the DNA hybridization patterns of the template DNA strand **1** with the complementary DNA strands **2A** and **2**. (a) [DNA strand] = 2 μM for each, [$GdCl_3$]/[DNA strand] = 0 (lanes 1, 2, 3) 3 (lanes 4) in 10 mM HEPES-NaOH buffer (pH 8.0), 100 mM NaCl. 20% gel, TAMg buffer (pH 8.0), at 4 °C. The DNA strand **2A** (a) or **2** (b) was labeled by 6-FAM as a fluorescence tag.

the single-stranded **2A** in the ratio of 6:4 (Figure 4-3a, lane 4). Thus, the strand **1** was likely to partially hybridize with the $\mathbf{U^{OH}}$-containing strand **2** through the formation of $\mathbf{U^{OH}}$–Gd^{III}–$\mathbf{U^{OH}}$ base pairs.

The FAM-labeled DNA strand **2** was then prepared to directly detect the metallo-DNA duplex on the gel. A mixture of strand **1**, FAM-labeled **2**, and label-free **2A** was annealed and the hybridization patterns were analyzed on the same protocol. The DNA duplex **1·2** was not formed in the absence of Gd^{III} ions (Figure 4-3b, lane 3). In contrast, the duplex **1·2** with Gd^{III} was generated in ca. 40% in the presence of Gd^{III} ions. These results exactly agreed with the previous results by using the FAM-labeled strand **2A** as shown in Figure 4-3a. Thus, it was concluded that the complexation of $\mathbf{U^{OH}}$ nucleobases with Gd^{III} altered the hybridization patterns of the $\mathbf{U^{OH}}$-containing DNA strand **1** although the yield of the metallo-DNA duplex was relatively low.

To raise the efficiency of the formation of the metallo-DNA duplex, the number of $\mathbf{U^{OH}}$ nucleobases incorporated was increased. A DNA strand **5**, containing four $\mathbf{U^{OH}}$ nucleobases, and its complementary DNA strands **6A** and **6** (Table 4-1) were prepared. These strands can form DNA duplexes **5·6A** and **5·6** through the formation of $\mathbf{U^{OH}}$–**A** and $\mathbf{U^{OH}}$–Gd^{III}–$\mathbf{U^{OH}}$ base pairs, respectively. To investigate the effects of the number of $\mathbf{U^{OH}}$ nucleobases on the DNA hybridization preference, melting experiments were conducted for DNA duplexes **5·6A** and **5·6**. The T_m values of duplexes **1·2A** and **1·2** as well as those of duplexes **5·6A** and **5·6** are shown in Figure 4-4. In addition, the differences in T_m values (ΔT_m) between the $\mathbf{U^{OH}}$–**A**- and the $\mathbf{U^{OH}}$–$\mathbf{U^{OH}}$-containing duplexes are also indicated. In the absence of metal ions, the ΔT_m values of the three-$\mathbf{U^{OH}}$ system and of the four-$\mathbf{U^{OH}}$ systems are +22 °C and +29 °C, respectively. The ΔT_m values of the three-$\mathbf{U^{OH}}$ system with 3 equivalents of Gd^{III} and of the four-$\mathbf{U^{OH}}$ systems with 4 equivalents of Gd^{III} are –10 °C and –14 °C, respectively. Thus, the stability difference between the $\mathbf{U^{OH}}$–**A**- and the $\mathbf{U^{OH}}$–$\mathbf{U^{OH}}$-containing duplexes in the four-$\mathbf{U^{OH}}$ system was larger than that in the three-$\mathbf{U^{OH}}$ system. It was expected that the DNA hybridization patterns are more clearly altered by complexation with Gd^{III} in the four-$\mathbf{U^{OH}}$ system.

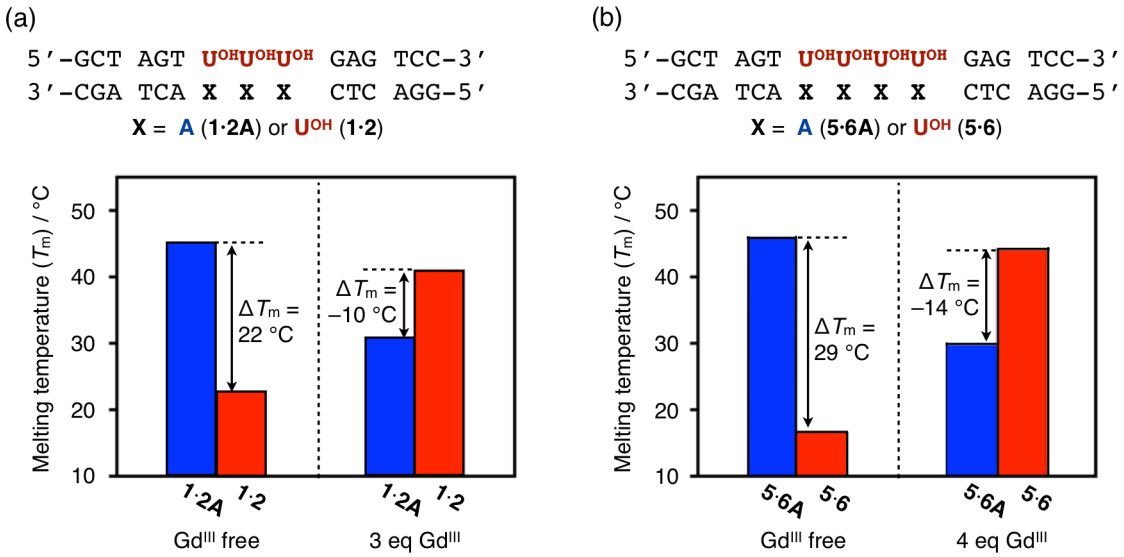

Figure 4-4. Melting temperatures (T_m) of the DNA duplexes containing three and four $\mathbf{U^{OH}}$–**X** base pairs [**X** = **A** and $\mathbf{U^{OH}}$]. [duplex] = 2 μM, [$GdCl_3$]/[duplex] = 0, 3 (a), 4 (b) in 10 mM HEPES-NaOH buffer (pH 8.0), 100 mM NaCl. (a) $\Delta T_m = T_{m\mathbf{1\cdot2A}} - T_{m\mathbf{1\cdot2}}$; $T_{m\mathbf{1\cdot2A}}$ and $T_{m\mathbf{1\cdot2}}$ represent the T_m values of the DNA duplexes **1·2A** and **1·2**, respectively. (b) $\Delta T_m = T_{m\mathbf{5\cdot6A}} - T_{m\mathbf{5\cdot6}}$; $T_{m\mathbf{5\cdot6A}}$ and $T_{m\mathbf{5\cdot6}}$ represent the T_m values of the DNA duplexes **5·6A** and **5·6**, respectively.

The native PAGE analysis was conducted for the annealed mixture of the template DNA strand **5** containing four $\mathbf{U^{OH}}$ nucleobases, and its complementary DNA strands **6A** and **6**. The natural strand **6A** was labeled by 6-FAM. In the absence of Gd^{III} ion, the DNA duplex **5·6A**, containing four $\mathbf{U^{OH}}$–**A** base pairs, was quantitatively observed (Figure 4-5, lane 3). In the presence of 4 equivalents of Gd^{III} ions, the FAM-labeled DNA strand **6A** was detected as a single strand in ca.

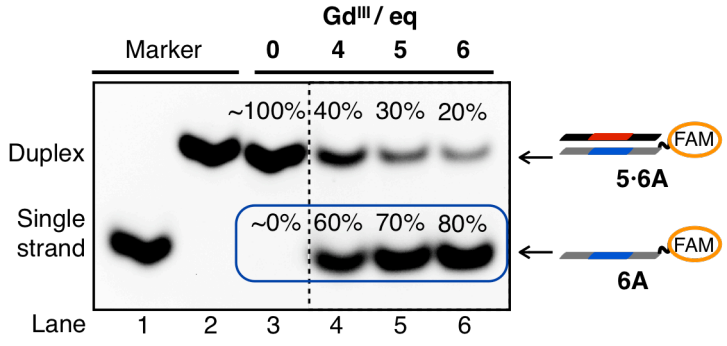

Figure 4-5. Native PAGE analysis to investigate the DNA hybridization patterns of the template DNA strand **5** with the complementary DNA strands **6A** and **6**. (a) [DNA strand] = 2 μM for each, [$GdCl_3$]/[DNA strand] = 0 (lanes 1, 2, 3), 4 (lanes 4), 5 (lane 5), 6 (lane 6), in 10 mM HEPES-NaOH buffer (pH 8.0), 100 mM NaCl. 20% gel, TAMg buffer (pH 8.0), at 4 °C. DNA strand **6A** was labeled by 6-FAM as a fluorescence tag.

60% (Figure 4-5, lane 4). This result suggested that 60% of strand **5** hybridized with the $\mathbf{U^{OH}}$-containing strand **6** through the formation of the $\mathbf{U^{OH}}$–Gd^{III}–$\mathbf{U^{OH}}$ base pairs. Compared with the three-$\mathbf{U^{OH}}$ system as shown in Figure 4-3, the yield of the metallo-DNA duplex was increased by 20%. Furthermore, more than 4 equivalents of Gd^{III} ions were added to further improve the efficiency. As the result, the ratio was raised up to 80% in the presence of 6 equivalents of Gd^{III} ions (Figure 4-5, lanes 5, 6). Thus, when a mixture of strand **5** and complementary strands **6A** and **6** was annealed, the DNA duplex **5·6A** and **5·6** were preferentially formed in the absence and in the presence of 6 equivalents of Gd^{III} ions, respectively.

4-3. Reversible DNA strand exchange reactions induced by addition and removal of Gd^{III} ions

Herein I describe the DNA strand exchange reactions through the base pair switching between $\mathbf{U^{OH}}$–**A** and $\mathbf{U^{OH}}$–Gd^{III}–$\mathbf{U^{OH}}$ base pairs. In section **4-2**, the DNA hybridization patterns of template DNA strand **5**, containing four $\mathbf{U^{OH}}$ nucleobases, were found to be regulated by complexation with Gd^{III}. In this section, the reaction was conducted under an isothermal condition, that is, at a certain temperature (Figure 4-6).

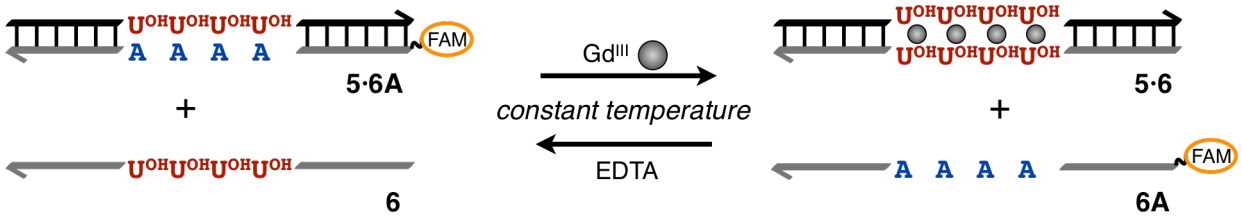

Figure 4-6. The DNA strand exchange reactions at a certain temperature. After the three DNA strands **5**, **6A**, and **6** are mixed and annealed without Gd^{III} ions, Gd^{III} ion was added to the annealed DNA strands, and then the reaction mixture was incubated.

When three DNA strands **5**, **6A**, and **6** were mixed and annealed without Gd^{III} ions, both DNA duplex **5·6A** and single strand **6** were quantitatively formed. Gd^{III} was added to trigger the strand exchange and then the reaction mixture was incubated for 0 to 22 h. Based on the results of the melting analysis as shown in Figure 4-4b, the reaction temperature was kept constant at 30 °C, where the proposed products, that is, DNA duplexes **5·6A** and **5·6** would not be dissociated without and with Gd^{III}, respectively. The products were analyzed by native PAGE, in which **6A** was labeled by 6-FAM. Figure 4-7 shows the results of native PAGE analysis after the strand exchange reactions in the absence and in the presence of 6 equivalents of Gd^{III} ions. Without Gd^{III} ions, the gel bands derived from the $\mathbf{U^{OH}}$–**A**-containing duplex **5·6A** was not changed even after 22 h (Figure 4-7a). In contrast, upon addition of Gd^{III} ions, the DNA duplex **5·6A** was gradually dissociated into single strands in up to 80% yield. This observation suggested the DNA strand exchange reaction proceeded even at the given temperature and eventually a metallo-DNA of **5·6** with Gd^{III} ions was formed. The highest conversion yield was comparable to the yield of the thermodynamically stable

products obtained through the annealing process. Thus, the strand exchange reaction reached the end after 22 h.

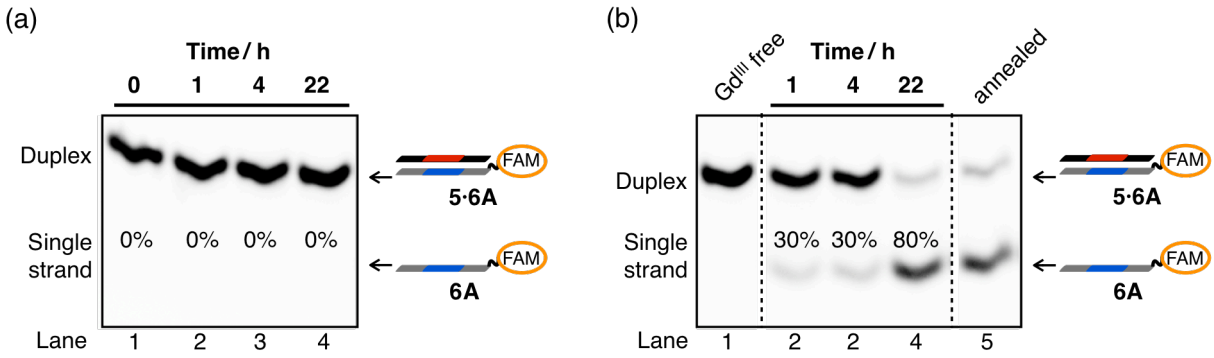

Figure 4-7. Native PAGE analysis to investigate the DNA strand exchange reactions by using the template DNA strand **5** and the complementary strands **6A** and **6**. [DNA strand] = 2 μM for each, [$GdCl_3$]/[DNA strand] = 0 (a, lane 1 of b), 6 (lanes 2–5 of b), in 10 mM HEPES-NaOH buffer (pH 8.0), 100 mM NaCl, 30 °C for 0–22 h. 20% gel, TAMg buffer (pH 8.0), at 4 °C. The DNA strand **6A** was labeled by 6-FAM as a fluorescence tag.

A control experiment was also conducted to confirm if the exchange reaction occurs based on the base pair switching of $\mathbf{U}^{\mathbf{OH}}$ nucleobases based on the complexation with Gd^{III}. Its complementary DNA strand **6T** was utilized instead of strand **6**, in which four $\mathbf{U}^{\mathbf{OH}}$ nucleobases were fully replaced by **T** (Table 4-1). Native PAGE analysis showed that the addition of Gd^{III} did not induce the strand exchange reaction (Figure 4-8). This result strongly supported that the formation of $\mathbf{U}^{\mathbf{OH}}$–Gd^{III}–$\mathbf{U}^{\mathbf{OH}}$ base pairs is a key process for the DNA strand exchange reaction through the base pair switching.

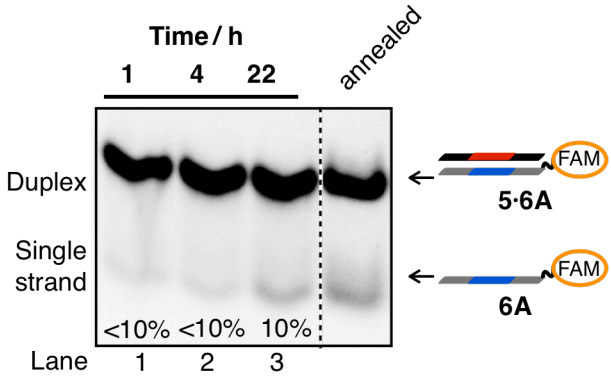

Figure 4-8. Native PAGE analysis to investigate the DNA strand exchange reactions by using the template DNA strand **5** and the complementary strands **6A** and **6T**. [DNA strand] = 2 μM for each, [$GdCl_3$]/[DNA strand] = 6, in 10 mM HEPES-NaOH buffer (pH 8.0), 100 mM NaCl, 30 °C for 1–22 h. 20% gel, TAMg buffer (pH 8.0), at 4 °C. The DNA strand **6A** was labeled by 6-FAM as a fluorescence tag.

Next, the reverse DNA strand exchange reaction was examined by the removal of Gd^{III} ions. EDTA was chosen as a chelate reagent to remove the Gd^{III} ions bound to $\mathbf{U^{OH}}$ nucleobases. When a mixture of DNA strands **5**, **6A**, and **6** with 6 equivalents of Gd^{III} ions was annealed, a mixture of the metallo-DNA of **5·6** with Gd^{III} and the DNA duplex **5·6A** was obtained in the ratio of 8:2. Equimolar amount of EDTA against Gd^{III} ions was then added to trigger the strand exchange in the reverse direction. Figure 4-9 indicates the results of native PAGE analysis after incubation at 30 °C for 1, 4, and 22 h. As expected, the Gd^{III} complex of **5·6** was dissociated and then the DNA duplex **5·6A** was formed even after 1 h. It was concluded that the DNA strand exchange reaction proceeded to the reverse direction by removing Gd^{III} ions by using EDTA. The exchange reactions would be repeatable because Gd^{III} ions can be quantitatively trapped by equimolar amount of EDTA.

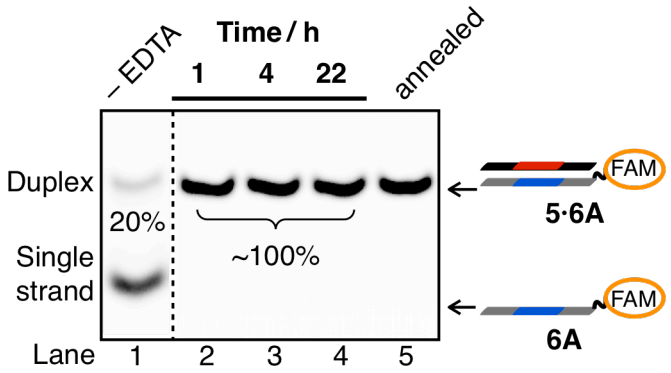

Figure 4-9. Native PAGE analysis to investigate the EDTA-induced reverse DNA strand exchange reactions by using the template DNA strand **5** and the complementary strands **6A** and **6** with Gd^{III} ions. [DNA strand] = 2 μM for each, [$GdCl_3$]/[DNA strand] = 6, [EDTA]/[DNA strand] = 0 (lane 1), 6 (lanes 2–5), in 10 mM HEPES-NaOH buffer (pH 8.0), 100 mM NaCl, 30 °C for 1–22 h. 20% gel, TAMg buffer (pH 8.0), at 4 °C. DNA strand **6A** was labeled by 6-FAM as a fluorescence tag.

The Gd^{III}- and EDTA-induced DNA strand exchange reactions require approximately 1 day and less than 1 h, respectively, for completion. In general, the toehold-mediated strand displacement reactions are faster (e.g. less than 1 h[16]) than the strand exchange reactions in full-matched DNA duplexes (e.g. longer than 1 day[17]). In the case of the Gd^{III}-induced strand exchange, the starting DNA duplex containing the $\mathbf{U^{OH}}$–A base pairs is relatively stable (T_m = ca. 30 °C) even after the destabilization by complexation with Gd^{III}. On the other hand, in the case of the $\mathbf{U^{OH}}$-based EDTA-induced reverse reaction, the starting duplex containing mismatched $\mathbf{U^{OH}}$–$\mathbf{U^{OH}}$ base pairs is unstable (T_m = ca. 17 °C) after the removal of Gd^{III} ions. Thus, the central $\mathbf{U^{OH}}$–$\mathbf{U^{OH}}$ region would be fully mismatched and would effectively interact with the nucleobases of the invading strand. The difference in the thermodynamic stability is likely to cause the difference in the reaction rate.

4-4. Summary

I have developed the metal-responsive DNA strand exchange reactions through the reversible base pair switching between $\mathbf{U^{OH}}$–**A** and $\mathbf{U^{OH}}$–Gd^{III}–$\mathbf{U^{OH}}$ base pairs. The highest conversion yield was 80% when the DNA strands containing four $\mathbf{U^{OH}}$ nucleobases and a small excess amount of Gd^{III} ions were employed. The reverse exchange reaction quickly proceeded by using equimolar amount of EDTA to remove the Gd^{III} ions bound to $\mathbf{U^{OH}}$ nucleobases.

In DNA-based nanotechnology, the toehold-mediated DNA strand exchange/displacement reaction is a cardinal technology to dynamically obtain the thermodynamically stable DNA duplexes without annealing process.[6] In the toehold-mediated systems, additional DNA strands are required to give reversibility for the strand exchange. It is worthy of note that the bifacial $\mathbf{U^{OH}}$ nucleobases allow for the bidirectional strand exchange reaction to obtain the thermodynamically stable duplexes with neither annealing process nor additional DNA strands. Thus, I believe that the $\mathbf{U^{OH}}$-based DNA strand exchange reactions serve as a new motive power of DNA-based nanomachines, logic gates, and drug delivery systems.

4-5. Experimental section

DNA synthesis

DNA oligonucleotides containing 5-hydroxyuracil ($\mathbf{U}^{\mathbf{OH}}$) nucleobases were synthesized on the same procedure as shown in section **2-7**. Unmodified and FAM-labeled $\mathbf{U}^{\mathbf{OH}}$-containing oligonucleotides purified by HPLC were purchased from Japan Bio Services and used without further purification.

Characterization of the DNA strands possessing $\mathbf{U}^{\mathbf{OH}}$ nucleosides

ODN1. Shown in section **2-7**.

ODN2. Shown in section **2-7**.

ODN5. HPLC retention time: 11.0 min (gradient: 5%A (0 min), 6%A (20 min)). ESI-MS: *m*/*z* cacld for $[C_{154}H_{194}N_{49}O_{104}P_{15} - 10H]^{10-}$: 485.0; found: 484.9. $\varepsilon_{260} = 1.33 \times 10^5\ M^{-1}\ cm^{-1}$.

ODN6. HPLC retention time: 11.0 min (gradient: 5%A (0 min), 6%A (20 min)). ESI-MS: *m*/*z* cacld for $[C_{154}H_{192}N_{55}O_{100}P_{15} - 10H]^{10-}$: 486.8; found: 486.7. $\varepsilon_{260} = 1.40 \times 10^5\ M^{-1}\ cm^{-1}$.

Metal sources

$GdCl_3 \cdot 6H_2O$ (99.9%) as a metal source was purchased from Soekawa Chemical Co.

Sample preparation

(Melting analysis) All samples were prepared by mixing the DNA strands (2 μM) in 10 mM HEPES-NaOH buffer (pH 8.0) containing 100 mM NaCl. After addition of $GdCl_3$ (0 or 8 μM), the solutions were heated to 85 °C and cooled slowly to 4 °C at the rate of –1.0 °C/min.

(Investigation of DNA hybridization patterns) All samples were prepared by mixing the DNA strands (2 μM) in 10 mM HEPES buffer (pH 8.0) containing 100 mM NaCl. After addition of $GdCl_3$ (0–12 μM), the solutions were heated to 85 °C and cooled slowly to 4 °C at the rate of –1.0 °C/min.

(DNA strand exchange) All samples were prepared by mixing the DNA strands (2 μM) and

$GdCl_3$ (0 or 12 μM) in 10 mM HEPES buffer (pH 8.0) containing 100 mM NaCl. The solutions were heated to 85 °C and cooled slowly to 4 °C at the rate of –1.0 °C/min. After addition of $GdCl_3$ (12 μM) or EDTA (12 μM) on ice, the solutions were incubated at 30 °C for 0–22 h.

Melting analysis

UV absorbance at 260 nm was recorded on a UV-1700 spectrophotometer (Shimadzu) equipped with a TMSPC-8 temperature controller while the temperature was raised from 4 °C to 60 °C at the rate of 0.2 °C/min. A drop of mineral oil was laid on the sample to prevent the evaporation.

The melting temperatures (T_m) were determined as an inflection point of a melting curve using a T_m analysis software LabSolutions (Shimadzu) with a 17-point adaptive smoothing program.

Native polyacrylamide gel electrophoresis (PAGE)

The polyacrylamide gels (20%) were prepared using TAMg buffer (40 mM Tris, 76 mM $MgCl_2$, 14 mM acetic acid, pH 8.0). The sample (10 μL) was mixed with 6× loading buffer (30% ethylene glycol, bromophenol blue, 2 μL) and applied on the gel. After running at 120 V for 3 h in the cool incubator (4 °C), the gels were observed using an Alpha imager mini (LMS) with a blue-LED transilluminator (Optocode). The conversion yield of each product was determined by comparing the band intensities of the duplex (**1·2A** or **5·6A)** with that of single strand (**2A** or **6A**), in which DNA strand **2A** and **6A** were labeled by 6-FAM.

4-6. References

[1] S. C. Kowalczykowski, A. K. Eggleston, *Annu*. *Rev*. *Biochem*. **1994**, *63*, 991–1043.

[2] B. Yurke, A. J. Turberfield, A. P. Mills Jr., F. C. Simmel, J. L. Neumann, *Nature* **2000**, *406*, 605–608.

[3] R. P. Goodman, M. Heilemann, S. Doose, C. M. Erben, A. N. Kapanidis, A. J. Turberfield, *Nat*. *Nanotechnol*. **2008**, *3*, 93–96.

[4] E. S. Andersen, M. Dong, M. M. Nielsen, K. Jahn, R. Subramani, W. Mamdouh, M. M. Golas, B. Sander, H. Stark, C. L. P. Oliveira, J. S. Pedersen, V. Birkedal, F. Besenbacher, K. V. Gothelf, J. Kjems, *Nature* **2009**, *459*, 73–76.

[5] S. F. J. Wickham, J. Bath, Y. Katsuda, M. Endo, K. Hidaka, H. Sugiyama, A. J. Turberfield, *Nat*. *Nanotechnol*. **2012**, *7*, 169–173.

[6] D. Y. Zhang, G. Seelig, *Nat*. *Chem*. **2011**, *3*, 103–113.

[7] Y. Xing, Z. Yang, D. Liu, *Angew*. *Chem*. *Int*. *Ed*. **2011**, *50*, 11934–11936.

[8] K. Morihiro, T. Kodama, R. Wakia, S. Obika, *Chem*. *Sci*. **2014**, *5*, 744–750.

[9] B. Kou, J. Zhang, X. Huai, X. Liang, S.-J. Xiao, *RSC Adv*. **2015**, *5*, 5055–5058.

[10] A. Amodio, B. Zhao, A. Porchetta, A. Idili, M. Castronovo, C. Fan, F. Ricci, *J. Am*. *Chem*. *Soc*. **2014**, *136*, 16469–16472.

[11] C.-H. Lu, A. Cecconello, J. Elbaz, A. Credi, I. Willner, *Nano Lett*. **2013**, *13*, 2303−2308.

[12] W. Tang, H. Wang, D. Wang, Y. Zhao, N. Li, F. Liu, *J. Am*. *Chem*. *Soc*. **2013**, *135*, 13628−13631.

[13] W. Ding, W. Deng, H. Zhu, H. Liang, *Chem*. *Commun*. **2013**, *49*, 9953–9955.

[14] T.-G. Cha, J. Pan, H. Chen, H. N. Robinson, X. Li, C. Mao, J. H. Choi, *J. Am*. *Chem*. *Soc*. **2015**, *137*, 9429−9437.

[15] Z. Liu, C. Tian, J. Yu, Y. Li, W. Jiang, C. Mao, *J. Am*. *Chem*. *Soc*. **2015**, *137*, 1730−1733.

[16] D. Y. Zhang, E. Winfree, *J. Am*. *Chem*. *Soc*. **2009**, *131*, 17303−17314.

[17] W. J. Kim, T. Ishihara, T. Akaike, A. Maruyama, *Chem*. *Eur*. *J*. **2001**, *7*, 176–180.

Chapter 5.

Metal-responsive triplex-forming oligonucleotides with 5-hydroxyuracils

5-1. Introduction

A triplex-forming oligonucleotide (TFO) recognizes a target double-stranded DNA in a sequence-specific manner and consequently a triple-stranded DNA is formed. The binding of TFO inhibits the access of DNA-binding proteins such as RNA polymerases.[1,2] If the association and dissociation of TFO are reversibly controlled by specific external stimuli, biological events related to DNA-binding proteins can be possibly regulated.

In **chapter 3**, I mentioned that the addition of metal ions (Gd^{III} and Zn^{II}) thermally destabilized the double-stranded DNA containing Watson–Crick-type $\mathbf{U^{OH}}$–**A** base pairs ($\mathbf{U^{OH}}$ = 5-hydroxyuracil). Thus, it was expected that a $\mathbf{U^{OH}}$-containing TFO ($\mathbf{U^{OH}}$-TFO) would recognize a target DNA duplex through formation of a $\mathbf{U^{OH}}$**·A–T** base triplet in a manner similar to a **T·A–T** base triplet (Figure 5-1). Moreover, the metal complexation of $\mathbf{U^{OH}}$ nucleobases was likely to decrease the binding ability of the $\mathbf{U^{OH}}$-TFO to the target duplex. Thus, the introduction of $\mathbf{U^{OH}}$ nucleobases would confer the metal responsiveness on the TFOs.

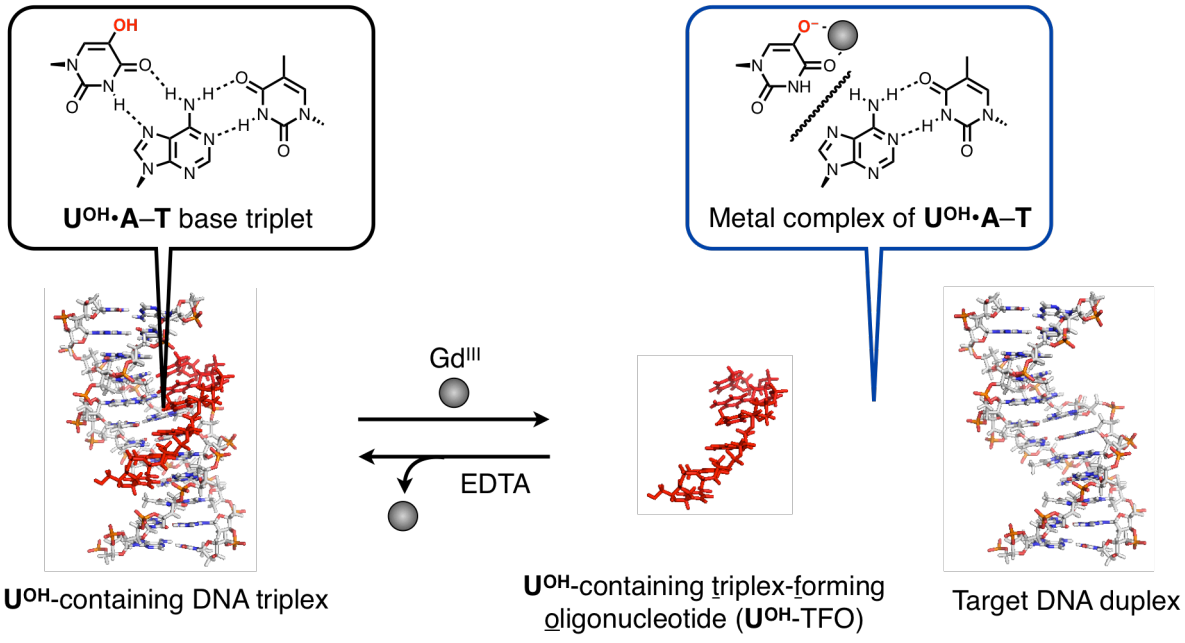

Figure 5-1. Schematic representation of the metal-responsive dissociation of triple-stranded DNA consisting of a $\mathbf{U^{OH}}$-containing triplex-forming oligonucleotide ($\mathbf{U^{OH}}$-TFO) and the target double-stranded DNA. A $\mathbf{U^{OH}}$ nucleobase is most likely to form a $\mathbf{U^{OH}}$**•A–T** base triplet. The metal complexation of a $\mathbf{U^{OH}}$**•A–T** base triplet promoted dissociation of $\mathbf{U^{OH}}$-TFO from the target DNA duplex.

5-2. Design and synthesis of a triplex-forming oligonucleotide containing 5-hydroxyuracil nucleobases

I designed and synthesized a TFO containing three $\mathbf{U}^{\mathbf{OH}}$ nucleobase ($\mathbf{U}^{\mathbf{OH}}$-TFO), which forms a DNA triplex with a target double-stranded DNA (dsDNA) through the formation of three $\mathbf{U}^{\mathbf{OH}}\cdot\mathbf{A}$–**T** as well as natural **T**·**A**–**T** and $\mathbf{C}^{+}\cdot\mathbf{G}$–**C** ($\mathbf{C}^{+}$ is protonated **C**) base triplets (Table 5-1, Figure 5-2). A natural TFO, in which $\mathbf{U}^{\mathbf{OH}}$ nucleobases are fully replaced by the natural **T** nucleobases, was also prepared for control experiments.

Table 5-1. Sequences of DNA strands used

Name	Sequence
$\mathbf{U}^{\mathbf{OH}}$-TFO	5´-TTT TTC $\mathbf{U}^{\mathbf{OH}}\mathbf{U}^{\mathbf{OH}}\mathbf{U}^{\mathbf{OH}}$ CTC TCT-3´
Natural TFO	5´-TTT TTC **TTT** CTC TCT-3´
dsDNA	5´-GCT AAA AAG **AAA** GAG AGA TCG-3´ 3´-CGA TTT TTC **TTT** CTC TCT AGC-5´

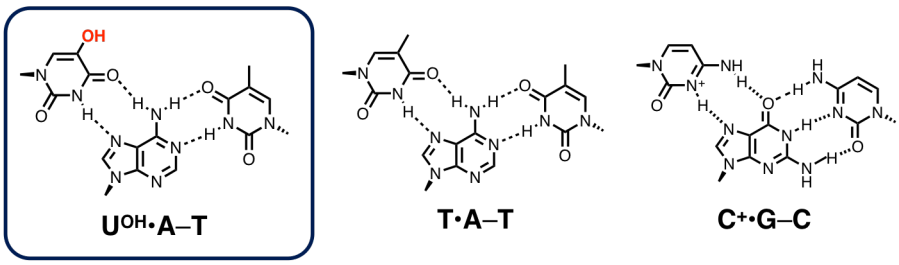

Figure 5-2. Chemical structures of $\mathbf{U}^{\mathbf{OH}}\cdot\mathbf{A}$–**T** and natural **T**·**A**–**T** and $\mathbf{C}^{+}\cdot\mathbf{G}$–**C** base triplets ($\mathbf{C}^{+}$ = protonated cytosine).

5-3. Control of the binding ability of the triplex-forming oligonucleotides based on the Gd^{III} complexation of 5-hydroxyuracil nucleobases

The ability of $\mathbf{U}^{\mathbf{OH}}$-containing TFO ($\mathbf{U}^{\mathbf{OH}}$-TFO) to recognize a target double-stranded DNA (dsDNA) and the effect of the addition of metal ions on the binding ability of $\mathbf{U}^{\mathbf{OH}}$-TFO to dsDNA (Table 1) were then examined. Gd^{III} ion was used here because the binding of Gd^{III} ions to $\mathbf{U}^{\mathbf{OH}}$–**A** base pairs significantly decreased the duplex stability as shown in section **3-2**. Melting experiments were conducted for a mixture of $\mathbf{U}^{\mathbf{OH}}$-TFO and dsDNA in the absence and in the presence of Gd^{III} ions (Figure 5-3a). Without Gd^{III} ions, the melting curve indicated two transitions at different temperatures. By compared with the melting transition of dsDNA (Figure 5-3b), the second transition at a higher temperature around 65 °C was assigned to the dessociation of dsDNA into single strands. Based on this, the first transition around 25 °C was deductively ascribed to the dissociation of $\mathbf{U}^{\mathbf{OH}}$-TFO from dsDNA. This melting profile showed that $\mathbf{U}^{\mathbf{OH}}$-TFO can bind to dsDNA to form a triplex.

Upon addition of 3 equivalents of Gd^{III} ions, the first transition curve, derived from the dissociation of $\mathbf{U}^{\mathbf{OH}}$-TFO, was shifted to the left side (Figure 5-3a). In contrast, the second transition was hardly changed. The results strongly suggested that the $\mathbf{U}^{\mathbf{OH}}$-containing DNA triplex

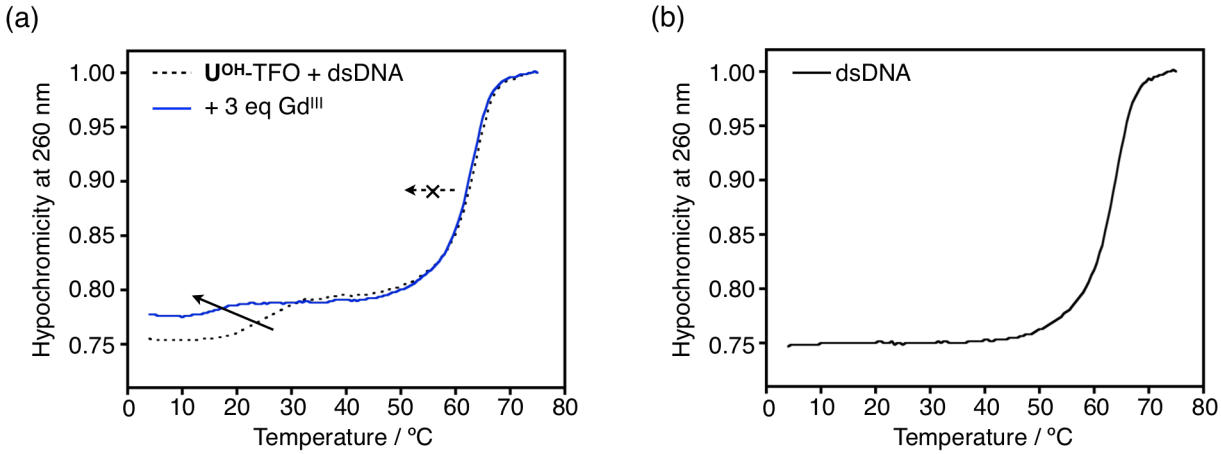

Figure 5-3. Melting curves of the $\mathbf{U}^{\mathbf{OH}}$-containing DNA triplex (a, $\mathbf{U}^{\mathbf{OH}}$-TFO + dsDNA) and only dsDNA (b) in the absence and in the presence of Gd^{III} ions. [$\mathbf{U}^{\mathbf{OH}}$-TFO] = 0 (b), 1.5 μM (a), [dsDNA] = 1.5 μM, [$GdCl_3$] = 0 (a, black dashed line; b), 3 (a, blue solid line) in 10 mM HEPES-NaOH buffer (pH 7.0), 140 mM NaCl, 10 mM $MgCl_2$, 0.2 °C/min.

was selectively destabilized by addition of Gd^{III}. That is, the binding affinity of $\mathbf{U^{OH}}$-TFO to dsDNA was decreased due to the Gd^{III} complexation of $\mathbf{U^{OH}}$ nucleobases.

Control experiments were also conducted to confirm if the destabilization behavior was derived from the Gd^{III} complexation of $\mathbf{U^{OH}}$ nucleobases. The triple-stranded DNA consisting of a natural TFO and dsDNA was utilized (Table 5-1). This fully natural triplex contains **T·A–T** base triplets instead of $\mathbf{U^{OH}}$**·A–T**. Figure 5-4 shows the melting curves of the natural DNA triplex. The two melting curves with and without Gd^{III} ions were well overlapped. This result supported that Gd^{III} ions selectively interacted with the $\mathbf{U^{OH}}$ nucleobases of the oligonucleotides, and therefore decreased the binding ability of $\mathbf{U^{OH}}$-TFO in a sequence-specific manner.

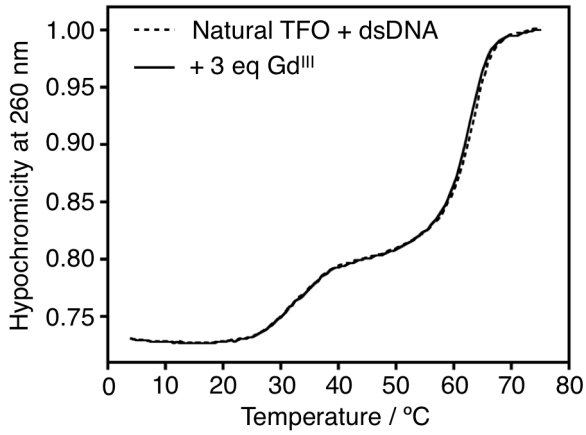

Figure 5-4. Melting curves of the natural DNA triplex (natural TFO + dsDNA) in the absence and in the presence of Gd^{III} ions. [Oligonucleotides] = 1.5 μM for each, [$GdCl_3$] = 0 (dashed line), 3 (solid line) in 10 mM HEPES-NaOH buffer (pH 7.0), 140 mM NaCl, 10 mM $MgCl_2$, 0.2 °C/min.

5-4. Summary

I have designed and synthesized a metal-responsive triplex-forming oligonucleotide based on 5-hydroxyuracil ($\mathbf{U}^{\mathbf{OH}}$) nucleobases as the metal binding sites. The $\mathbf{U}^{\mathbf{OH}}$-containing TFO ($\mathbf{U}^{\mathbf{OH}}$-TFO) was found to have an ability to recognize a complementary DNA duplex in a sequence-specific manner. Moreover, the binding ability of $\mathbf{U}^{\mathbf{OH}}$-TFO was altered in response to Gd^{III} ions.

A number of previous excellent papers have demonstrated that the binding of TFOs results in controlling biological events such as transcription and mutation in the specific regions of endogenous double-stranded DNAs.[1–3] With a view to these findings, the $\mathbf{U}^{\mathbf{OH}}$-TFOs have a potential to regulate the biological functions depending on the type of metal ions. For instance, the $\mathbf{U}^{\mathbf{OH}}$-TFOs would serve as artificial transcription factors like natural metal-responsive proteins related to homeostasis. Furthermore, the sequence of the metal-responsive TFOs can be easily designed by substituting **T** bases for $\mathbf{U}^{\mathbf{OH}}$ bases. It is believed that even simple design strategy helps developing a novel TFO to be versatilely utilized in many fields.

5-5. Experimental section

DNA synthesis

DNA oligonucleotides containing 5-hydroxyuracil ($\mathbf{U}^{\mathbf{OH}}$) nucleobases were synthesized on the same procedure as described in section **2-7**. Unmodified oligonucleotides purified by HPLC were purchased from Japan Bio Services and used without further purification.

Characterization of the DNA strands possessing $\mathbf{U}^{\mathbf{OH}}$ nucleosides

$\mathbf{U}^{\mathbf{OH}}$-TFO. HPLC retention time: 8.7 min (gradient: 6%A (0 min), 8%A (20 min)). ESI-MS: *m*/*z* calcd for $[C_{143}H_{186}N_{34}O_{102}P_{14} - 7H]^{7-}$: 634.2; found: 634.1. $\varepsilon_{260} = 1.06 \times 10^5\ M^{-1}\ cm^{-1}$.

Metal sources

$GdCl_3 \cdot 6H_2O$ (99.9%) as a metal source was purchased from Soekawa Chemical Co.

Sample preparation

All samples for the melting analyses were prepared by mixing the DNA strands (1.5 μM) in 10 mM HEPES-NaOH buffer (pH 7.0) containing 140 mM NaCl, 10 mM $MgCl_2$. After addition of $GdCl_3$, the solutions were heated to 85 °C and cooled slowly to 4 °C at the rate of –1.0 °C/min.

Melting analysis

UV absorbance at 260 nm was recorded on a UV-1700 spectrophotometer (Shimadzu) equipped with a TMSPC-8 temperature controller while the temperature was raised from 4 °C to 85 °C at the rate of 0.2 °C/min. A drop of mineral oil was laid on the sample to prevent the evaporation. Hypochromicity shown in the Figures were calculated as follows:

$$Hypochromicity\ at\ 260\ nm = Abs_{260}(t\ °C)/Abs_{260}(60\ °C)$$

5-6. References

[1] L. J. Maher III, B. Word, P. B. Dervan, *Science* **1989**, *245*, 725–730.

[2] L. J. Maher III, *Biochemistry* **1992**, *31*, 7587–7594.

[3] K. M. Vasquez, L. Narayanan, P. M. Glazer, *Science* **2000**, *290*, 530–533.

Chapter 6.

Conclusion

In this study, I have demonstrated the metal-responsive "bifacial" DNA base pairing based on the 5-hydroxyuracil ($\mathbf{U}^{\mathbf{OH}}$) nucleobase (Figure 6-1). The consecutive $\mathbf{U}^{\mathbf{OH}}$ nucleobases formed both metal-mediated $\mathbf{U}^{\mathbf{OH}}$–M–$\mathbf{U}^{\mathbf{OH}}$ (M = Zn^{II}, Gd^{III} etc) and hydrogen-bonded $\mathbf{U}^{\mathbf{OH}}$–**A** base pairs. The $\mathbf{U}^{\mathbf{OH}}$–M–$\mathbf{U}^{\mathbf{OH}}$ base pairing thermally stabilized the resulting DNA duplexes while the metal complexation of the $\mathbf{U}^{\mathbf{OH}}$–**A** base pairs destabilized the duplex. It is worthy of note that the metal-driven stabilization and destabilization induced the bidirectional DNA strand exchange reactions through the base pair switching of $\mathbf{U}^{\mathbf{OH}}$ nucleobases. In addition, the bifacial property of $\mathbf{U}^{\mathbf{OH}}$ nucleobase allowed the regulation of the binding ability of the triplex-forming oligonucleotide (TFO) to the target DNA duplex in response to Gd^{III} ions.

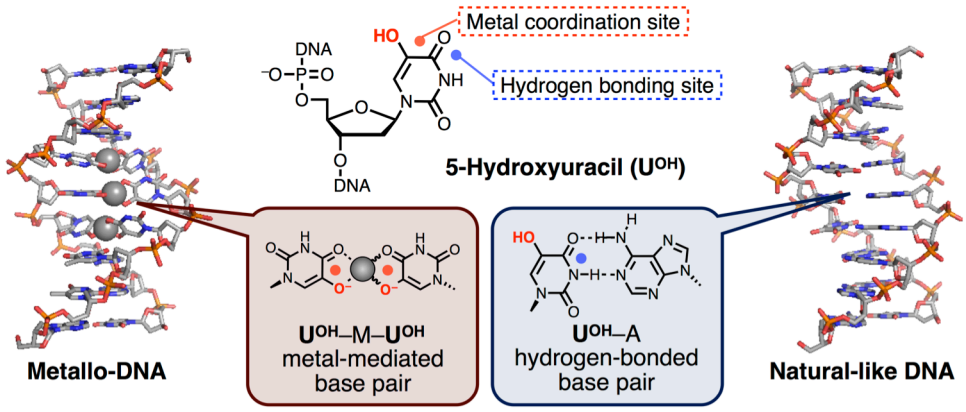

Figure 6-1. Schematic representation of the metal-responsive bifacial base pairing of 5-hydroxyuracil ($\mathbf{U}^{\mathbf{OH}}$) DNA bases. $\mathbf{U}^{\mathbf{OH}}$ bases form both the $\mathbf{U}^{\mathbf{OH}}$–M–$\mathbf{U}^{\mathbf{OH}}$ (M = Zn^{II}, Gd^{III} etc) and the $\mathbf{U}^{\mathbf{OH}}$–**A** base pairs. Other possible additional ligands on the metal ion are omitted for clarity.

In chapter **2**, the consecutive three $\mathbf{U}^{\mathbf{OH}}$–$\mathbf{U}^{\mathbf{OH}}$ base pairs were found to form the zinc- and lanthanide-mediated $\mathbf{U}^{\mathbf{OH}}$–M–$\mathbf{U}^{\mathbf{OH}}$ base pairs inside DNA duplexes. The $\mathbf{U}^{\mathbf{OH}}$-based metal-mediated base pairing thermally stabilized the resulting DNA duplexes. From another viewpoint, the introduction of multiple $\mathbf{U}^{\mathbf{OH}}$–M–$\mathbf{U}^{\mathbf{OH}}$ base pairs permitted the precise metal arrangement within the DNA helical scaffold. The novel metal-mediated base pairing would contribute not only to develop the metal-responsive bifacial base pairing but also to induce the chiral properties such as circular polarized luminescence and asymmetric catalysts. To utilize various metal ions, other bifacial nucleobases can be designed by systematic alteration of the 5-modifying functional group and of the pyrimidine scaffold. For instance, 5-mercaptouracil, 5-mercaptocytosine, and 5-aminocytosine

would serve as soft metal ligands and then bind to soft metal ions such as Pd^{II} and Pt^{II}.

In chapter **3**, the hybridization preference of the $\mathbf{U^{OH}}$-containing DNA strands was altered by the Gd^{III} complexation of $\mathbf{U^{OH}}$ nucleobases through the stabilization of $\mathbf{U^{OH}}$–$\mathbf{U^{OH}}$ base pairs and the destabilization of $\mathbf{U^{OH}}$–**A** base pairs. The reverse changes in the duplex stability resulted from the bifacial structure of $\mathbf{U^{OH}}$ nucleobase. The unique metal-responsive property is a strong foundation to achieve the reversible DNA strand exchange reactions through the base pair switching. In addition, Zn^{II}-pH dual responsiveness would also expand the DNA-based nanotechnology and biotechnology.

In chapter **4**, it was found that the DNA strand exchange reaction occurred through the base pair switching from $\mathbf{U^{OH}}$–**A** base pairs to $\mathbf{U^{OH}}$–Gd^{III}–$\mathbf{U^{OH}}$ base pairs upon addition of Gd^{III} ions. The exchange reaction also proceeded to the reverse direction based on EDTA to remove the Gd^{III} ions bound to $\mathbf{U^{OH}}$ nucleobases. The $\mathbf{U^{OH}}$-based bidirectional reaction requires neither the additional DNA strands nor the annealing process and consequently would become a versatile motive power for the DNA-based nano-machines, logic gates, and drug delivery systems.

In chapter **5**, the metal responsiveness and the bifacial property of $\mathbf{U^{OH}}$ nucleobases were applied to the triple-stranded DNA structure. The $\mathbf{U^{OH}}$-containing triplex-forming oligonucleotide ($\mathbf{U^{OH}}$-TFO) bound to the target DNA duplex and then the binding ability of $\mathbf{U^{OH}}$-TFO to the duplex was selectively decreased by addition of Gd^{III}. In general, TFOs recognize the DNA duplexes in a sequence-specific manner and the TFO binding inhibits the access of RNA polymerases. Thus, the $\mathbf{U^{OH}}$-TFO is expected to serve as an artificial transcription factor, which works in response to the specific metal ions. Furthermore, the introduction of the metal-responsiveness into the other higher-order structures is also a versatile technic because the $\mathbf{U^{OH}}$-containing DNA structures can be easily designed by replacing **T** nucleobase for $\mathbf{U^{OH}}$ nucleobase.

Taken all together, it is concluded that the novel metal-responsive “bifacial” base-pairing behaviors strongly contributed to construction of dynamic self-assembly systems. I believe that the achievement in this study is a beneficial and expansive first step for many fields such as supramolecular chemistry, nanotechnology, and biotechnology.

A list of publications

1. "Bifacial Base-Pairing Behaviors of 5-Hydroxyuracil DNA Bases through Hydrogen Bonding and Metal Coordination"

   Yusuke Takezawa, Kotaro Nishiyama, Tsukasa Mashima, Masato Katahira, Mitsuhiko Shionoya, *Chem*. *Eur*. *J*. **2015**, *21*, 14713–14716.

2. "pH-Dependence of the Thermal Stability of Metallo-DNA Duplexes Containing Ligand-Type 5-Hydroxyuracil Nucleobases"

   Kotaro Nishiyama, Yusuke Takezawa, Mitsuhiko Shionoya, *Inorg*. *Chim*. *Acta* **2016**, *452*, 176–180.

Acknowledgement

This research was promoted under supervision of Professor Dr. Mitsuhiko Shionoya (The University of Tokyo). I greatly appreciate him for his dedicated tutelage and warmest encouragement.

I'm deeply grateful to Assistant Professor Dr. Yusuke Takezawa (The University of Tokyo) for his courteous leadership in my life as a researcher.

I appreciate Associate Professor Dr. Shohei Tashiro and Assistant Professor Dr. Hitoshi Ube (The University of Tokyo) for their shrewd advice and polite support.

I give thanks to Mr. Tsutomu Umeki, Mr. Atsushi Kawaguchi, Mr. Yoshinori Takamatsu, Mr. Yoshihiro Yasuda, and Mr. Shuhei Yoneda for their inspiring words and actions.

I heartfelt thank to all members of Shionoya laboratory for the friendly competition with each other.

I would like to say a lot of thanks to Professor Dr. Masato Katahira and Assistant Professor Dr. Tsukasa Mashima (Kyoto University) for conducting NMR structural analysis of the $\mathbf{U}^{\mathbf{OH}}$-based metallo-DNA duplex.

I'm strongly grateful to Professor Dr. Yasuhiko Yamamoto (University of Tsukuba) for his kind support from my undergraduate study to now.

I'm thankful for Advanced Leading Graduate Course for Photon Science (ALPS) for the financial support and the encouragement.

Finally, I would like to express sincerely appreciation to my family, Mr. Takayoshi Nishiyama, Ms. Yumiko Sakai, Mr. Kentaro Nishiyama, Mr. Toyoaki Saito, Mrs. Kyoko Saito, and Mrs. Mika Nishiyama for warm and painstaking supports.

Kotaro Nishiyama